POWER GENERATION FROM LOW-GRADE ENERGY SOURCE USING ORGANIC RANKINE CYCLE TECHNOLOGY

Owoputi, Adefemi Oluwaniyi B.Eng (Hons)
(Student Number: 214585093)

Supervisor: Prof Freddie L. Inambao

Dissertation submitted in fulfilment of the requirement for the degree of
MASTER OF SCIENCE IN ENGINEERING (MSc. Eng)
(MECHANICAL)

School of Engineering, University of KwaZulu-Natal, Durban, South Africa

2017

DECLARATION 1: PLAGIARISM

I, **Owoputi Adefemi Oluwaniyi** declare that:

1. The research reported in this thesis, except where otherwise indicated is my original research work.

2. This thesis has not been submitted for any degree or examination at any other university.

3. This thesis does not contain other persons' data, pictures, graphs or other information, unless specifically acknowledged as being sourced from other persons.

4. This thesis does not contain other persons' writing, unless specifically acknowledged as being sourced from other researchers. Where other written sources have been quoted, then:
   a. Their words have been re-written but the general information attributed to them has been referenced
   b. Where their exact words have been used, then their writing has been placed in italics and inside quotation marks, and referenced.

5. This thesis does not contain text, graphics or tables copied and pasted from the Internet, unless specifically acknowledged, and the source being detailed in the thesis and in the References sections.

Signed:  .....

DECLARATION 2: PUBLICATIONS

DETAILS OF CONTRIBUTION TO PUBLICATIONS that form part and/or include research presented in this thesis (including publications in preparation, submitted, in press and published and give details of the contributions of each author to the experimental work and writing of each publication)

Publication 1: **Owoputi Adefemi Oluwaniyi,** Andrew Oyieke and Freddie Inambao: "Simulation of a Hypothetical Geothermal Powered ORC System Using R134a", Presented at 14th Botswana Institution of Engineers Biennial Conference, October 6 - 8, 2015, Gaborone, Botswana.

In the above paper, I, Owoputi Adefemi Oluwaniyi was the main and corresponding author.

Signed: 

As the candidate's supervisor, I have approved this thesis for submission.

Signed  Date 25th of January, 2017

Name: **Professor Freddie Inambao**

ACKNOWLEGEMENTS

My profound gratitude goes to The Almighty, the giver and sustainer of life. I would also like to appreciate the priceless role Professor Freddie Inambao, my research supervisor, has played in the attainment of this degree. My sincere thanks goes to Professor Glen Bright, the Head of Discipline, and the entire staff of the Mechanical Engineering Discipline for providing an enviable and holistic academic research environment for me during this period. Special thanks to every individual member of Green Energy Solutions Cluster for their support and encouragement all through this exciting journey. Finally, my deepest appreciation goes to my parents and siblings for their ever reliable and unfailing support as well as sacrifice towards my attainment of this degree. I am forever grateful.

ABSTRACT

This thesis focuses on power generation from low-grade heat sources using Organic Rankine Cycle (ORC) technology. Growing concerns over the gradual deterioration of the ozone layer leading to extreme and adverse weather and climatic conditions have necessitated the need to develop technology which can be used to harness and generate energy from low-grade sources efficiently and effectively, rather than rely on traditional energy sources such as coal and crude oil which significantly increase the atmospheric CO_2 content.

On the basis of a cleaner and greener alternative to power generation, a simulated heat source was adopted for the research. The methodological approach to this research is divided into two parts, this include a computer-based modelling and simulation of the processes involved in the cycle operation which can be used to predict the performance of a real life ORC system given the thermal content of the available renewable source. The second part to the methodological approach is a laboratory investigation to determine the power generating capacity of an IT10 Infinity Turbine ORC unit.

Modelling and simulation of the cycle were carried out using Engineering Equation Solver (EES) software. A net power output of 9.4 kW was obtained from the system cycle given the heat source temperature of 80^0C and refrigerant pump pressure of 2.46 MPa and flow rate of 0.4778 kg/s. The experimentation processes for this research work was carried out in the Mechanical Engineering Discipline Workshop of the University of KwaZulu-Natal, Durban. A single IT10 ORC unit procured from Global Energy and Infinity Turbine LLC, Madison, Wisconsin, USA, was used while the low-grade energy heat source was simulated using a hot water geyser with a regulated maximum temperature of 80^0C. Water was adopted as the Heat Transfer Fluid (HTF) and Cooling Fluid (CF) for this research while the refrigerant R-134a was used.

The result from the experimental investigation shows that with a system operating pressure of 2.46 MPa and a HTF fluid temperature of 80^0C, the IT10 Infinity Turbine was able to generate power of 9.57 kW while the speed of the turbine blade was observed to rotate at a speed of 1577 rpm. The outcome of this research shows that power generation from clean, renewable low-grade heat sources is possible using the ORC technology. The choice of the working fluid, and careful selection of the major component units of the ORC is the key determinant of the efficiency and overall performance of the cycle. Depending on the efficiency of the cycle, the quantity of heat available to be harnessed from a given source determines the amount of power that can be generated.

Keywords: *Organic Rankine Cycle, Renewable Energy, Working Fluid, Heat Transfer Fluid, Global Warming Potential, Low-grade Energy.*

TABLE OF CONTENTS

DECLARATION 1: PLAGIARISM ii
DECLARATION 2: PUBLICATIONS iii
ACKNOWLEGEMENTS v
ABSTRACT vi
TABLE OF CONTENTS vii
LIST OF FIGURES xi
LIST OF TABLES xiii
LIST OF APPENDIXES xiv
NOMENCLATURE xv
ACRONYMS AND ABBREVIATIONS xvii
CHAPTER 1 : INTRODUCTION 1
1.1 The Global Energy Trend 1
1.2 Background to Research 1
1.3 Motivation 2
1.4 Problem Statement 3
1.5 Research Questions 3
1.6 Aim and Objectives 4
1.7 Scope 4
1.8 Structure of Thesis 5
CHAPTER 2 : LITERATURE REVIEW 7
2.1 Introduction 7
2.2 Thermodynamic Cycle 7
2.2.1 Power Cycles 7
2.2.1.1 Ideal Rankine Cycle 7
2.2.1.2 Organic Rankine Cycle 10
2.2.1.3 Kalina Cycle 11
2.2.1.4 Goswami Cycle 13
2.2.1.5 Trilateral Cycle 14
2.2.1.6 Transcritical (CO_2) power cycle 15
2.2.1.7 Brayton Cycle 15
2.3 The Organic Rankine Cycle and Applications 16
2.3.1 Waste Heat Recovery Application 16

2.3.2 Geothermal Applications 17
2.3.3 Biomass Applications 18
2.3.4 Solar Applications 18
2.4 Working Fluid Selection for Organic Rankine Cycle Power Production 18
2.4.1 Types of Working Fluids 19
2.4.1.1 Single Component Working Fluids 19
2.4.1.2 Multicomponent Working Fluids 19
2.4.2 Working Fluid Selection Criteria 20
2.4.2.1 Thermal Stability 20
2.4.2.2 Critical Properties/Points 20
2.4.2.3 Fluid Molecular Weight 20
2.4.2.4 Fluid-Material Compatibility 21
2.4.2.5 System Performance 21
2.4.2.6 Safety 21
2.4.2.7 Environmental Consideration and Ethics 22
2.4.2.8 Accessibility and Cost Factors 23
2.5 The Choice of R-134a as Working Fluid 23
2.6 Summary 24
CHAPTER 3 : RESEARCH METHODOLOGY 25
3.1 Introduction 25
3.2 Modelling of ORC System Components 25
3.2.1 The Pump Model 25
3.2.2 The Evaporator Model 26
3.2.3 The Turbine Model 27
3.2.4 The Condenser Model 28
3.3 Process of Heat Exchange in the Evaporator 29
3.3.1 Factors Influencing Heat Exchangers Performance 31
3.3.2 Design Model for Evaporator Heat Exchanger 31
3.4 The Mathematical Model for the Organic Rankine Cycle 33
3.5 Summary 35
CHAPTER 4 : SIMULATION RESULTS 36
4.1 Introduction 36
4.2 Simulation Results of the Organic Rankine Cycle 36
4.3 Effect of the Heat Transfer Area on the Cycle Performance 39
4.3.1 Effect of Heat Transfer Area on Refrigerants Exit Temperature 39
4.3.2 Effect of Heat Transfer Area on Quantity of Heat Energy Transferred 41

4.3.3 Effect of Heat Transfer Area on Net Power Output 42
4.3.4 Effect of Heat Transfer Area on Cycle Efficiency 43
4.3.5 Effect of Heat Transfer Area on Back-work-ratio of Refrigerant Pump 43
4.4 Effect of Heat Transfer Fluid (Water) Inlet Temperature on Cycle Performance 44
4.4.1 Effect of Heat Transfer Fluid (Water) Inlet Temperature on Refrigerants Exit Temperature 44
4.4.2 Effect of Heat Transfer Fluid (Water) Inlet Temperature on Quantity of Heat Energy Transferred 45
4.4.3 Effect of Heat Transfer Fluid (Water) Inlet Temperature on Net Power Output 46
4.4.4 Effect of Heat Transfer Fluid (Water) Inlet Temperature on Cycle Efficiency .. 47
4.5 Effect of Refrigerant Mass Flow Rate on the Cycle Performance 48
4.5.1 Effect of Refrigerant Mass Flow Rate on Refrigerants Exit Temperature 48
4.5.2 Effect of Refrigerant Mass Flow Rate on Quantity of Heat Energy Transferred 49
4.5.3 Effect of Refrigerant Mass Flow Rate on Net Power Output 49
4.5.4 Effect of Refrigerant Mass Flow Rate on Cycle Efficiency 50
4.6 Effect of Refrigerant Pump Pressure on the Cycle Performance 51
4.6.1 Effect of Refrigerant Pump Pressure on Refrigerant Exit Temperature 51
4.6.2 Effect of Refrigerant Pump Pressure on Quantity of Heat Energy Transferred .. 52
4.6.3 Effect of Refrigerant Pump Pressure on Net Power Output 53
4.6.4 Effect of Refrigerant Pump Pressure on its Cycle Efficiency 53
4.6.5 Effect of Refrigerant Pump Pressure on Rotational Speed of Turbine Blades 54
4.6.6 Effect of Refrigerant Pump Pressure on Torque 55
4.7 Influence of Power on the Rotational Speed of the Turbine Blade 55
4.8 Summary 59
CHAPTER 5 : EXPERIMENTAL INVESTIGATION 61
5.1 Introduction 61
5.2 Detailed Description of Experimental Setup Units 61
5.2.1 Description of the Hot Water Geyser System 61
5.2.2 Description and Details of the IT10 ORC 62
5.3 Cycles in the Experimental Setup 63
5.3.1 The Heat Transfer Fluid (HTF) Cycle 63
5.3.2 The Working Fluid (WF) Cycle 64
5.3.3 The Cooling Fluid (CF) Cycle 65
5.4 Experimental Methodology 66
5.4.1 Leak Testing on the ORC System 66
5.4.1.1 Air Leak Test 66

5.4.1.2 Nitrogen Leak Test 67
5.4.1.3 Ultrasonic Leak Test 68
5.4.1.4 Vacuuming 68
5.4.2 Refrigerant Charging 69
5.4.3 Experimental Result and Analysis 70
5.4.3.1 Rise in HTF Temperature 71
5.4.3.2 Influence of System Working Pressure on Rotational Speed 72
5.4.3.3 Influence of System Working Pressure on Torque 73
5.4.3.4 Influence of System Working Pressure on Power 74
5.4.3.5 Influence of Power Output on Turbine Speed 75
5.4.3.6 Electrical Load Connection and Measurements 77
5.5 Model Validation with Experimental Results 78
5.5.1 System Refrigerant Pressure against Rotational Speed of Turbine blade 79
5.5.2 System Refrigerant Pressure against Torque 80
5.5.3 Power Output against Turbine Speed 80
5.6 Summary 81
CHAPTER 6 : CONCLUSIONS AND RECOMMENDATIONS 83
6.1 Conclusions 83
6.2 Recommendations 84
REFERENCES 85
APPENDIXES 90
Appendix I: Simulation Codes and Formatted Equations 90
Appendix II: Simulation Results 96
Appendix III: Parametric Tables for Plots 97
Appendix IV: IT10 Infinity Turbine Data Sheet 110

LIST OF FIGURES

Figure 2.1: Schematic Showing the Reheating Stage and Two Turbines 9
Figure 2.2: Schematic of an Organic Rankine Cycle Process 11
Figure 2.3: Diagrammatic Process of Kalina Cycle 13
Figure 2.4: Schematic Diagram for Trilateral Cycle (TLC) and Corresponding T-s Diagram ... 14
Figure 3.1: State Point 1 at the Pump Exit 26
Figure 3.2: State Point 2 at the Evaporator Exit 27
Figure 3.3: State Point 3 at the Turbine Exit 28
Figure 3.4: State Point 4 at the Condenser Exit 28
Figure 3.5 Parallel Flow Pattern 29
Figure 3.6 Counter Flow Pattern 29
Figure 3.7: Cross flow Pattern 30
Figure 3.8: Shell and Tube Exchanger 30
Figure 3.9: Compact Type Heat Exchangers 30
Figure 3.10: Schematic Setup of the ORC 33
Figure 4.1 Temperature Profile of the Fluids in the Evaporator 36
Figure 4.2: Temperature-Entropy Diagram for the Cycle 38
Figure 4.3: Pressure-Enthalpy Diagram for the Cycle 39
Figure 4.4: Effect of Heat Transfer Area on Refrigerant Exit Temperature 40
Figure 4.5: Effect of Increased Heat Transfer Area on Exit Temperature of Refrigerant 40
Figure 4.6: Effect of Heat Transfer Area on Quantity of Heat Energy Transferred 41
Figure 4.7: Effects of Increased Heat Transfer Area on Heat Energy Transferred 42
Figure 4.8: Effect of Heat Transfer Area on Net Power Output 42
Figure 4.9: Effect of Heat Transfer Area on Cycle Efficiency 43
Figure 4.10: Effect of Heat Transfer Area on Back-work-ratio of Refrigerant Pump 44
Figure 4.11: Effect of Heat Transfer Fluid (Water) Inlet Temperature on Refrigerants Exit Temperature 45
Figure 4.12: Effect of Heat Transfer Fluid (Water) Inlet Temperature on Quantity of Heat Energy Transferred 46
Figure 4.13: Effect of Heat Transfer Fluid (Water) Inlet Temperature on Net Power Output 47
Figure 4.14: Effect of Heat Transfer Fluid (Water) Inlet Temperature on Cycle Efficiency 47
Figure 4.15: Effect of Refrigerant Mass Flow Rate on Refrigerants Exit Temperature 48
Figure 4.16: Effect of Refrigerant Mass Flow Rate on Quantity of Heat Energy Transferred ... 49
Figure 4.17: Effect of Refrigerant Mass Flow Rate on Net Power Output 50
Figure 4.18: Effect of Refrigerant Mass Flow Rate on Cycle Efficiency 51
Figure 4.19: Effect of Refrigerant Pump Pressure on Refrigerant Exit Temperature 52

Figure 4.20: Effect of Refrigerant Pump Pressure on Quantity of Heat Energy Transferred 52
Figure 4.21: Effect of Refrigerant Pump Pressure on Net Power Output 53
Figure 4.22: Effect of Refrigerant Pump Pressure on its Cycle Efficiency 54
Figure 4.23: Effect of Refrigerant Pump Pressure on Rotational Speed of Turbine Blades 54
Figure 4.24: Effect of Refrigerant Pump Pressure on Torque 55
Figure 4.25: Influence of Power on the Rotational Speed of the Turbine Blade 56
Figure 5.1 Cross-section of the Heat Source (Hot Water Geyser) 62
Figure 5.2: IT10 Organic Rankine Cycle Unit 63
Figure 5.3 Schematic of the HTF Cycle 64
Figure 5.4 Schematic Layout of the WF cycle 65
Figure 5.5 Schematic of Cooling Fluid Cycle 65
Figure 5.6 Air Compressor Unit 67
Figure 5.7: Nitrogen Charging Setup 68
Figure 5.8: System Vacuuming Pump Setup 69
Figure 5.9: Refrigerant Charging 70
Figure 5.10: Schematic Diagram of Experimental Setup 71
Figure 5.11: Rise in HTF Temperature with Time 72
Figure 5.12: Variation of Rotational Speed of Turbine with Refrigerant Pressure 73
Figure 5.13: Variation of Torque with Refrigerant Pressure 74
Figure 5.14: Variation of Power with Refrigerant Pressure 75
Figure 5.15: Generator Power Versus Turbine Speed 76
Figure 5.16: Turbine Speed and Generator Characteristics [49] 76
Figure 5.17: Schematic Showing the Load Connection on the ORC 77
Figure 5.18: Current Variation with Load Resistance at Different System Operating Pressures 78
Figure 5.19: Model Validation for Rotational Speed of Turbine blade 79
Figure 5.20: Model Validation for Torque Produced at the Turbine 80
Figure 5.21: Model Validation for Power Output versus Turbine Speed 81

LIST OF TABLES

Table 2.1: Properties of R-134a 23
Table 4.1 Variable Parameters 37
Table 4.2 Simulation Results 37
Table 4.3: Variation of ORC Units and Performance with Heat Source Temperature 57
Table 4.4: Variation of ORC Units and Performance with Refrigerant Pump Pressure 57
Table 4.5: Variation of ORC Units and Performance with Heat Transfer Area 58
Table 4.6: Variation of ORC Units and Performance with Refrigerant Mass Flow Rate 59

LIST OF APPENDIXES

Appendix I: Simulation Codes and Formatted Equations……..90

Appendix II: Simulation Results…….96

Appendix III: Parametric Tables for Plots…….……...97

Appendix IV: IT10 Infinity Turbine Data Sheet…….110

NOMENCLATURE

LATIN SYMBOLS

C	Heat Capacity of Fluids (J)
D	Diameter
F	Force (N)
h	Enthalpy (kJ/kg)
kW	Kilowatt
$\dot{m}$	Mass flow rate (kg/s)
P	Pressure (MPa)
$\dot{Q}$	Heat Energy (J)
R_f	Fouling resistance
s	Specific entropy (kJ/kgK)
T	Temperature (K)
U	Heat Transfer Coefficient (W/m^2K)
$\dot{W}$	Work (kW)
x	Fluid quality

GREEK SYMBOLS

ε	Effectiveness
η	Rankine efficiency (%)
τ	Torque

SUBSCRIPTS

b	Evaporator (Boiler)
cond	Condenser
c	Working Fluid (Refrigerant)
h	Heat Transfer Fluid (Hot Water)
in	Inlet

out	Outlet
p	Pump
r	Ratio
t	Turbine
[ ]	Denote state points

CHEMICAL COMPOUNDS

NH_3-H_2O	Ammonia-water
CH_2FCF_3	1,1,1,2-Tetrafluoroethane
CO_2	Carbon dioxide

ACRONYMS AND ABBREVIATIONS

ASHRAE	American Society of Heating, Refrigerating, and Air-Conditioning Engineers
ALT	Atmospheric Life Time
BWR	Back-Work-Ratio
BC	Brayton Cycle
CAPEX	Capital Expenditure
CFCs	Chlorofluorocarbons
CF	Cooling Fluid
DORC	Dual-loop Organic Rankine Cycle
EES	Engineering Equation Solver
FER	Fossil Energy Resources
GWP	Global Warming Potential
GHG	Green House Gases
HTA	Heat Transfer Area
HTF	Heat Transfer Fluid
ORC	Organic Rankine Cycle
ODP	Ozone Depletion Potential
TEG-ORC	Thermo-Electric Generator Organic Rankine Cycle
TLC	Trilateral Cycle
WF	Working Fluid

CHAPTER 1 : INTRODUCTION

1.1 The Global Energy Trend

There has been a tremendous advancement in technology through the years as research has intensified on effective and optimum use of energy resources available to generate the power that is needed to keep up with the rate of industrialization. The world is getting closer to the stage where its need for energy to carry out day-to-day domestic and industrial activities becomes seemingly impossible to meet if alternate energy sources are not utilized maximally. This is due to the heavy reliance on fossil fuel deposits as the main energy sources which are finite and non-renewable [1]. The continual reliance on and usage of fossil fuel resources over time has led to an increase in environmental challenges such as air pollution and global warming [2].

Traditionally, the main energy sources are non-renewables like coal, crude oil and gas. In 2012, non-renewable sources supplied 81% of global final energy consumption and although the value dropped to 77.9% at the end of 2013, it was still apparent how heavily the global energy production relied on fossil fuels [3]. The formation of acid rain, rapidly deterioration of climatic conditions, and increase in Green House Gas (GHG) emission effects can be linked to the extensive use of carbon-based fossil fuel reserves as the main source of energy. Consequently, obtaining energy from renewable sources such as solar, wind, hydro, biomass, geothermal and industrial waste heat is becoming attractive. Additionally, research into effective and efficient energy harnessing techniques from renewable sources is intensifying worldwide.

Renewable energy sources as alternatives to conventional fossil fuel sources for energy come in various forms and can be harnessed through various means. There is no region in the world that does not have one form of renewable energy source or another, however small or limited these might be. Geothermal, hydropower, wind, solar and biomass are renewable energy sources which have been tapped into in different parts of the world. According to Li, et al. [2] hydropower and solar renewable energy alone accounted for 33.3% increase in renewable energy capacity globally in 2013.

1.2 Background to Research

The Rankine cycle technology is one of the earliest energy conversion techniques used to harness energy from renewable sources. It was developed as an improvement of the already existing Carnot cycle in which the compression of wet vapor became problematic [1]. The

Rankine cycle consists of four main thermodynamic processes of compression, evaporation, expansion and condensation which are associated with the four major components of the cycle. These are the pump, boiler/evaporator, turbine/expander, and condenser. The Rankine cycle can be used in various applications such as geothermal, hydropower, wind, solar, biomass and municipal/industrial waste heat recovery. The resources for power generation using the Rankine cycle can be from renewable as well as non-renewable sources. A typical instance of this is observed in the life cycle analysis of a thermal power plant in Egypt where natural gas and low-quality fuel oil (also known as *mazout*) as Heat Transfer Fluid (HTF) is used to raise the temperature of steam in the boiler to produce electricity [4]. The Rankine cycle has been used in various renewable energy sources applications around the world. Solar application was reported by [5] in "New Energy Externalities Development For Sustainability". Furthermore, other applications such as geothermal, biomass and waste heat recovery have been well documented in various works of literature and reports [2, 6-8]. The various sources for these applications can be categorized into high, medium and low-grade heat sources depending on their temperature. While the system efficiency of an Ideal Rankine Cycle is comparatively high for medium and high thermal sources with temperatures above 370^0C, the Organic Rankine Cycle (ORC) which operates on the same principle as the Ideal Rankine Cycle with the exception of using an organic fluid as the working fluid, possesses even higher efficiency when used to harness energy from low-grade thermal sources [9, 10]. These sources usually have their temperature around 150^0C and below [10].

Increase in the global use of energy has led to a corresponding increase in demand. This upsurge has propelled the exploitation of energy from low-grade sources as an alternative and viable means to meet the rising demands. The ORC, hence, poses a great advantage in the effective utilization of this grade of energy which could have otherwise been wasted. Features of the organic Rankine technology such as dry expansion process, low adverse environmental impact, high thermal efficiency, simple expander design among others, makes it a desirable technology [11].

1.3 Motivation

Research into clean and sustainable power generation has been the trend for a long time now with no signs of slowing down soon. This is due to various factors including industrialization, socio-economic and environmental factors. Results from this research work could prove useful in addressing some of the fundamental issues which are associated with the conventional way of energy generation from fossil fuel reserves while further presenting the benefits of renewable

energy production. Beyond the general motivation for this study, there is a more specific and urgent need to utilize old and abandoned mine shafts all across the country for energy generation via geothermal means. Abandoned mine shafts present unique niches for siting geothermal plants for the following reasons:

- A temperature range of 50^0C to 200^0C can easily be obtained by drilling a horizontal directional shaft from the greatest depth into the sub-terrain at a much lower CAPEX (capital expenditure) than from the surface;
- Technical and human knowhow for such undertaking already exists in great abundance all across the country and
- It has the potential to solve two major problems at once – the challenge of unemployment among mine workers and the current shortfall in energy generation.

Being a renewable source, geothermal means has the potential to move dependence away from fossil coal as our base load carrier to a cleaner source of energy thus creating a hedge against possible unsustainable global liability in the form of the much talked about carbon tax, if and when it is introduced.

1.4 Problem Statement

Factors such as ozone layer diminution, air pollution resulting from GHG emissions and depletion in the Fossil Energy Resources (FER) has made the quest for renewable energy resources for power production more desirable. As a result, research into ways of generating clean and sustainable energy are intensifying. Furthermore, the increase in power shortages experienced in developing nations such as South Africa is a direct result of continual increase in energy demand for production needed for sustained industrialization. Finally, the increase in human population and civilization are also contributing factors to the imbalance in the energy demand and supply. The impetus of this research is derived from the challenges highlighted above and thus seeks to explore the use of alternative energy sources for power generation in order to complement existing energy sources such as coal and natural gas, while also reducing harmful environmental impacts.

1.5 Research Questions

To ensure the success of this research, the essential questions to which this study seeks to offer solutions are stated below:

- What is the current global trend in energy/power generation?

- What are the model parameters for on ORC system output?
- What design characteristics influence the heat exchanger performance?
- What HTF source characteristics are required for desired output?
- What is the power generating capacity of the experimental IT10 ORC system?

In a bid to answer these preformed questions, an in-depth literature review was conducted to understand the underlying principles of the Rankine technology in energy and power generation. This helped in developing the model adopted for this study.

1.6 Aim and Objectives

The aim of this study was to harness and convert low-grade thermal energy from renewable source to electrical power using the Organic Rankine Cycle (ORC). The main objectives of this research were to:

i. Conduct an extensive literature survey on the praxis of renewable energy resources and the technology used to harness them.
ii. Develop a suitable model for the heat exchanger evaporator unit for the ORC.
iii. Determine the operating parameters of heat transfer fluid and working fluid to give optimum performance.
iv. Develop a mathematical model for the ORC and refrigerant state point properties.
v. Present the ORC system output in terms of power generated and efficiency.
vi. Show the influence of variation in input parameters of pressure, heat source temperature and refrigerant flow rates, for the model developed and presented in (iv) on the ORC performance and determining optimum performance conditions.
vii. Perform a laboratory investigation on the available IT10 ORC system to determine how variation in pressure influences system performance.
viii. Present result of experimental investigation and validate against results obtained from model.

1.7 Scope

This research seeks to present the power generating potential that is available in renewable energy sources with low to medium thermal deposits. In the course of this study, there is extensive review of various renewable energy sources which have been developed and adopted for use. The peculiarities, advantages, and disadvantages of the various renewable energy

sources are highlighted. Factors which affect the choice of working fluid for the ORC technology are discussed after which selection of a suitable refrigerant is made. The flow rate, pressures, evaporator heat exchanger outlet temperatures for both water and refrigerant are determined for the desired power output. In the model formulation for this research work, the conservation law of energy which states the indestructible nature of energy, rather, its transformation from one form to another, was carefully considered. It is important to note that cost analyses and evaluation of equipment used for this study were not taken into account.

1.8 Structure of Thesis

Chapter 1 of the thesis is aimed at providing the background to the concept of energy and power generation from renewable and non-renewable sources. The Rankine technology is introduced and its various applications explored. Additionally, some challenges encountered from the conventional use of fossil fuel reserve for energy production was highlighted. The objectives and scope of this research work were stated in the first chapter as well as the chosen course of action.

Chapter 2 contains an extensive literature review of the subject area. Types of non-renewable and renewable energy resources are discussed. Global energy usage and current trends and their implications on the environment, as well as socio-economic impacts, are discussed. Thermodynamic cycles are critically analyzed with special emphasis on the ORC's working principle, components, and applications. The working fluid characteristics, selection and comparison between different working fluids for ORC application are discussed.

Chapter 3 presents the methodological approach to this research, which included both computer based simulations and laboratory experiments. Individual models for the components of a typical ORC system and the process of heat exchange. Factors which influence heat exchanger performance and also the mathematical model developed for the ORC are also being presented.

Chapter 4 presents and discusses the results of simulation and parametric analysis conducted using the model presented in Chapter Three. The effects of various input parameters on the system performance were also discussed.

Chapter 5 presents the experimental methodology employed in this research. The experimental approach includes cycle description, leak test analysis, refrigerant charging, experimental procedures and experimental results presentation and model validation with experimental results.

Chapter 6 presents the conclusion of this research and provides recommendations on the ORC system for future work.

CHAPTER 2 : LITERATURE REVIEW

2.1 Introduction

The study of thermodynamics in heat, refrigeration and power cycles has intensified in recent years. As a result, this chapter presents the thermodynamic cycle, with the focus on power cycles. Two main types of power cycles, the ideal Rankine cycle, and the ORC, are presented while their various applications as obtained in works of literature are reviewed. The criteria for the selection of working fluid for Rankine cycle are presented with a description of the working fluid refrigerant of choice for the research.

2.2 Thermodynamic Cycle

A thermodynamic cycle is a cycle which comprises a series of thermodynamic processes connected together so that heat and work can be done in the system while state parameters such as temperature and pressure are varied. Being a cycle, the process eventually returns to its original state. Work is done through the conversion of energy from one form to another, but upholding the principle of conservation of energy in accordance with the first law of thermodynamics. The thermodynamic cycle is classified into Power Cycles and Heat/Refrigeration Cycles. This research centers on power generation, hence, Power Cycles only are discussed.

2.2.1 Power Cycles

These cycles convert energy input in the form of heat into a system to mechanical work or/and electrical power outputs. In view of power generation, the cycles considered herein are the ideal (steam) Rankine cycle and the organic Rankine cycle. Some generic novel cycles such as the Kalina cycle, Goswami cycle and Trilateral cycle, Transcritical cycle and Brayton cycle are also discussed.

2.2.1.1 Ideal Rankine Cycle

The Ideal Rankine cycle has the simplest configuration consisting of four stages –compression, heating, expansion, and cooling. Water serves as the working fluid and efficiency is high when operating at a temperature greater than 600^0C [12]. Water is heated by a source to a high temperature and expands as it passes through the turbine causing the turbine blade to rotate. The working fluid loses energy as it exits the turbine and is then further cooled in the condenser.

From the condenser it goes through the pump and back to the heat exchanger where it gains thermal energy and the cycle is repeated. Working fluid alternates between liquid and vapor phase for the Ideal Rankine cycle.

Production and generation of electrical power are achieved in power plants using steam as the working fluid. Solar, hydropower, and biogas among others, are also renewable sources. Kapooria, et al. [13], investigated the operations of a theoretical steam power plant using the Rankine technology. In their comparative investigation between the Carnot cycle and the Rankine cycle systems, the Carnot cycle was made to have a fixed high and low temperatures for the thermal addition and heat rejection. Conversely, the Rankine cycle had heat addition and rejection occurring over a range of temperatures. Consequently, it was observed that the Carnot cycle efficiency is always higher than the Rankine cycle. The irreversibility and mechanical friction which occurs in the Rankine cycle compared to the Carnot cycle makes it less efficient in comparison with the Carnot. Although the Carnot cycle presents better efficiency, its practicability is almost impossible due to factors such as low work ratio, economic considerations among others. Hence, the use of the Rankine cycle in the study was opted for and analysis of more efficient performance was proposed.

Assuming a steady state condition, the efficiency of the Rankine cycle is dependent on the average rate of the heat addition and heat rejection from the source to the evaporator and from the condenser to the sink respectively. The turbine and pump were identified as critical components in improving the efficiency of the Rankine cycle. Reusing the low-pressure steam leaving the turbine to generate more power was explored, hence, the introduction of a second turbine in the cycle. Furthermore, a reheating stage was introduced to allow steam leaving the high-pressure turbine to pass through the low-pressure turbine as shown in Figure 2.1. Other factors such as feed water, heater, and controlling the pressure in the steam condenser, among others, were suggested for further enhancement of the thermal efficiency of the plant [13].

With the introduction of a second stage steam turbine, the efficiency of the cycle was improved. However, depending on the final exit temperature of the steam from the low-pressure turbine, it could serve as a heat source for an ORC in a dual stage cycle thereby producing even more power.

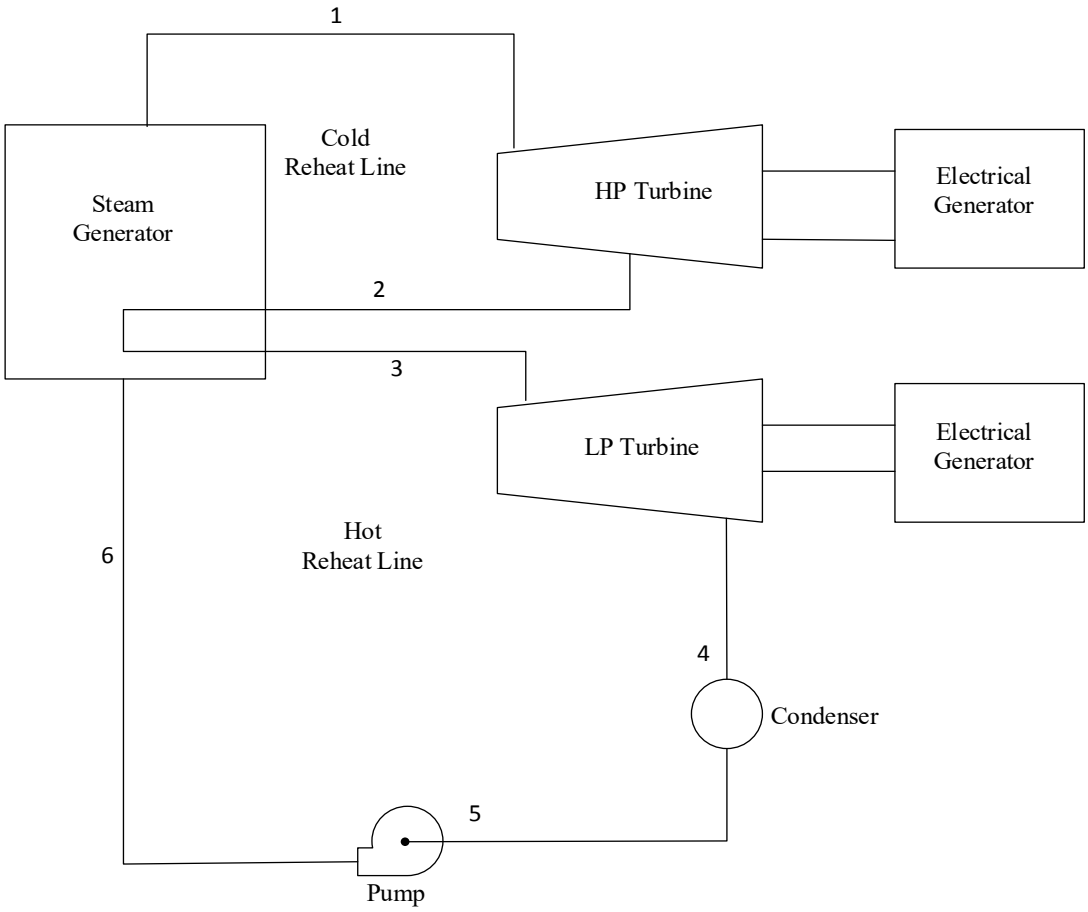

Figure 2.1: Schematic Showing the Reheating Stage and Two Turbines [13]

The Rankine cycle using steam, as is a modified Carnot cycle, has been identified as having limitations in its usage. Quoilin and Lemort [14] identified that the efficiency of the Rankine cycle can be increased by either increasing the mean hot temperature which consists of the evaporating temperature and turbine inlet temperature or reducing the temperature at which the steam condenses. Furthermore, the evaporating temperature can only be increased to a certain limit beyond which the turbine blade characteristics are adversely affected and the fluid quality at the turbine exit decreases below the accepted 0.9 limit. To eliminate the challenges of acceptable fluid quality, a two-stage expansion can be introduced with a heating stage between them. The two stages each consist of turbines (a high-pressure turbine with fluid from the boiler, and a low-pressure turbine with inlet fluid from the high-pressure turbine). With this modification, the overall efficiency of the Rankine cycle is improved. A similar Rankine cycle configuration is seen in [13]. Irreversibility in the Rankine cycle is a major concern in determining the efficiency of the cycle. This is mitigated by including a regeneration process in

the cycle. For a low-grade heat source, however, the steam Rankine cycle falls short compared to the ORC in terms of overall system efficiency.

2.2.1.2 Organic Rankine Cycle

The ORC technology as a bottoming cycle has proven to be a dependable means by which high thermal energy can be converted into power in an efficient manner when utilized in a combined power plant. In evaluating two separate working fluid media, Masheiti, et al. [15] asserted that the low-temperature exhaust from other Rankine cycle processes makes the use of ORCs as a bottoming cycle in a combined configuration highly desirable. The ORC is ideal for temperature ranges between 50^0C and 350^0C and small scale power generation below 50 kW have been reported in [10, 16].

The ORC works on the same principle as the Steam Rankine cycle with the difference being the use of organic compounds as its working fluid rather than steam. The working fluid has a low boiling point and high molecular mass. The ORC has a major advantage over the steam or Brayton cycle in that it can be used to generate power from low thermal heat sources with a temperature below 300^0C. The ORC components are the pump, expander, condenser, and evaporator as shown in Figure 2.2.

For improved efficiency of the ORC, factors such as the heat source temperature, choice of working fluid, expander types are considered. Auxiliary equipment such as the recuperator and regenerator can also be incorporated when necessary as suggested by [17].

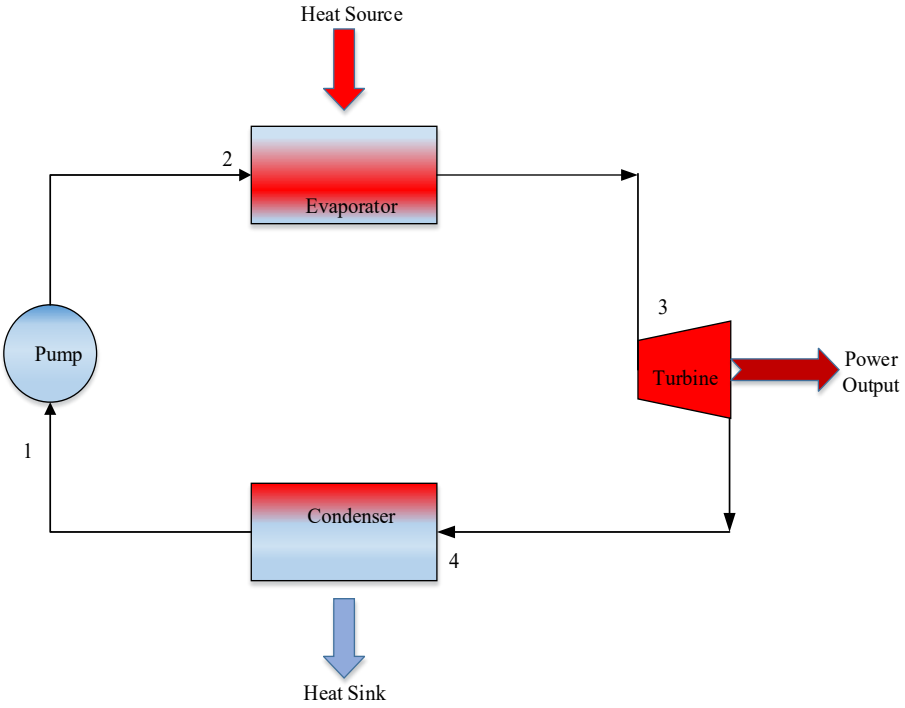

Figure 2.2: Schematic of an Organic Rankine Cycle Process

In addition to the two basic thermodynamic cycles mentioned in section 2.2.1.1 and section 2.2.1.2, various other novel cycles developed by researchers over the years such as the Kalina cycle, the Goswami cycle, the Trilateral cycle, the Brayton cycle and the Transcritical (CO_2) cycle are hereby discussed.

2.2.1.3 Kalina Cycle

This power cycle was developed in 1970 by Aleksander Kalina and is commonly used in recovery and conversion of thermal energy from low-grade heat sources to produce electrical power. The Kalina cycle has a design configuration different from the conventional Rankine cycle and requires supplementary equipment such as a separator and intermediate heat exchangers [18]. Another unique characteristic of the cycle is the use of a mixture of ammonia and water as a working fluid. This proves advantageous as it provides variation in boiling and condensing temperature thereby minimizing exergy destruction [19]. Also, the mixture as a working fluid helps in increasing the cycle efficiency and decreasing the thermodynamic irreversibility [20]. Zhang, et al. [21] proposed an integrated system of Ammonia-Water Kalina Rankine cycle for power generation as well as for central heating purposes. They submitted that the advantages of ammonia-water cycle and the Kalina Rankine cycle can be capitalized upon when both cycles are combined. At a heat source temperature of 300^0C, the turbine outlet

temperatures for the Kalina and Rankine cycles in the research work were found to be 83.75^{0}C and 117.15^{0}C while their thermal efficiency was 20.85% and 17.09% respectively. The huge difference in the temperature during evaporation for both the Kalina and Rankine cycle and also the high-temperature difference in condensation for Rankine cycle makes the integrated cycles suitable to generate heating water as a by-product for domestic application. The ORC with a refrigerant of sub-zero boiling temperature can use the hot water temperature from the system presented by [21] as its heat source producing a higher thermal efficiency of the entire system while also increasing power output. Theoretically, it has been shown that the Kalina cycle has a conversion rate of up to 45% of heat input into electricity, hence, a relatively higher efficiency level. Additionally, approximately 32% more power can be generated from waste heat application using the Kalina cycle in comparison to the conventional Steam Rankine cycle [22]. Although the Kalina cycle has a cycle configuration similar to the Ideal Rankine cycle, it possesses an additional degree of freedom than the Ideal Rankine cycle, and the variation in the ratio of ammonia-water all through the cycle process also influences the cycle's thermodynamic performance [22]. As stated earlier, the Kalina cycle produces higher efficiency which results from the close proximity in temperature between the cycle heat and the source heat [23]. The ratio of the composition of ammonia-water determines, to a large extent, the boiling and condensation temperature of the mixture which also contributes to its high efficiency. Hence, there is no fixed temperature point for the mixture. The more the amount of ammonia there is in the mixture, the lower the boiling point of the mixture. Figure 2.3 shows the cycle process in the Kalina cycle in which constant heat is transferred to the NH_3-H_2O working fluid mixture from a low-temperature renewable source. This increases the temperature of the working fluid and as the evaporation starts to occur, ammonia which has a lower boiling point compared to water starts to vaporize first. Before inlet of the working fluid mixture into the turbine, the vapor which contains a large concentration of ammonia is separated in a separator from the liquid phase after which it goes through the turbine. The turbine coupled with a generator then produces electricity. On exit from the turbine, the ammonia-rich fluid mixes with the initially separated low ammonia concentration fluid and undergoes condensation in the condenser. From the condenser, the working fluid mixture is pumped through a heat recuperator, which enhances the cycle efficiency, and then through the evaporator thereby repeating the cycle [24].

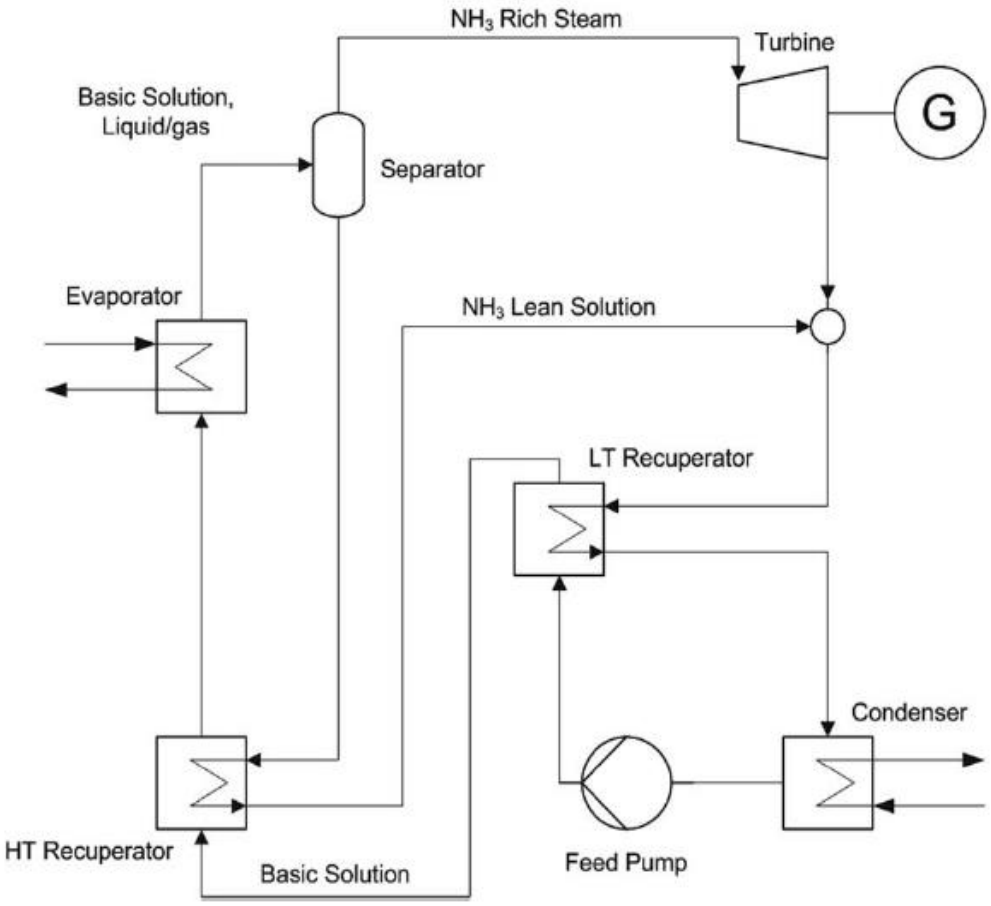

Figure 2.3: Diagrammatic Process of Kalina Cycle [24]

2.2.1.4 Goswami Cycle

The Goswami cycle was first proposed in the 1990s and is characterized by improved energy conversion and a considerable decrease in energy cost [25]. The Goswami cycle is a heat and power cycle combined. Like the Kalina cycle, the Goswami cycle uses a mixed working fluid of ammonia-water for its operation and possesses improved overall energy conversion efficiency. Ammonia and water are soluble in each other and can also be easily separated [26]. Various research work has been conducted, and indeed is still been conducted, to study the characteristics and advantages of a multi-component fluid mixture as seen in the Kalina and Goswami cycles, compared to single component fluid as is the case in the Ideal Rankine cycle. Comparative study shows significant improvement of 10-20% in the thermal efficiency of the mixed component working fluid [27]. The Goswami cycle, which is a more recent developed cycle, combines the refrigeration and Rankine cycle into one cycle. It improves on the shortfalls

of the Kalina cycle by replacing the usual process of condensation used by Kalina cycle which limits the lowest temperature of working that exists in the turbine with an absorption condensation process, while retaining the Kalina cycle's advantages. For low thermal sources like solar collectors, Xu, et al. [27] submitted that the use of NH_3/H_20 as a working fluid limits the thermal transfer irreversibility. The high concentration of ammonia in the turbine during operation allows for expansion of the ammonia vapor without being condensed. Power is therefore generated when the vapor drives the turbine and refrigeration occurs simultaneously as the ammonia temperature becomes very low.

2.2.1.5 Trilateral Cycle

The Trilateral cycle is a power cycle in which expansion of the working fluid at the turbine is at a saturated liquid phase instead of a saturated vapor phase [19, 20]. At the expander outlet, there is a two-phase working fluid mixture. The system comprises the following components: the two-phase turbine, the condenser, pump and the heater. The Trilateral cycle is such that the saturated liquid which is at a low pressure coming from the condenser exit, is pumped to the heater. This raises the liquid's temperature and also the pressure entering the turbine where it expands and drives the turbine. The liquid leaving the expander drops in temperature and pressure and condenses in the condenser and the cycle is repeated. Figure 2.4 shows the TLC process cycle. The thermal efficiency of the Trilateral cycle is relatively lower than the ORC because of the lower temperature at which heat is transferred to the working fluid [19]. A simplified schematic diagram of the trilateral cycle and its corresponding T-s diagram is shown in Figure 2.4.

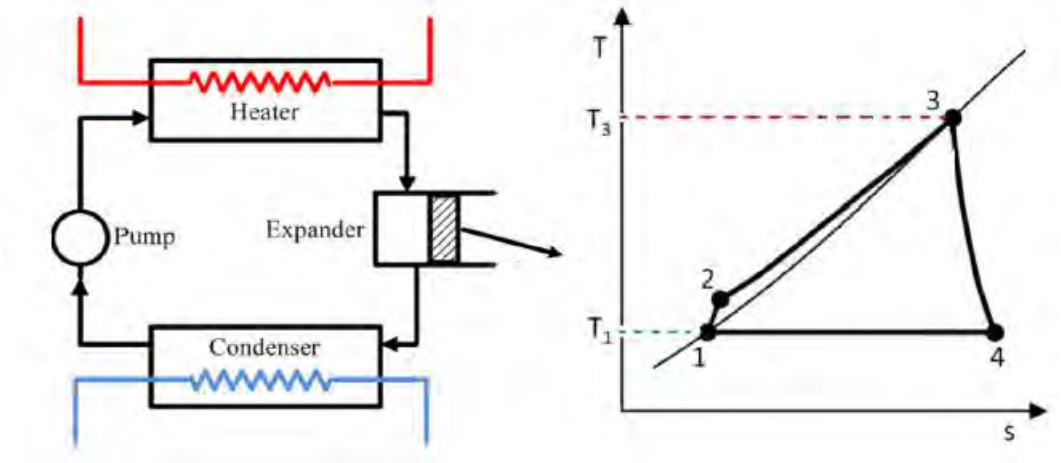

Figure 2.4: Schematic Diagram for Trilateral Cycle (TLC) and Corresponding T-s Diagram [19]

The advantage of the Trilateral cycle is avoidance of boiling part of the thermodynamic cycle and the decrease in irreversibility. On the flip side, the lack of appropriate expander to handle a two-phase mixture working fluid poses a drawback to the wide usage of this cycle [20]. Yari, et al. [19] argued that should the isentropic efficiency of the Trilateral cycle be close to a regular turbine it could prove advantageous thermodynamically in comparison to other cycles. However, its main credit over other cycles in thermal efficiency is the close temperature matching of the heat source and fluid inlet temperature which increases the net power output of the cycle. Furthermore, with a medium thermal source of a temperature of 150^0C as inlet temperature, using water and propane as working fluids for a Trilateral cycle and ORC respectively, Fischer [28] demonstrated that the exergy efficiency of the TLC compared to the ORC in power production is higher by 29%.

2.2.1.6 Transcritical (CO_2) power cycle

The Transcritical (CO_2) cycle has a similarity with the Kalina cycle in that the change in phase of the working fluid occurs over a range of temperatures. Enthalpy transfer within the working fluid of the Transcritical cycle is enhanced compared to other working fluid media. Li [29] stated that although power production of the Transcritical cycle is greater than the ORC, the dual phase properties of the working fluid in the cycle poses challenges in the design and development of an appropriate cycle expander. However, with new feats attained, designs of suitable turbine blades to handle multi-phased working fluid are available today making the use of the Transcritical cycle more realistic and viable in renewable energy production.

2.2.1.7 Brayton Cycle

The Brayton cycle has a configuration similar to the Rankine cycle but differs on a number of things such as having its working fluid remains in vapor state without phase change all through the process [12]. Depending on the component of steam and material used in the Steam Rankine cycle, the thermal efficiency obtained from the Steam Rankine cycle compared to the Brayton cycle is higher at a temperature range of about 600^0C. Above 600^0C the Brayton cycle with CO_2 recompression offers a higher thermal efficiency. Dunham and Iverson [12] argue that at 30 MPa and temperature greater than 1000^0C the Brayton cycle could attain up to 60% thermal efficiency. Due to the high temperature of the fluid leaving the turbine at 1146^0C, the Brayton cycle can be made to operate as a topping cycle serving as a source of heat for an ORC in a dual cycle arrangement, hence, improving the overall thermal efficiency. The Brayton cycle using superheated carbon dioxide as its working fluid has the advantage of zero toxicity and also non-

flammability. Aside from the fact that CO_2 is abundant in nature, it also possesses desirable thermodynamic properties such as a good work-to-expansion ratio [30].

2.3 The Organic Rankine Cycle and Applications

The ORC technology has been well researched as a viable method of power generation from low thermal sources. It has found usefulness in various applications either as a sole system or in combined systems. Various applications where ORC has been used are presented in sub–section 2.3.1 to sub-section 2.3.4, bearing in mind that the use of ORCs are not limited to these applications.

2.3.1 Waste Heat Recovery Application

The sources of waste heat can be manufacturing industries, plants and also municipal solid waste. Many types of research have been carried out on the waste heat recovery application of the ORC technology [6, 8, 31]. However, the limitation for the ORC application for heat recovery becomes pronounced when the temperature exceeds 300^0C. Hence, to effectively recover this grade of heat, Zhang, et al. [32] proposed combined systems techniques which involved a combination of different Rankine cycles with the ORC in a two-stage setup as opposed to the prevalent single stage Rankine systems. The work compared three different systems, each having the ORC as a bottoming cycle. The systems compared are the Dual-loop Organic Rankine Cycle (DORC) which had a steam cycle combined with the organic cycle, the CO_2 Brayton-ORC (BC-ORC) and the Thermo-electric Generator Organic Rankine Cycle (TEG-ORC). Performance indicators compared among the three systems are the net power generated, thermal recovery and also the exergy efficiency. With the same system operating parameter for all three combined systems under investigation, the overall net power produced by the DORC was the highest with 32.63 kW. Furthermore, efficiencies of 26.55%, 23.04%, and 19.14% were observed for DORC, BC-ORC and TEG-ORC respectively. The use of ORC as a bottoming cycle in each of the combined system presented by Zhang, et al. [32] reiterates its distinctiveness in harnessing low thermal energy for power generation either in combined systems or in a single stage system as presented in this thesis.

David, et al. [33] proposed constructing an ORC system which would utilize waste heat from a capstone gas turbine engine as its heat source. The thermal capacity of the waste heat source is 90 kW with a temperature of 220^0C. The flowrate of the waste heat is at 0.3 kg/s. A model was developed to determine the performance of the proposed system. It was found that using R-

245fa as refrigerant at a pressure of 0.695 MPa and a flowrate of 0.06 kg/s, and having an evaporation and condensation temperature of 80^0C and 30^0C, an efficiency of 5.7% and a net power output of 2.2 kW was obtained.

Minea [10] examined the efficiency, reliability and feasibility of a prototype laboratory 50 kW ORC prototype machine in converting heat from a renewable source to electricity. The ORC prototype was designed and built and the heat source for the system was simulated by a boiler to produce hot water with temperature ranging from 85^0C to 125^0C. An organic fluid pump range of 0 Hz to 60 Hz was adopted for the setup. The thermodynamic performance of the prototype machine was adequately monitored through the use of transmission systems. The result obtained showed that the overall cycle performance is dependent on the temperature lift of the system. The higher the lift, the higher the network output of the system. With the heat source temperature ranging from 85^0C to 125^0C and heat sink temperature ranging from 15^0C to 30^0C, the ORC produced a power output of between 22.3 kW and 39.9 kW. The efficiency of conversion of heat to electricity varied from 6.62% to 7.57%. This, however, can be increased to 10% higher with a heat source temperature over 116^0C.

2.3.2 Geothermal Applications

Due to its reliability and independence on climatic or weather conditions, a geothermal source is regarded as a much more dependable renewable energy source for continuous and constant energy supply compared to other sources such as solar, wind or biomass. Several works of literature exist on geothermal applications of the ORC using different fluid media while varying several factors to enhance power output. Masheiti, et al. [15] presented a comparative study of a geothermal powered ORC system using two different organic fluids – R-134a and R-245fa. The heat source (73^0C) and sink (25^0C) for his work was adopted from the Al-Jufrah region of Libya while IPSEpro simulation tool was used for the process. The performance of two different organic fluids was analyzed under the same prefixed working parameters. The result of the simulation shows that R-245fa produced a more desirable system output in comparison to R-134a. The pump power consumption for ORC system with R134a was significantly greater than R-245fa. Furthermore, the higher pinch temperature obtained with R-245fa compared to R-134a makes it a more desirable refrigerant for the simulated ORC system. The work of Zyhowski, et al. [34] also lends support to the use of R-245fa as organic working fluid for ORC, albeit, waste heat recovery was used as heat source in his work. A further sensitivity analysis shows the effect of increasing source temperature on performance such as net power, turbine pressure drop

and efficiency of the ORC system. Masheiti, et al. [15], reported that performance of the ORC system is largely dependent on the condenser unit of the system.

Potentials for geothermal application of ORC has been a source of interest for energy research in South Africa. Taufeeq Dhansay, et al. [35] examined the feasibility of power generation from heat energy obtained from thermal springs with temperatures reaching 343 K in the Limpopo region. In his estimation, using an enhanced geothermal system (EGS), the region is capable of producing a 75 MW power in a 30 years period.

2.3.3 Biomass Applications

The system presented by Qiu, et al. [7] is a combined heat and power system. This simultaneously produces electrical power while also generating heated water which can be used for domestic purposes. The heat source adapted for the ORC was a 50 kW biomass boiler and working fluid selected was HFE 7000 while the system power output was expected at 1 kW. The outcome of the investigation showed that only 860.7 W of electricity was produced at source temperature (water from biomass boiler) of 128.9^0C and the pump capacity of ORC being kept at the maximum. Qiu, et al. [7] reported that the ORC efficiency obtained was 3.78% and could be improved upon with improvement in evaporator temperature. Though the power efficiency of 1.41% for the model presented is comparatively low, the combined heat and power efficiency of 78.69% is laudable. This leaves the cooling water from the condenser at a moderately heated temperature suitable for domestic heating.

2.3.4 Solar Applications

The ORC has also found application using solar irradiation as its thermal source. In harnessing the sun's thermal energy, flat and concentrated type solar panels have been used. However, the mode of application is a deciding factor as to which type of collector is employed [36]. Other types of solar collector used for solar ORC application are the evacuated tube solar collector. A comparison made between the evacuated tube and the flat plate collectors for the ORC using R-245fa reported a better efficiency in the power output for evacuated tube compared to flat plate collectors [37].

2.4 Working Fluid Selection for Organic Rankine Cycle Power Production

For an ORC to produce electricity, it has need of fluid which will drive the turbine for the power to be generated. This fluid is often referred to as "Working Fluid". It is organic in nature, hence,

the name organic Rankine cycle. Determination of appropriate working fluid for a particular ORC system is determined by various factors among which are the type of turbine, heat source, heat sink and expected output (power) of the system. Selection of the proper working fluid for an ORC application has an overall effect on the total energy/system efficiency, the impact on the environment and condition of operation among others.

2.4.1 Types of Working Fluids

Working fluids used for the ORC systems can either be single component working fluid substances or multicomponent working fluid substances.

2.4.1.1 Single Component Working Fluids

Li [29], analyzed the effects of temperature and pressure on three different pure refrigerants used as working fluids for an organic Rankine cycle for solar application. The system's estimated output lies between 5 kW to 1 MW. A recuperator was added after the turbine to improve the system's overall efficiency. Refrigerants R-245fa, R-123and R-113 were studied independently with mono-ethylene glycol as the heat transfer fluid. With predetermined operating pressures for each fluid, it is reported that the thermal efficiency of the cycle increased with every 5^0C increase above each fluid's saturated temperature, with the exception of R-245fa at operating pressure of 800 kPa. R-113 was reported to yield the highest efficiency of the three fluids examined due to the little temperature difference between its saturated point and temperature at the evaporator inlet. Other works of literature such as [15, 38] among others, have documented the use of single component working fluid medium for various organic Rankine cycle applications.

2.4.1.2 Multicomponent Working Fluids

Two component fluids when used as a working fluid medium in an organic Rankine cycle, do so by complimenting the demerits of the other. The ratio of mixture between the components fluids involved to obtain the suitable working fluid combination is essential in determining the overall efficiency of the organic cycle [39]. This idea was reinforced by Garg, et al. [40] using the combination of iso-pentane and R-245fa in the ratio of 70/30 as a working fluid medium for ORC application. It was established that with the expansion ratio at the turbine kept between 7 and 10, the mixture produces better a performance as working fluid than would either individual component.

2.4.2 Working Fluid Selection Criteria

A major element in the operation of the ORC is the kind of refrigerant being used as its working fluid. The selection of this refrigerant determines the overall efficiency of the cycle in terms of either cost or generated power or both. Below are some of the criteria which need to be considered prior to selection of a suitable working fluid for ORC purposes.

2.4.2.1 Thermal Stability

Thermal stability is the potential of a substance to remain unchanged chemically during temperature change. The working fluid must possess a good thermal stability. It must be able to maintain its chemical integrity in cases of changes in temperature. When working fluid is not thermally stable, it tends to decompose easily and might require frequent replacement. This is undesirable as it decreases the overall efficiency of the ORC system. Chemical decomposition of the working fluid due to thermal instability also produce gasses which do not condense and can be of adverse effect on components of the ORC system [41]. Maximum working temperature of the system is determined by the chemical stability that the working fluid possesses, viz, the thermal stability of the selected working fluid must be considered when the working temperature of the ORC is to be determined or vice versa. Water does not suffer chemical decomposition when used as the working fluid [42].

2.4.2.2 Critical Properties/Points

The point on the Temperature-Entropy (T-s) curve whereby there is absolutely no distinguishable difference between the properties of a working fluid either in the liquid or gaseous state is referred to as the critical point. The fluid composition, its density and temperature at either phase, liquid or gas are the unchanged [41]. The peak point of the T-s diagram indicates this critical point. This point indicates the appropriate region of temperature at which the working fluid is optimally operating [42]. This is an important parameter in fluid selection.

2.4.2.3 Fluid Molecular Weight

The intended output for the ORC in terms of power produced and temperature worked at informs the selection of the fluid used for the system. The turbine for the ORC is also taken into consideration. From literature, for a high working temperature or high power output requirement using a multi-stage turbine, a working fluid with low molecular weight is

appropriate. Conversely, a high molecular weight working fluid is appropriate when low power output is desired [41]. During the expansion of fluid in the turbine, the working fluid with a heavy molecular mass would produce a slight decrease in enthalpy which is advantageous to the system operation but will result in a poor coefficient of heat transfer which is undesirable [43].

2.4.2.4 Fluid-Material Compatibility

The compatibility of a working fluid with the materials of the ORC system it comes in contact with and also the lubricating oil used (where applicable), is of utmost importance. Contact of fluid with materials should in no way adversely affect the system materials or the overall system efficiency. Working fluid that might facilitates corrosion of any section of the system should be avoided [41, 42]. Chen, et al. [42] reported a method presented by Anderson and Bruno in their work "Rapid screening of fluids for chemical stability in Organic Rankine Cycle application", which helps in determining how chemically stable a working fluid is using testing techniques like the ample technique. Basically, this method allows us to know how fast (or maybe slow) a working fluid decomposes while the working pressure and temperature are being varied.

2.4.2.5 System Performance

Another factor to consider is the system performance. Consequently, in selection of a good working fluid, the system performance of the ORC must be carefully considered. The quickest way to do this is by simulation of the system with the aid of a computer program and supplying the parameters of the fluid properties required [41].

2.4.2.6 Safety

The ORC working fluid must be one which is relatively safe to handle and possesses little or no hazard to the operator (and system as well). Due to the high level of toxicity, flammability and high corrosive tendency, some fluids are deemed inappropriate for the use of ORC operation. Inasmuch as these above listed criteria of non-toxicity, non-flammability and minimal corrosive tendency is desired, they are not always of critical importance as their effect or prevention , as the case may be, can always be safely handled [42]. The American Society of Heating, Refrigerating, and Air-Conditioning Engineers (ASHRAE) safety classification for refrigerant is used in the classification of ORC working fluid. The classification is governed by two key factors: the flammability level and the toxicity level of the fluid. These factors are further

divided into sub-factors: toxicity is divided into two sub-factors A and B, while flammability is divided into three sub-factors 1, 2 and 3.

- Toxicity **A**: Non-toxic
- Toxicity **B**: Toxic
- Flammability **1**: No Flammability Propagation
- Flammability **2**: Low Flammability Limit
- Flammability **3**: High Flammability Limit

By deduction, it is safe to say that the organic working fluid with the indices **A1** would possess the most appropriate combination as regards the two factors considered by American Society of Heating, Refrigerating, and Air-Conditioning Engineers (ASHRAE), namely, toxicity and flammability [41].

2.4.2.7 Environmental Consideration and Ethics

As the awareness level for the earth's environmental safety reaches an all-time high, consideration is being given to the effect of working fluid on the environment in ORC applications. In so doing, factors such as Ozone Depletion Potential (ODP), Atmospheric Life Time (ALT), and Global Warming Potential (GWP) of the chosen refrigerant(s) are examined. If the earth is going to be preserved and the rate of depletion of the ozone minimized, it is imperative that the engineer selects a working fluid for the ORC for which the above-mentioned considerations, i.e. ODP, ALT, and GWP are kept to the barest minimum. A fluid which will meet these criteria, as well as others, would be considered ideal organic working fluid [41, 42]. In the past various working fluids with desirable qualities have been used for many operations without proper attention being paid to their negative effect on the environment until Roland and Molina postulated that the chlorofluorocarbons (CFCs) contents of some refrigerants being used remain unchanged, and on reaching the stratosphere, release chlorine atoms as a result of the sun's intense radiation. These chlorine atoms, in turn, destroy the ozone layer thereby endangering living things through direct exposure to the sun's ultra-violet rays. Consequently, these organic compounds were prohibited [41]. Other substances like R-21, R-22, R-123, R-124, R-141b, and R-142b will also be banned come year 2020 or 2030. There is on-going work aimed at finding suitable replacements for these refrigerants which will have lesser harmful effect on the environment without the desired properties of the fluid being compromised [42].

2.4.2.8 Accessibility and Cost Factors

Needless to say, the overall cost effectiveness of the ORC system is relevant. How easy is it to produce or obtain the fluid? What is the cost of one unit mass of the fluid? These questions need to be carefully considered before the eventual selection of the fluid [41].

It is worth noting that it is near impossible to have a working fluid which will adequately satisfy all the above-stated factors. Hence, choice of the working fluid comes down to which of the properties is most desired and which fluid best meets these properties [43].

2.5 The Choice of R-134a as Working Fluid

The Hydrofluorocarbon (HFC) group of refrigerant has been extensively used as substitutes for the Chlorofluorocarbon (CFCs) and Hydrochlorofluorocarbons (HCFCs) refrigerants due to the negative effects of the latter on the ozone layer. The refrigerant 1,1,1,2-Tetrafluoroethane (R-134a) with chemical formula CF_3CH_2F, belongs to the family of Hydrofluorocarbon (HFC) refrigerants. The choice, however, of R-134a as the working fluid for this research, other than being an alternate substitute as recommended by the ORC IT10 supplier, was informed by some of the refrigerant's desirable qualities such as safety, zero ODP and considerably minimal GWP. The thermodynamic properties of the R-134a are presented in Table 2.1.

Table 2.1: Properties of R-134a

Property (Units)	**R-134a**
Molecular mass (kg/kmol)	102
Critical temperature (^{0}C)	101
Critical Pressure (MPa)	4.1
Latent heat of vaporization at 1 atm (kJ/kg)	217.2
Boiling temperature at 1 atm (^{0}C)	26.4
Safety	Non-flammable
Atmospheric Lifetime (years)	14
ASHRAE level of safety	A1
Ozone Depletion Potential	≈0
Net Greenhouse Warming Potential (100 years)	1430

2.6 Summary

This review has shown the principles of thermodynamics, the various thermodynamic cycles available today as well as their various applications in energy and power generation. Various novel cycles have also been presented. A critical aspect in the use of the ORC technology in harnessing energy from a low-grade source is the choice of the working fluid refrigerant; consequently, the criteria for the selection of the working fluid have also been presented.

CHAPTER 3 : RESEARCH METHODOLOGY

3.1 Introduction

The research methodology adopted in this work is in two parts: the first part is the modelling of an ORC thermodynamic system which is followed by simulation of the results obtained. The model is then validated by using experimental variables obtained from literature and comparing the results obtained with those found in literature. The second part of the research is a laboratory investigation on an IT10 Infinity Turbine ORC system and presentation of experimental outcomes. This is presented in Chapter 5.

3.2 Modelling of ORC System Components

The ORC comprises four main components which are evaporator, condenser, refrigerant circulation pump and expander. The individual components of the ORC system drive the four processes observed in the ORC operation. The model of the ORC components is presented in Sections 3.2.1 to 3.2.4.

3.2.1 The Pump Model

The cycle process begins at the pump with the refrigerant undergoing an isentropic compression without any significant change in its temperature. There is no additional heat loss or gain across this unit. The choice of the appropriate pump to use in an ORC system is dependent on the type of refrigerant used as a working fluid medium and also the pump pressure required to circulate the fluid [44]. Additional factors that influence pump selection are the arrangement of the plant, properties of the refrigerant and the operating temperature of the cycle. Although the pump work can be neglected in the operation of the steam turbine, its operation is taken into account in evaluating the net power output by the ORC, albeit its efficiency is often assumed [44]. Increase in the heat transfer within the system would lead to an increase in the work output at the turbine. However, the cost of operation for a system with high boiler pressure sets the limit to the extent to which the boiler pressure can continually be increased. The ratio of the power produced at the turbine and which is consumed by the pump is known as the back-work-ratio (BWR) [45]. It can be used in determining the performance of the cycle. The lower the BWR at the pump, the higher the performance of the cycle. The energy balance across the pump is given as shown in Equation 3.1

$$\frac{\dot{W}_p}{\dot{m}_c} = h_{[1]} - h_{[4]} \quad (3.1)$$

Where $h_{[1]}$ and $h_{[4]}$ are enthalpies of the refrigerant at states 1 and 4 respectively, $\dot{W}_p$ represents pump work and $\dot{m}_c$ represents the mass flow of refrigerant. Figure 3.1 shows the state point 1 of the ORC cycle as the refrigerant exits from the pump into the evaporator.

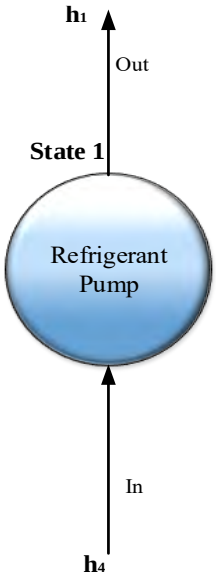

Figure 3.1: State Point 1 at the Pump Exit

3.2.2 The Evaporator Model

The evaporator is one of the heat exchanger components of the organic Rankine cycle used. It is at state 2 of the cycle. The heat transfer fluid from the heat source transfers its energy to the refrigerant in the evaporator / boiler. The working fluid temperature is raised thereby gaining energy as it goes into the turbine. Conversely, the heat transfer fluid loses energy and is returned to the heat source to be reheated. The process of heat exchange in the evaporator occurs under constant pressure supplied by the pump. The energy balance across the evaporator is given by Equation 3.2.

$$\frac{\dot{Q}_b}{\dot{m}_c} = h_{[2]} - h_{[1]} \quad (3.2)$$

Where $h_{[1]}$ and $h_{[2]}$ are enthalpies of the refrigerant across the evaporator unit, $\dot{Q}_b$ is heat across the evaporator unit and $\dot{m}_c$ represents the mass flow of refrigerant. Figure 3.2 shows the state point 2 of the ORC cycle as the refrigerant exits from the evaporator into the turbine.

Figure 3.2: State Point 2 at the Evaporator Exit

3.2.3 The Turbine Model

Also known as the "expander", the turbine, coupled with an alternator converts mechanical energy/power into electrical energy/power. The mechanical energy is as a result of the rotational motion generated by the impact of the working fluid on its blades. At the turbine, the working fluid undergoes an isentropic expansion. The output of the turbine is given at state 3 of the cycle. Furthermore, due to expansion, heat losses occur leading to a temperature difference of the working fluid between the points of entry and exit into and from the turbine. Pressure losses are also observed at the turbine. The energy balance across the turbine is given by Equation 3.3.

$$\frac{\dot{W}_t}{\dot{m}_c} = h_{[2]} - h_{[3]} \tag{3.3}$$

Where $\dot{W}_t$ the turbine is work, $h_{[2]}$ and $h_{[3]}$ are enthalpies of the refrigerant across the turbine unit, and $\dot{m}_c$ represents the mass flow of refrigerant. Figure 3.3 shows the state point 3 of the ORC cycle as the refrigerant exits from the turbine into the condenser.

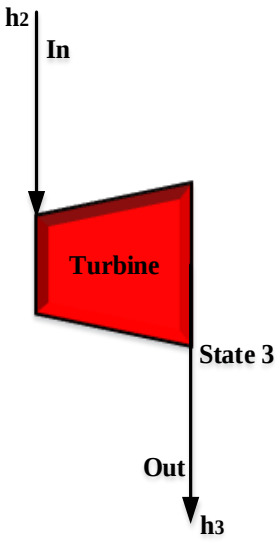

Figure 3.3: State Point 3 at the Turbine Exit

3.2.4 The Condenser Model

The condenser is the second heat exchanger unit in the system and is at state 4 of the process. After the expansion process in the turbine, the working fluid is depleted of heat energy and pressure. It then moves to the condenser where a further cooling of the temperature occurs returning the working fluid to its starting temperature. This process is aided by the transference of heat from the refrigerant to a cooling fluid medium from a cooling sink. The cooling, or heat rejection, process occurs with no significant change in the pressure of the working fluid. The energy balance across this unit is given by Equation 3.4.

$$\frac{\dot{Q}_{cond}}{\dot{m}_c} = h_{[3]} - h_{[4]} \tag{3.4}$$

Where $\dot{Q}_{cond}$ is the heat across the condenser, $h_{[3]}$ and $h_{[4]}$ are enthalpies of the refrigerant across the condenser unit, and $\dot{m}_c$ represents the mass flow of refrigerant. The state point 4 of the ORC cycle as the refrigerant exit from the condenser into the pump is shown in Figure 3.4.

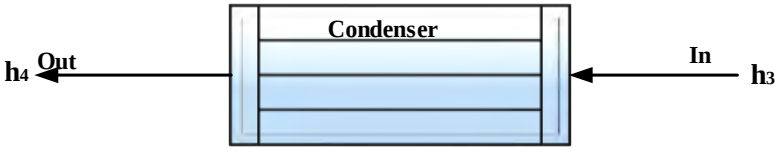

Figure 3.4: State Point 4 at the Condenser Exit

3.3 Process of Heat Exchange in the Evaporator

An ideal ORC configuration consist of two exchangers which are the evaporator and the condenser. The evaporator heat exchanger is where the transfer of heat energy from the heat transfer fluid to the working fluid medium occurs. Some ORC circle configurations may consist of additional heat exchangers such as the regenerator or the recuperator [23, 28]. Depending on the flow arrangement and the construction, heat exchangers are classified into three broad categories: the parallel flow, the counter-flow, and the cross flow as shown in Figure 3.5 to Figure 3.7. Furthermore, the fluids in the heat exchanger can either be mixed or unmixed. This plays an important role in determining the performance or effectiveness of the heat exchanger [46].

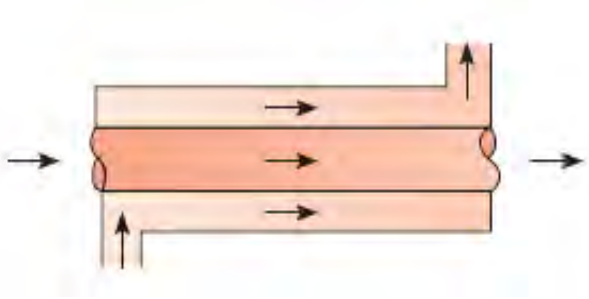

Figure 3.5 Parallel Flow Pattern [46]

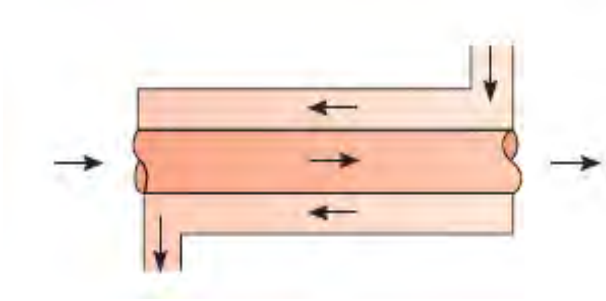

Figure 3.6 Counter Flow Pattern [46]

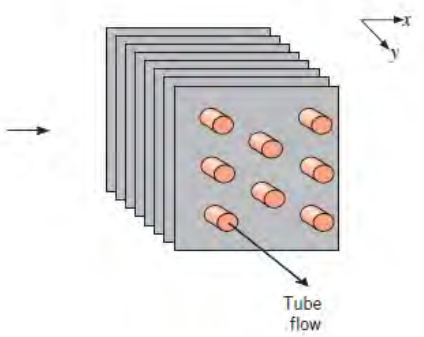

Figure 3.7: Cross flow Pattern [46]

Other heat exchanger types are the shell-and-tube with single or multiple passes and also the compact type heat exchangers with single or multiple passes as seen in Figure 3.8 and Figure 3.9 respectively

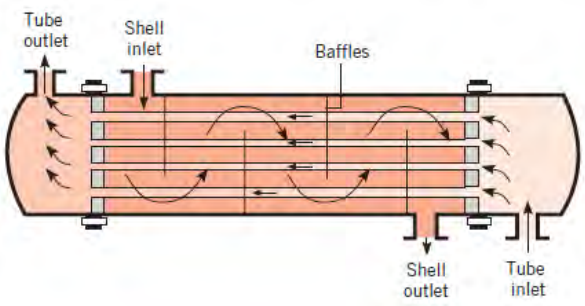

Figure 3.8: Shell and Tube Exchanger [46]

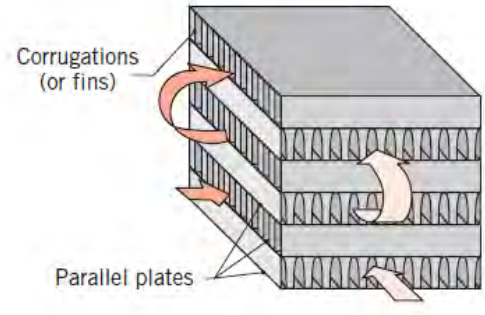

Figure 3.9: Compact Type Heat Exchangers [46]

3.3.1 Factors Influencing Heat Exchangers Performance

The overall performance of the heat exchanger in the transference of heat energy between fluids in the heat exchanger is dependent on factors such as the heat transfer surface area (A), the overall heat transfer coefficient (U), the Number of Transfer Units (NTU) among others. One prominent factor which determines the performance of heat exchange is the Fouling resistance, R_f. The Fouling resistance effect is a form of thermal resistance within the heat exchanger which arises as a result of impurities and rust along the heat transfer surface area of the heat exchanger. This prevents total heat transfer between the fluids within the exchanger.

3.3.2 Design Model for Evaporator Heat Exchanger

An evaporator heat exchanger model was developed to determine the quantity of heat exchange between the heat transfer fluid and the working fluid and also determine the exit temperatures of both fluids from the evaporator. It is imperative to bear in mind that the heat source for the ORC operation is a hot water geyser which represents the operation of a real life geothermal hot water source. Furthermore, the heat transfer fluid is water kept at a temperature of 80^0C.

The heat exchanger model was developed using the equations presented in Equations 3.5 to Equations 3.16. The heat transfer surface area was calculated using the geometry of the unit. Mass flow rates of the fluids required to obtain desired outputs were also determined. The evaporator effectiveness (ε) was determined as a function of the number of heat transfer units (NTU) and the heat capacity ratio (C_r) between both fluids, while the calculated value of 851.2 W/m^2K for the heat transfer coefficient (U) of the evaporator was adapted from [47]. The overall heat transfer coefficient is the inverse of the total resistance to thermal flow between fluids within the heat exchanger.

In developing this heat exchanger model, the following listed basic thermodynamic assumptions were made:

i. No heat loss to the surrounding from the system or connecting hoses.
ii. Thermal exchange within the heat exchanger unit occurs at steady state.
iii. The total heat transfer surface area (A) was taken to be 1 m^2.
iv. The mass flow rates of the refrigerant and the heat transfer fluid were taken as 0.4778 kg/s and 5.833 kg/s respectively.
v. Pump pressure of the refrigerant and the heat transfer fluid were 2.46 MPa and 1.6 MPa respectively.

The specific heat capacity at constant pressure of the hot and cold fluid media is represented by Equations 3.5 and 3.6 respectively.

$$c_{p,c} = c_p(F\$, T = T_{c,in}, P = P_{c,in}) \tag{3.5}$$

$$c_{p,h} = c_p(water, T = T_{h,in}, P = P_{h,in}) \tag{3.6}$$

$$\left.\begin{matrix} C_h = \dot{m}_h c_{p,h} \\ C_c = \dot{m}_c c_{p,c} \end{matrix}\right\} C_{min,max} \tag{3.7}$$

Where C_h and C_c signify the Heat Capacities of the HTF and WF while their mass flow rates are denoted with $\dot{m}_h$ and $\dot{m}_c$ respectively. $T_{c,in}$ and $T_{h,in}$ are the inlet temperatures of WF (refrigerant) and HTF (water) respectively into the evaporator unit. The minimum capacity C_{min} is the lesser of the value between C_h and C_c while C_{min} is the greater value. The heat capacity ratio is given by C_r.

$$C_r = \frac{C_{min}}{C_{max}} \tag{3.8}$$

$$NTU = \frac{UA}{C_{min}} \tag{3.9}$$

$$\varepsilon = f(NTU, C_r) \tag{3.10}$$

$$q_{max} = C_{min}\left(T_{h,in} - T_{c,in}\right) \tag{3.11}$$

If $C_r < 1$, then

$$\varepsilon = \frac{1 - e^{[-NTU(1-C_r)]}}{1 - C_r e^{[-NTU(1-C_r)]}} \tag{3.12}$$

If $C_r = 1$, then

$$\varepsilon = \frac{NTU}{1 + NTU} \tag{3.13}$$

$$q = \varepsilon . q_{max} \tag{3.14}$$

Where q represents the heat transfer between the fluids within the exchanger and ε is the heat exchanger effectiveness

$$T_{h,out} = T_{h,in} - \frac{q}{\dot{m}_h c_{p,h}} \tag{3.15}$$

$$T_{c,out} = T_{c,in} + \frac{q}{\dot{m}_c c_{p,c}} \tag{3.16}$$

The Equations 3.15 and 3.16 give the exit temperatures of the Heat Transfer Fluid, $T_{h,out}$ and the refrigerant, $T_{c,out}$ respectively from the heat exchanger unit.

3.4 The Mathematical Model for the Organic Rankine Cycle

The model for the simulation study of the ORC is presented here. However, in the formulation of this model, the thermodynamic properties at specific state points of the cycle were taken into consideration. Thermodynamic assumptions of a steady state system were also applied. Other assumed parameters are as stated in section 3.3.2. The schematic representation of the model is presented in Figure 3.10.

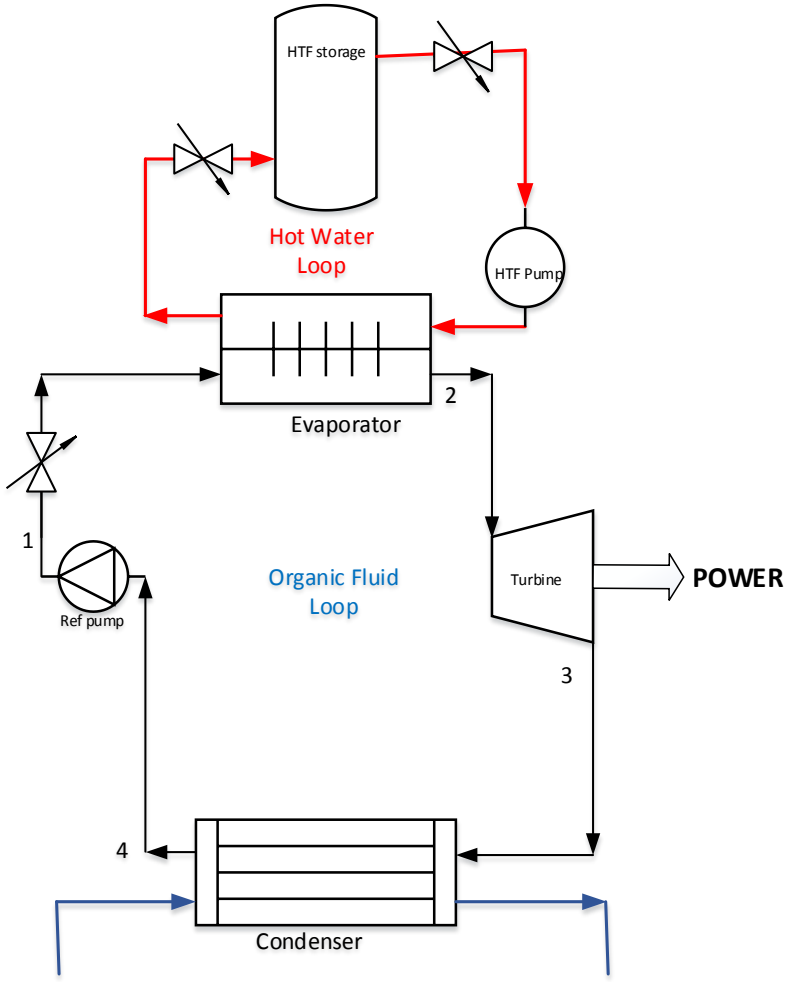

Figure 3.10: Schematic Setup of the ORC

The setup consists of two closed loops – the heat transfer fluid loop and the organic fluid loop. The hot water is pumped from the heat source using a hot water circulation pump with a flow rate of 5.833 kg/s into the evaporator. At the exit of the evaporator, it is re-injected back to the heat source for reheating. The refrigerant cycle is described with state points as follows: State 1 describes the refrigerant properties from the pump outlet to the evaporator inlet; the evaporator exit and turbine inlet is state point 2; the turbine exit and condenser inlet is state point 3; the

condenser outlet and pump inlet is state point 4. Equations 3.17 to Equation 3.33 describe the properties of the working fluid at various state points within the cycle.

State 1 occurs across the pump and the properties of the working fluid such as the entropy, pressure, enthalpy, and temperature are determined by Equation 3.17 to Equation 3.20 respectively.

$$s_{[1]} = s_{[4]} \tag{3.17}$$

$$P_{[1]} = P_{[2]} \tag{3.18}$$

$$h_{[1]} = enthalpy(F\$, s = s_{[1]}, P = P_{[1]}) \tag{3.19}$$

$$T_{[2]} = temperature(F\$, s = s_{[1]}, P = P_{[1]}) \tag{3.20}$$

State 2 is at the evaporator exit and is governed by Equation 3.21 to Equation 3.24

$$P_{[2]} = P_{c,in} \tag{3.21}$$

$$T_{[2]} = T_{c,out} \tag{3.22}$$

$$h_{[2]} = enthalpy(F\$, P = P_{[2]}, T = T_{[2]}) \tag{3.23}$$

$$s_{[2]} = entropy(F\$, P = P_{[2]}, T = T_{[2]}) \tag{3.24}$$

State 3 is after the turbine and is represented by Equation 3.25 to Equation 3.28

$$s_{[3]} = s_{[2]} \tag{3.25}$$

$$P_{[3]} = P_{[4]} \tag{3.26}$$

$$h_{[3]} = enthalpy(F\$, s = s_{[3]}, P = P_{[3]}) \tag{3.27}$$

$$T_{[3]} = temperature(F\$, s = s_{[3]}, P = P_{[3]}) \tag{3.28}$$

The properties of the refrigerant at **state 4** is thus represented by Equation 3.29 to Equation 3.33

$$T_{[4]} = T_{c,in} \tag{3.29}$$

$$P_{[4]} = pressure(F\$, x = x_{[4]}, T = T_{[4]}) \tag{3.30}$$

$$h_{[4]} = enthalpy(F\$, x = x_{[4]}, T = T_{[4]}) \tag{3.31}$$

$$s_{[4]} = entropy(F\$, x = x_{[4]}, T = T_{[4]}) \tag{3.32}$$

$$x_{[4]} = 0 \tag{3.33}$$

Where x is the fluid quality.

The work done by the turbine is given by:

$$\dot{W}_t = \dot{W}_{net} - \dot{W}_p \tag{3.34}$$

While Net Power output $\dot{W}_{net}$ is given by:

$$\frac{\dot{W}_{net}}{\dot{m}_c} = \frac{\dot{W}_t}{\dot{m}_c} - \frac{\dot{W}_p}{\dot{m}_c} \tag{3.35}$$

Thermal Efficiency of the Rankine cycle is thus given by:

$$\eta_{rankine} = \frac{\frac{\dot{W}_{net}}{\dot{m}_c}}{\frac{\dot{Q}_b}{\dot{m}_c}} \tag{3.36}$$

Where $\dot{W}_{net}$ is the Net power output by the system, $\dot{W}_t$ is the work output at the turbine, $\dot{W}_p$ is the work done by the refrigerant pump, $\eta_{rankine}$ is the Rankine efficiency of the system and $\dot{Q}_b$ is the heat input to the evaporator.

3.5 Summary

Computer-based simulation of real life engineering processes has proven to be a vital engineering tool for research in predicting the performance and also evaluation of engineering systems and processes. Consequently, this tool was adopted in this chapter to help develop models for the ORC system components and to determine the ORC system performance under varying input conditions. This was accomplished using the Engineering Equation Solver (EES) software. Parametric analysis is then carried out using these model and the results are presented in Chapter 4.

CHAPTER 4 : SIMULATION RESULTS

4.1 Introduction

The ORC model was used to obtain initial results from the available operating variable parameters which is been presented in Table 4.1. Simulation of these results were also carried out as the operating parameters were being varied helping to determine the optimum operating conditions of the system yielding maximum output.

4.2 Simulation Results of the Organic Rankine Cycle

The Engineering Equation Solver (EES) program was used so solve the set of equations which were used in developing the model used. The temperature profile of the fluids in the evaporator is shown in Figure 4.1.

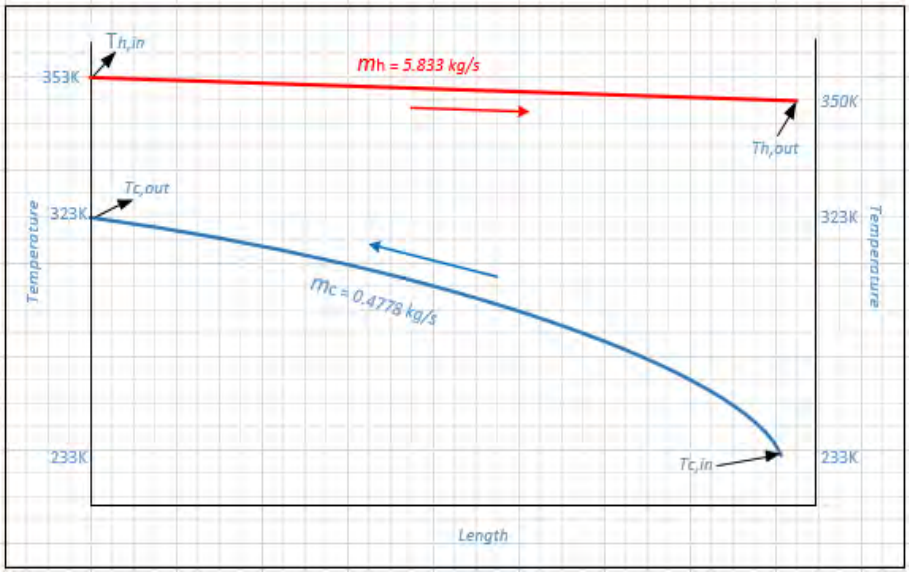

Figure 4.1 Temperature Profile of the Fluids in the Evaporator

The heat transfer fluid (water) enters the evaporator at 353 K at a flow rate of 5.833 kg/s and leaves at 350 K. However, the working fluid is pumped into the evaporator unit in liquid phase at a temperature of 233 K at a mass flow rate of 0.4778 kg/s. On absorbing heat energy through convection from the heat transfer fluid, its temperature is raised and it exits the evaporator at 323 K. It should be noted that the fluids are unmixed within the evaporator and flow counter-

current to each other. The variable parameters used for the simulation model and the results are presented in the Table 4.1 and Table 4.2.

Table 4.1 Variable Parameters

Heat Transfer Area, $\boldsymbol{A}$	1 m^2
Refrigerant mass flow rate, $\dot{\boldsymbol{m}}_{\boldsymbol{c}}$	0.4778 kg/s
Hot Water mass flow rate, $\dot{\boldsymbol{m}}_{\boldsymbol{h}}$	5.833 kg/s
Refrigerant pump inlet pressure, $\boldsymbol{p}_{\boldsymbol{c,in}}$	2.46x10^6 MPa
Hot Water pump inlet pressure, $\boldsymbol{p}_{\boldsymbol{h,in}}$	1.6x10^6 MPa
Hot Water inlet temperature, $\boldsymbol{T}_{\boldsymbol{h,in}}$	353 K
Refrigerant inlet temperature, $\boldsymbol{T}_{\boldsymbol{c,in}}$	233 K
Heat transfer coefficient, $\boldsymbol{U}$	851.2 W/m^2K
Turbine Inlet	0.005 m
Turbine Blade Diameter, $\mathbf{Di}_{\mathbf{turbineblade}}$	0.305 m

Table 4.2 Simulation Results

Back-work-ratio, $\boldsymbol{bwr}$	7.94%
Refrigerant Heat capacity, $\boldsymbol{C}_{\boldsymbol{c}}$	596.9 J
Water Heat Capacity, $\boldsymbol{C}_{\boldsymbol{h}}$	24.4 KJ
Refrigerant specific heat capacity at constant pressure, $\boldsymbol{c}_{\boldsymbol{p,c}}$	1.25 KJ/kgK
Water specific heat capacity at constant pressure, $\boldsymbol{c}_{\boldsymbol{p,h}}$	4.19 KJ/kgK
Heat capacity ratio, $\boldsymbol{C}_{\boldsymbol{r}}$	0.024
Heat exchanger effectiveness, $\boldsymbol{\varepsilon}$	0.7558
Rankine Efficiency, $\boldsymbol{\eta}_{\boldsymbol{rankine}}$	16.09%
Number of Transfer Unit, *NTU*	1.426
Turbine Power produced, $\dot{\boldsymbol{W}}_{\boldsymbol{t}}$	10.22 kW
Pump power consumed, $\dot{\boldsymbol{W}}_{\boldsymbol{p}}$	0.81 kW
Net Power, $\dot{\boldsymbol{W}}_{\boldsymbol{net}}$	9.41 kW
Torque, $\boldsymbol{\tau}$	58.93 N.m
Rotational Speed	1524 rpm
Force	193.2 N

The performance of the ORC was measured by the result listed in Table 4.2, and of particular interest are the Net power generated by the cycle, the power consumed by the pump, and the overall Rankine efficiency of the cycle. The T-s and P-h diagrams are presented in Figure 4.2

and Figure 4.3 respectively. The slope on the T-s diagram shows that the refrigerant R-134a is an isentropic fluid. This is important as it helps in preventing condensation at the turbine which could lead to damages of the turbine blades. The area bounded by the curve represents a mixture of phases of the refrigerant, that is, saturated liquid phase and saturated vapour phase. The point at which the saturated liquid line and the saturated vapour line meet at the apex of the curve as shown in the T-s diagram in Figure 4.2 and the P-h diagram in Figure 4.3 is the critical point of the refrigerant. The value of the point for both curves has been presented in Table 2.1

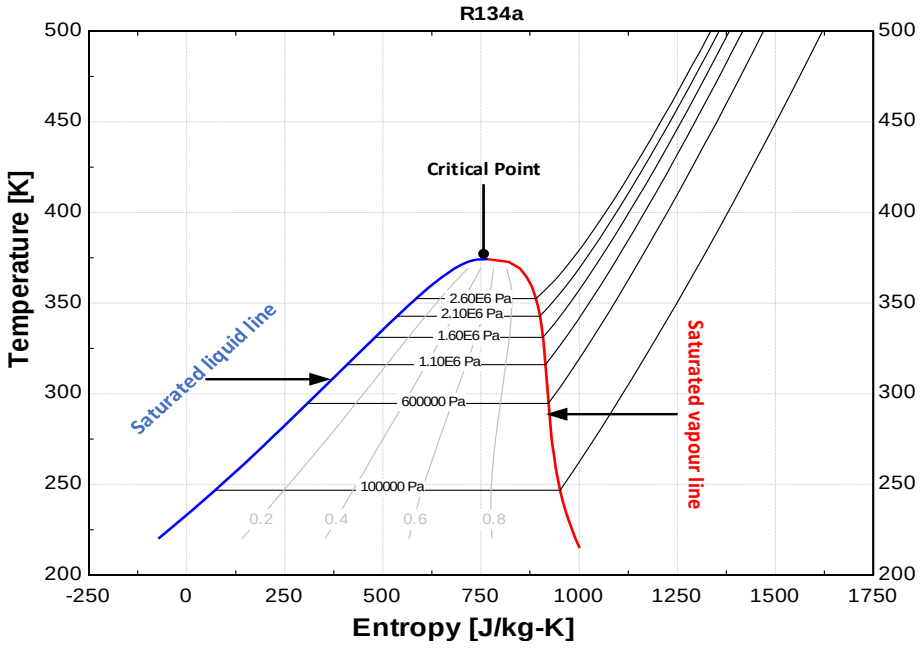

Figure 4.2: Temperature-Entropy Diagram for the Cycle

Conversely, a plot of the pressure of the refrigerant against its enthalpy at the various state points within the system shows the behavior of the refrigerant as the pressure is varied. It can be observed that the enthalpy at temperature range of 233 K to 285 K, the enthalpy of the refrigerant is independent on the pressure. However, along the isothermal line of 350 K, a decrease in the pressure shows a slight increase in the enthalpy at high pressure. A further lowering of the pressure shows no significant change in the enthalpy of the refrigerant.

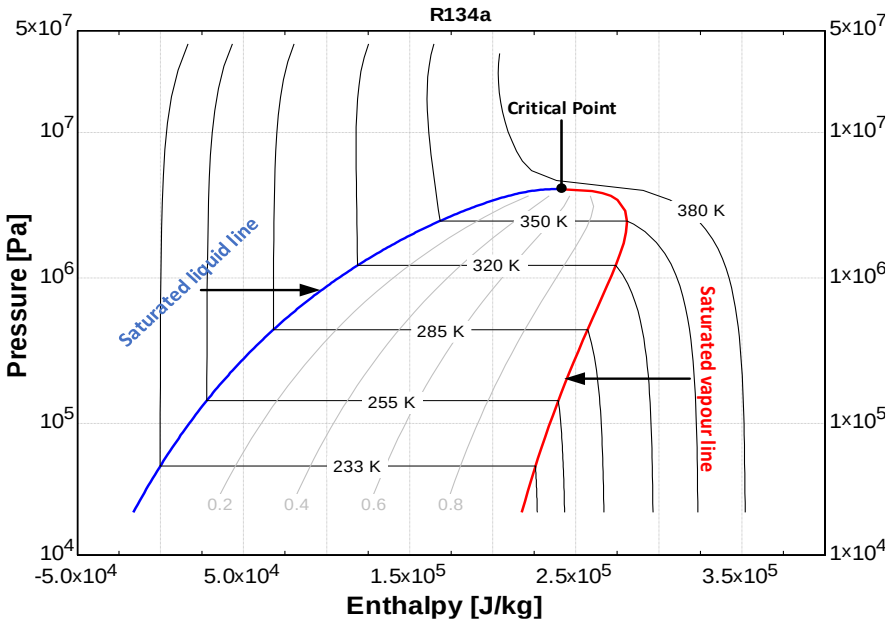

Figure 4.3: Pressure-Enthalpy Diagram for the Cycle

The effect of the inlet properties of the heat transfer fluid and that of the refrigerant at the exchanger inlet on the overall performance of the ORC is presented hereafter. The values of the parameters used to obtain the results presented in section 4.2 were varied so as to determine the effects these varied parameters have on the overall performance of the cycle. The analyses are presented in sections 4.3 to 4.6.

4.3 Effect of the Heat Transfer Area on the Cycle Performance

The amount of available surface area with which the fluids have to interact within the evaporator plays a significant role in the amount of heat energy that is transferred between them, their exit temperature from the evaporator, the net power generated by the cycle and the cycle's efficiency. These relationships are further discussed in the following subsections.

4.3.1 Effect of Heat Transfer Area on Refrigerants Exit Temperature

The model of the evaporator used has been presented in section 3.3.2. The selected flow type was a counter-flow while the fluids are unmixed within the evaporator. The effectiveness-NTU method was used in the evaporator analysis. Consequently, the analysis shows that the exit properties of the fluids entering the evaporator can be influenced by the size of the contact area on the evaporator available for heat exchange as shown in Figure 4.4 and Figure 4.5.

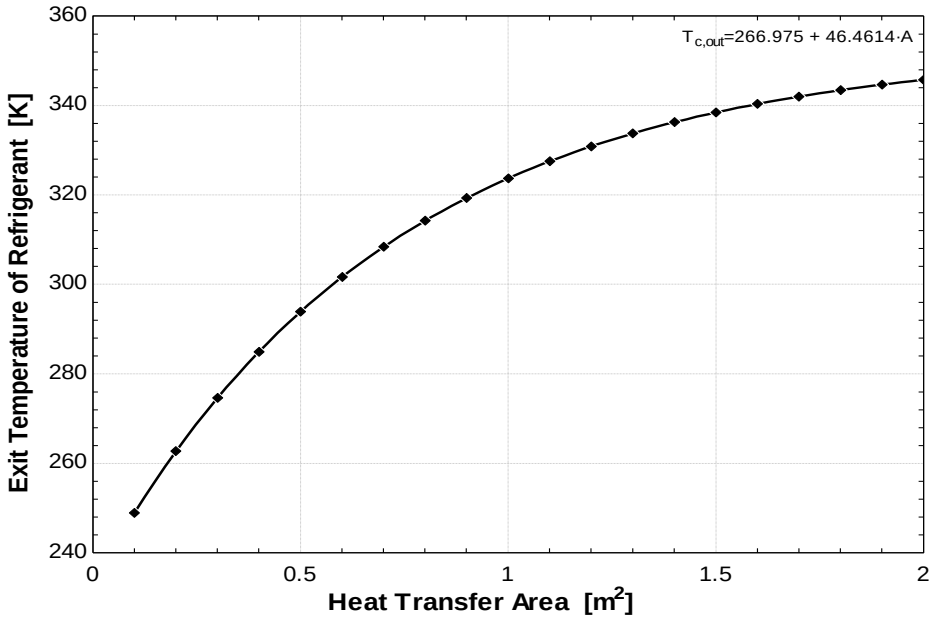

Figure 4.4: Effect of Heat Transfer Area on Refrigerant Exit Temperature

The graph presented in Figure 4.4 displays the effect of the surface area of the evaporator on the exit temperature of the refrigerant. The temperature of the refrigerant was shown to increase as the surface area made available for the heat transfer process to occur is increased. However, further increase in the heat transfer area beyond 3 m^2 will produce a negligible rise in temperature of the refrigerant fluid as it approaches the inlet temperature of the HTF as is shown in Figure 4.5. If there is no additional heat supply to the working fluid except from the HTF medium, then the temperature to which the refrigerant can rise to within the evaporator can be no greater than the temperature at which the HTF enters into the evaporator medium.

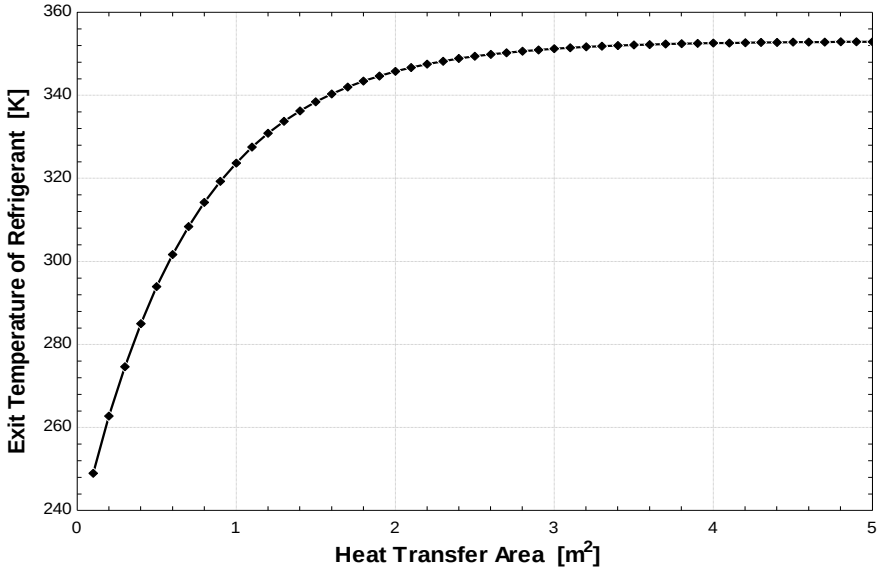

Figure 4.5: Effect of Increased Heat Transfer Area on Exit Temperature of Refrigerant

4.3.2 Effect of Heat Transfer Area on Quantity of Heat Energy Transferred

As the fluids interact within the evaporator, heat energy is transferred between them and the energy lost by the heat transfer fluid is invariably gained by the refrigerant facilitating its transformation from liquid phase to vapor phase. The quantity of energy which is transferred between both fluid media is a function of how long and how well both fluids interact within the evaporator. The interaction between the heat transfer area and the quantity of heat energy transferred is shown in Figure 4.6.

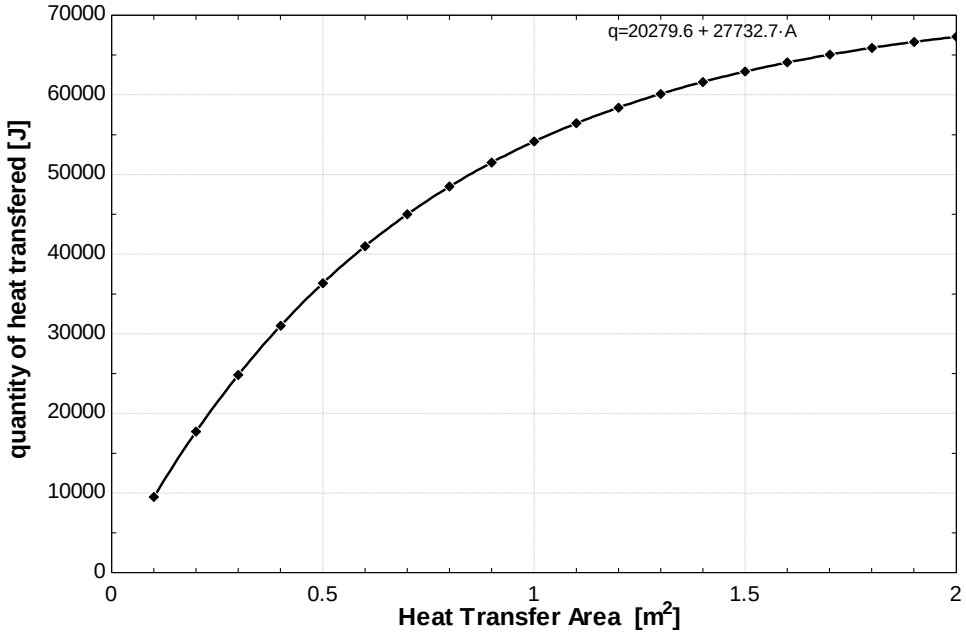

Figure 4.6: Effect of Heat Transfer Area on Quantity of Heat Energy Transferred

The quantity of heat energy transferred from the hot fluid to the refrigerant increases progressively from 9.5 KJ to 67 KJ as the surface area is increased from 0.1 m^2 to 2 m^2. However, as with Figure 4.5, Figure 4.7 indicates that an increase in the surface area for the fluid interaction of more than 3 m^2 leads to no significant increments on the quantity of heat transferred to the refrigerants from the hot fluid. This is because the heat energy of the refrigerant approaches the heat energy of the HTF bringing about heat energy equilibrium.

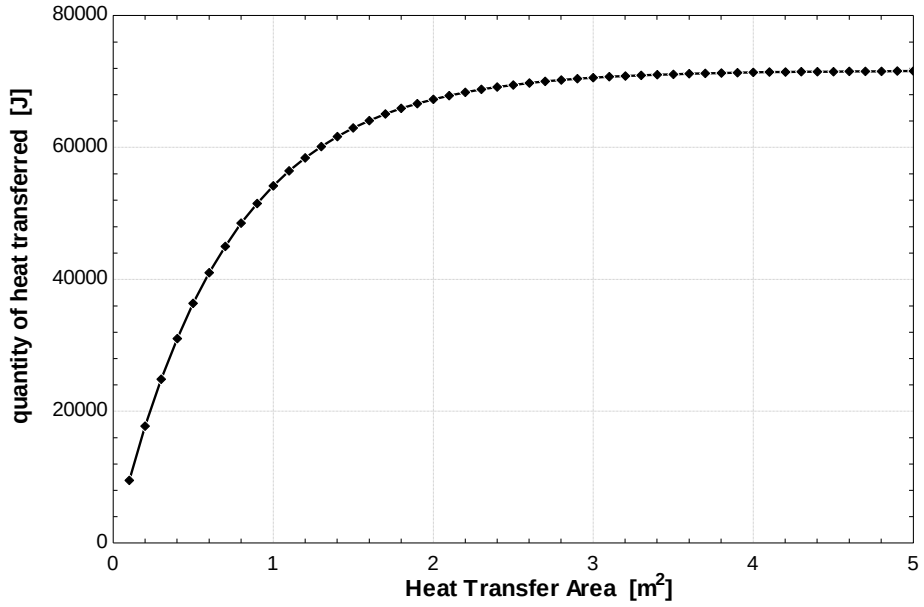

Figure 4.7: Effects of Increased Heat Transfer Area on Heat Energy Transferred

4.3.3 Effect of Heat Transfer Area on Net Power Output

The net power output of the cycle as it relates to the total surface area with which the fluids in the evaporator interact is represented by the graph in Figure 4.8. It follows that the net power produced by the ORC increases from 0.314 kW to 9.406 kW as the surface area for fluid interaction increases from 0.1 m^2 to 1 m^2. A further increase in the size of the evaporator increasing the interacting heat transfer area from 1 m^2 to 2 m^2 also shows an increase in the net power output of the system to 14.7 kW.

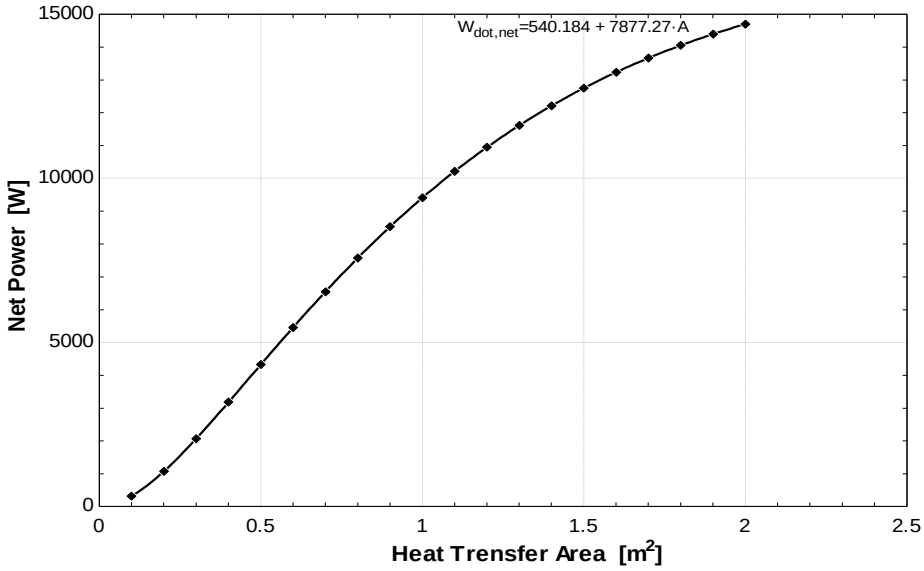

Figure 4.8: Effect of Heat Transfer Area on Net Power Output

4.3.4 Effect of Heat Transfer Area on Cycle Efficiency

Figure 4.9 shows how the heat transfer surface area between the fluids in the evaporator affects the Rankine efficiency of the ORC. It is observed that as the heat transfer surface area is increased, so also does the efficiency. It follows that the efficiency of the cycle increases from 3.4% to 16.09% as the surface area for fluid interaction increases from 0.1 m^2 to 1 m^2. A further increase in the size of the evaporator increasing the interacting heat transfer area from 1 m^2 to 2 m^2 also shows an increase in the cycle efficiency of the system to 19.37%. However, for every increase of the HTA by 10 cm^2, there is less than 0.15% increase in the overall system efficiency.

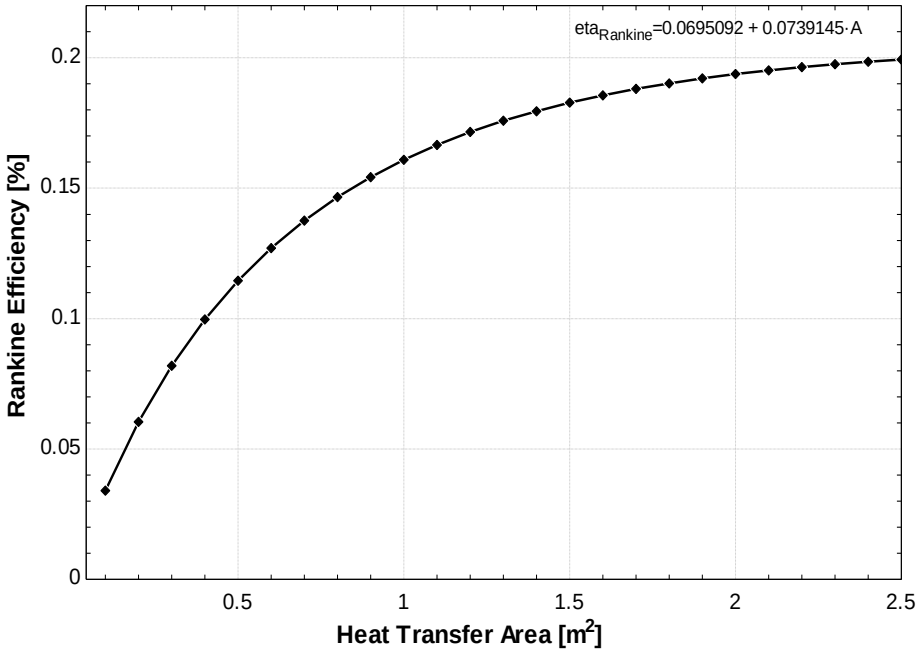

Figure 4.9: Effect of Heat Transfer Area on Cycle Efficiency

4.3.5 Effect of Heat Transfer Area on Back-work-ratio of Refrigerant Pump

The back-work-ratio of the cycle represents the ratio of the work at the pump to the work at the turbine. For a typical cycle however, the lower this ratio, the better the cycle performance. Figure 4.10 shows how varying the heat transfer area between the fluids affects the back-work-ratio of the refrigerant pump. The relationship above shows how the power needed by the pump is reduced as the fluids within the heat exchanger are given more contact surface area to interact. At a heat transfer area of 2 m^2, the ratio of the pump work to turbine work is seen to be at its minimum value of 0.05.

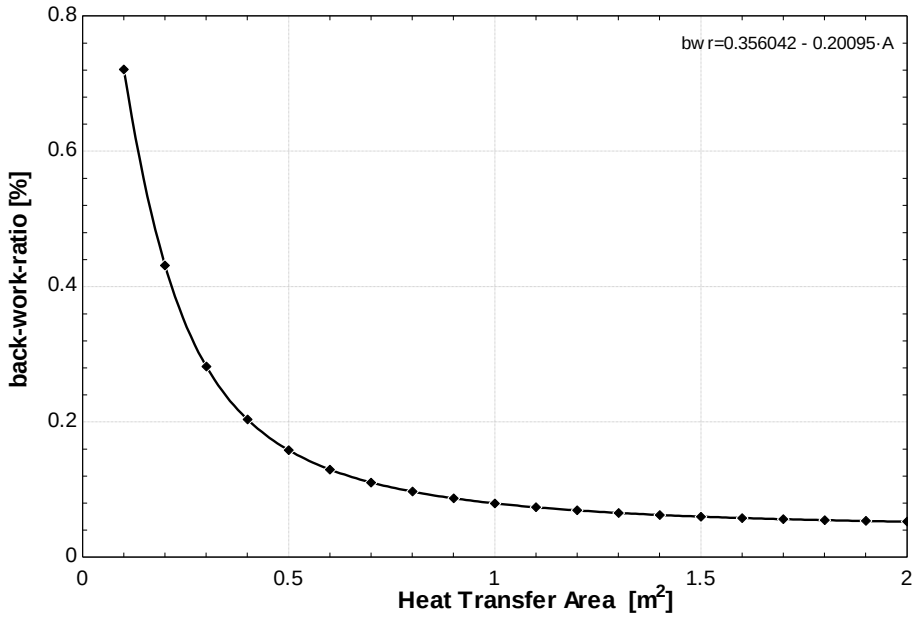

Figure 4.10: Effect of Heat Transfer Area on Back-work-ratio of Refrigerant Pump

4.4 Effect of Heat Transfer Fluid (Water) Inlet Temperature on Cycle Performance

The temperature of the heat transfer fluid (in this case, water) plays a significant role in the overall output that can be expected in terms of power. The heat source produces heated water at temperature of 353 K as presented in Section 4.2. A net output power of 9.4 kW was produced. However, the relationship between the inlet temperature of the heat transfer fluid and the ORC performance parameters are further analyzed.

4.4.1 Effect of Heat Transfer Fluid (Water) Inlet Temperature on Refrigerants Exit Temperature

The heat source temperature of water entering into the evaporator plays a significant role in determining the temperature at which the refrigerant exits the evaporator. The relationship between these temperatures is presented in Figure 4.11.

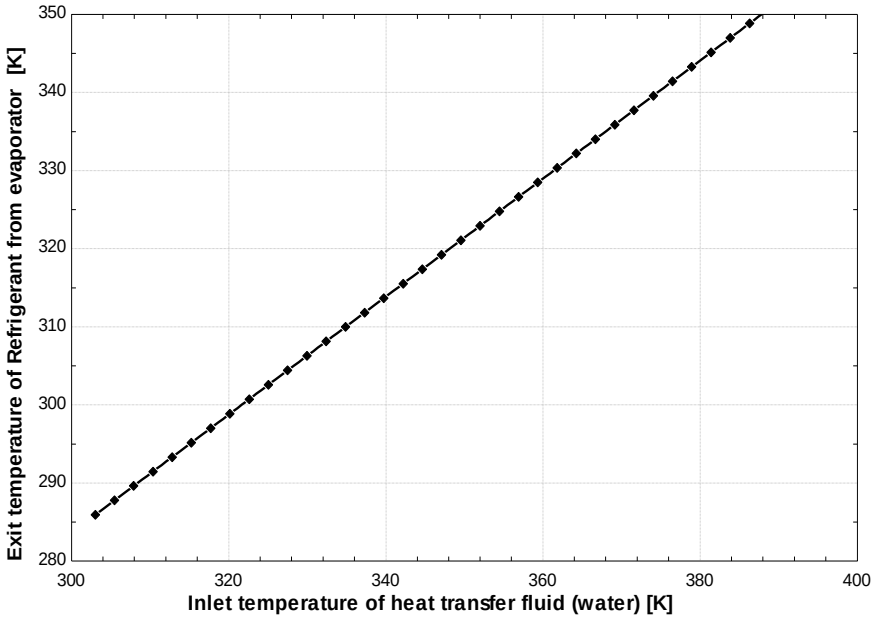

Figure 4.11: Effect of Heat Transfer Fluid (Water) Inlet Temperature on Refrigerants Exit Temperature

It is seen that a linear relationship exists between the heat source fluid temperature and the exit temperature of the refrigerant from the evaporator. The increase in temperature of the heating fluid from 303 K to 383 K will raise the temperature within the evaporator from 286 K to 446 K. The temperature of the refrigerant, in turn, has significance on the overall cycle performance.

4.4.2 Effect of Heat Transfer Fluid (Water) Inlet Temperature on Quantity of Heat Energy Transferred

Similar to the effect of the heat source temperature on the refrigerant outlet temperature from the evaporator, the quantity of heat energy which is transferred between the two fluids within the evaporator is dependent on the amount of the temperature profile of the hot fluid. The relationship between these two parameters is represented by Figure 4.12. The heat energy transferred from the hot fluid medium to the working fluid medium increases as the temperature of the hot fluid medium is increased. At the initial modelled temperature for the heat transfer fluid of 353 K, the heat transferred is 51.14 KJ. Further analysis however, shows that the heat energy transferred continuously increases as the hot fluid temperature also increases.

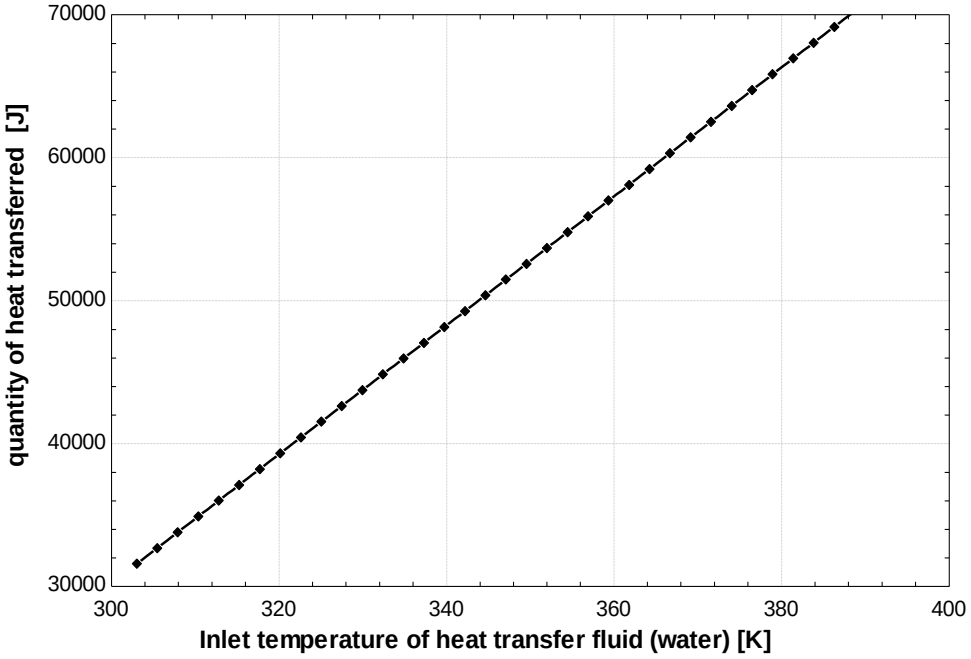

Figure 4.12: Effect of Heat Transfer Fluid (Water) Inlet Temperature on Quantity of Heat Energy Transferred

4.4.3 Effect of Heat Transfer Fluid (Water) Inlet Temperature on Net Power Output

The net power output obtained from the system at water inlet temperature of 353 K is 9.4 kW. However, from further investigations, increased net power output can be obtained from the ORC should there be an increase in the temperature of the heat transfer fluid from the source into the evaporator. This is shown by Figure 4.13. From the above figure, it can be stated that the power output of the cycle can further be increased to 14.9 kW if the hot fluid temperature can rise to 383 K.

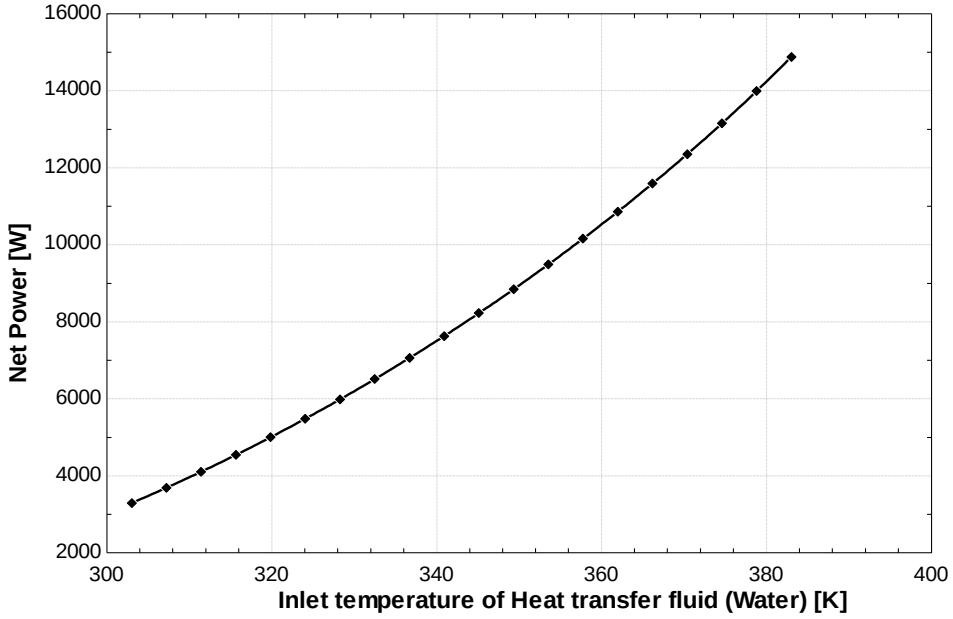

Figure 4.13: Effect of Heat Transfer Fluid (Water) Inlet Temperature on Net Power Output

4.4.4 Effect of Heat Transfer Fluid (Water) Inlet Temperature on Cycle Efficiency

The efficiency of the cycle is determined by how much of the heat energy input is available to be converted to power output. As illustrated in the graph in Figure 4.14, the efficiency of the cycle increases with the availability if heat energy provided due to increasing temperature.

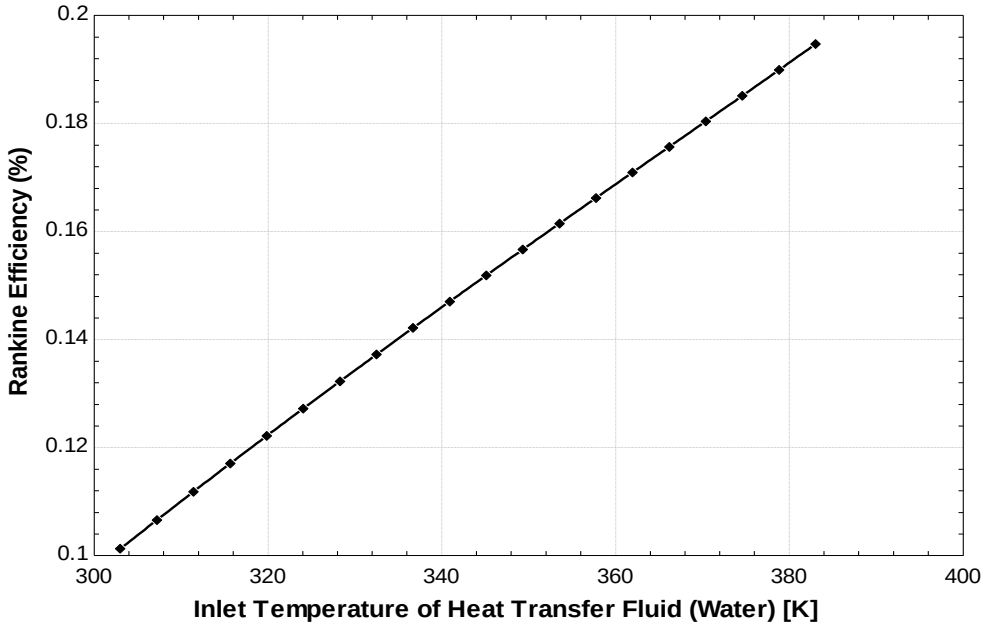

Figure 4.14: Effect of Heat Transfer Fluid (Water) Inlet Temperature on Cycle Efficiency

4.5 Effect of Refrigerant Mass Flow Rate on the Cycle Performance

The rate at which the refrigerant travels within the system is dependent on the refrigerant pump size / rating. The refrigerant flow rate used in obtaining the cycle outputs represented in this work is 0.4778 kg/s. The net power output and the efficiency of the cycle obtained are 9.4 kW and 16.1% respectively. The increase (or decrease) of the mass flow rate of the working fluid medium influences the output of the cycle as presented in the subsections below.

4.5.1 Effect of Refrigerant Mass Flow Rate on Refrigerants Exit Temperature

The effect of the mass flow rate of the refrigerant pump was studied by varying it from 0.01 kg/s to unity. As shown in Figure 4.15, increasing the rate of flow of the refrigerant can cause a decrease in the temperature of the refrigerant exiting the heat exchanger. The longer the time the refrigerant stays in contact with the hot fluid, the higher the rise in its temperature. This scenario enhances the vaporization of the working fluid at the exit of the evaporator.

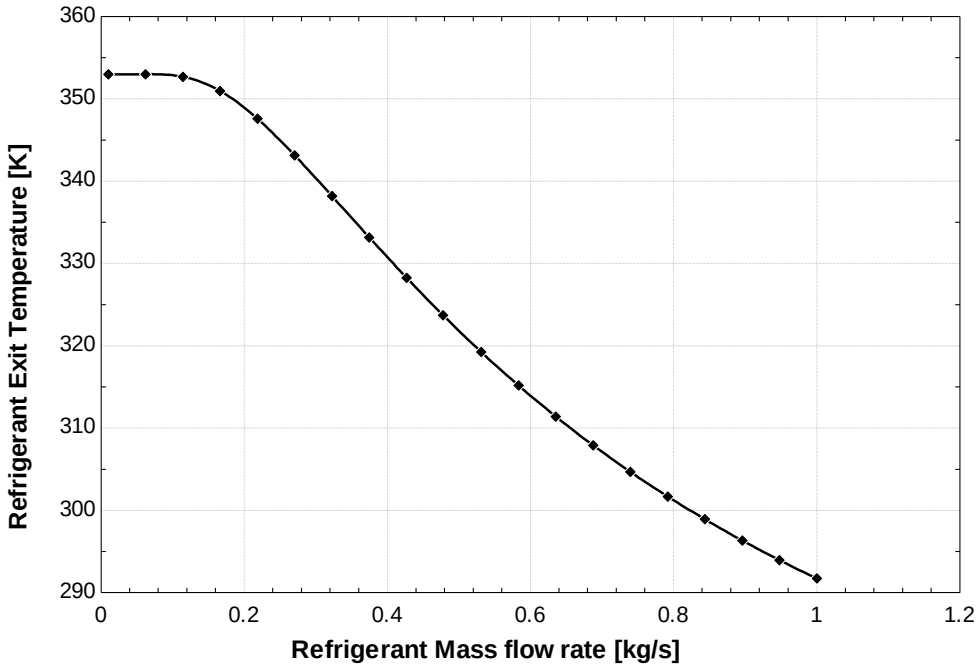

Figure 4.15: Effect of Refrigerant Mass Flow Rate on Refrigerants Exit Temperature

When the refrigerant has a low mass flow rate of 0.01 kg/s, its temperature can be raised up to 353 K. At this temperature, the working fluid is in a complete vapor phase ready to go into the turbine. Conversely, the faster the working fluid moves through the evaporator, having less time to interact with the hot fluid within the evaporator, the less the temperature is increased. An

incomplete vaporization may result from this which would lead to a two phase fluid proceeding into the turbine. This can in turn damage the turbine blade, thus affecting the cycle performance adversely.

4.5.2 Effect of Refrigerant Mass Flow Rate on Quantity of Heat Energy Transferred

The amount of heat transferred from the hot fluid (water) to the refrigerant is also dependent on the refrigerant mass flow rate across the heat exchanger. The heat energy transferred to the organic fluid with the cycle flow rate of 0.4778 kg/s, from the hot water fluid is 54.1 kJ, however, with increase in the mass flow rate of the refrigerant to 1 kg/s, the heat energy transferred to it from the hot water increases from 54.1 kJ to over 73.3 kJ. This increase, in turn, improves on the cycle overall output as can be seen in Figure 4.16.

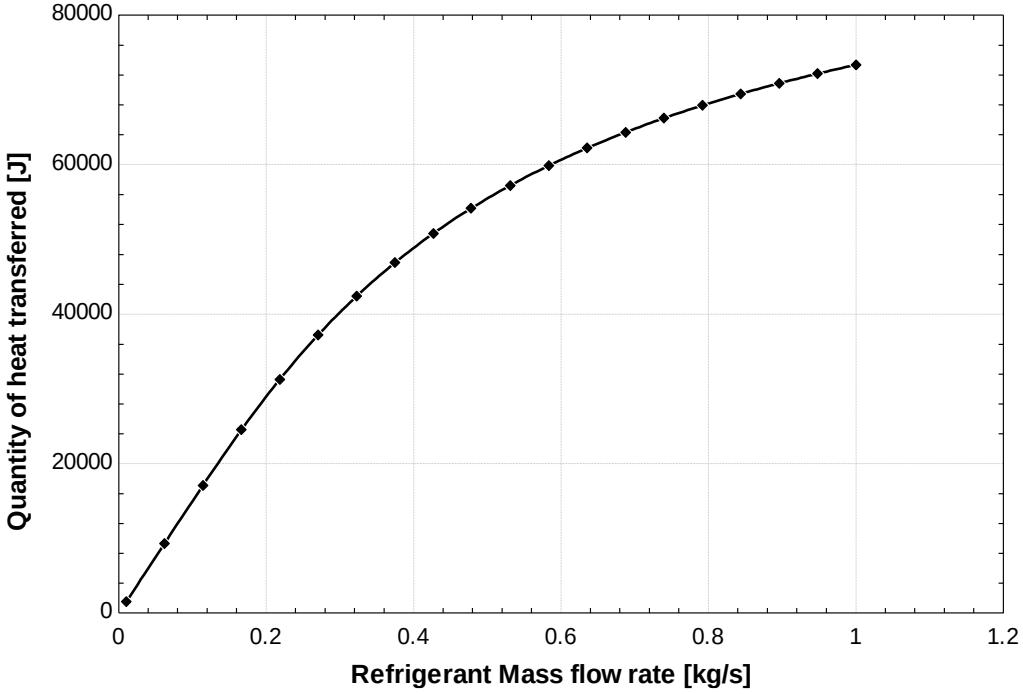

Figure 4.16: Effect of Refrigerant Mass Flow Rate on Quantity of Heat Energy Transferred

4.5.3 Effect of Refrigerant Mass Flow Rate on Net Power Output

The significance of the mass flow rate in determining the net power produced by the cycle can be observed in Figure 4.17. The net mechanical power produced from the cycle with refrigerant mass flow rate of 0.4778 kg/s is 9.4 kW.

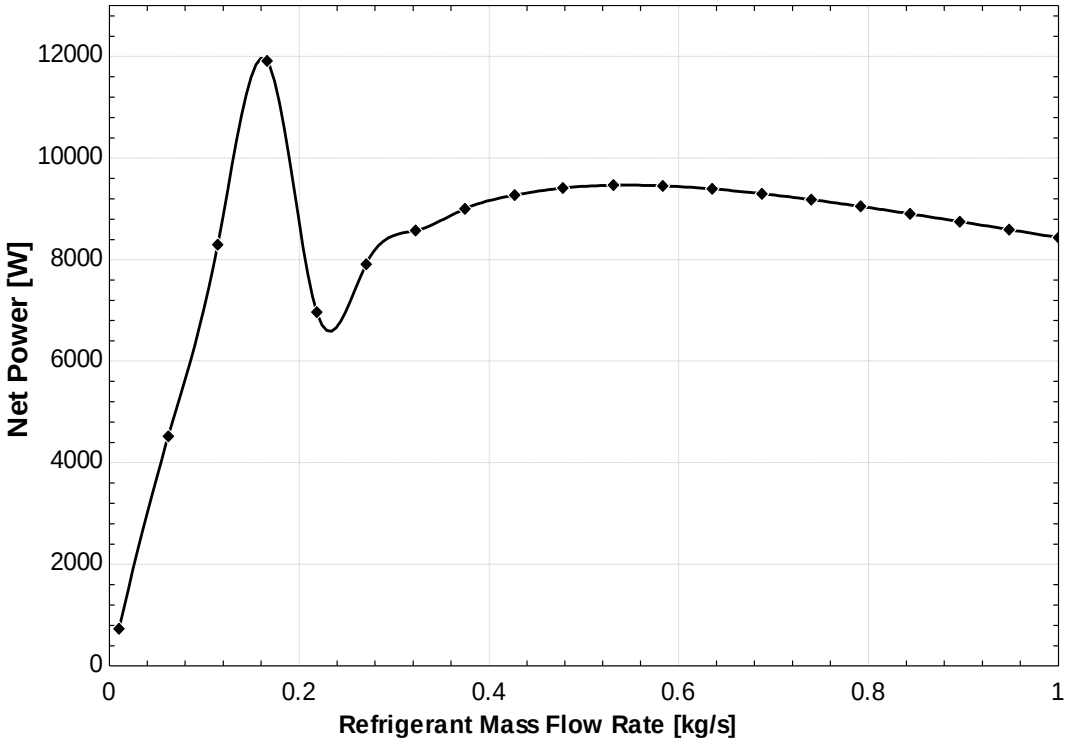

Figure 4.17: Effect of Refrigerant Mass Flow Rate on Net Power Output

It is seen that the heat energy transferred to the refrigerant fluid at flow rate of 0.1663 kg/s is 11.912 kW. The value of the heat energy decreases to 6.96 kW as the mass flow rate of the refrigerant increases to 0.22 kg/s. However, further increment in the flow rate to 0.5311 kg/s produces a net power of 9.46 kW from the cycle. On further increase of the flow rate to 1 kg/s, the net power output of the cycle is observed to decrease to 8.43 kW.

4.5.4 Effect of Refrigerant Mass Flow Rate on Cycle Efficiency

The overall efficiency of the ORC is partly dependent on the rate at which the refrigerant pump supplies the refrigerant fluid through the evaporator. The Rankine efficiency of the cycle modelled at the refrigerant flow rate of 0.4778 kg/s is obtained to be 16.09%. Figure 4.18 however shows that the efficiency of the cycle generally decreases as the refrigerant flow rate increases if all other parameters are unchanged. At a mass flow rate of 1 kg/s of the refrigerant, cycle efficiency drops to about 11% as seen in Figure 4.18.

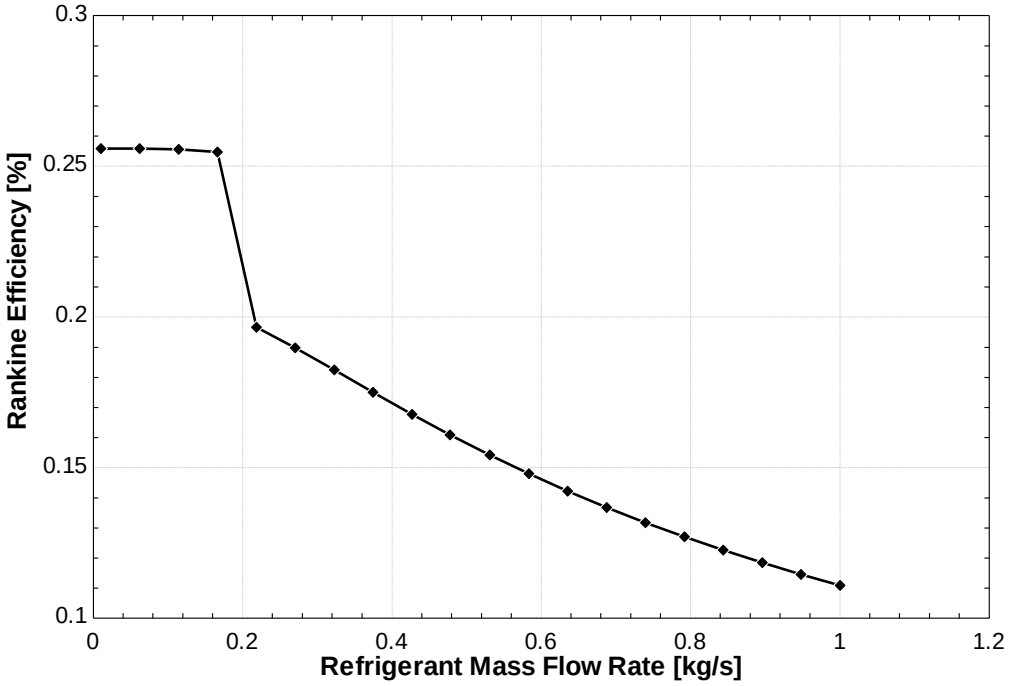

Figure 4.18: Effect of Refrigerant Mass Flow Rate on Cycle Efficiency

4.6 Effect of Refrigerant Pump Pressure on the Cycle Performance

The last factor to be considered is that the cycle performance is dependent is the pump pressure of the refrigerant. The refrigerant circulation pump used in the modelling has a pressure of 2.46 MPa which resulted in an output of 10.2 kW power at the turbine. The power consumed by the pump is 0.81 kW. The effects of the pump pressure on the cycle outputs are further discussed in the subsections below.

4.6.1 Effect of Refrigerant Pump Pressure on Refrigerant Exit Temperature

Operation across the evaporator unit is assumed to be isobaric. The temperature of the refrigerant at the exit of the evaporator depends also partly on the pressure of the fluid at the inlet of the evaporator. This is shown in the Figure 4.19. It can be observed that the temperature of the refrigerant at which it exits the evaporator unit is 323 K. Significant variation of the pump pressure above or below the initial pressure of 2.46 MPa would yield no significant change in raising the temperature of the refrigerant.

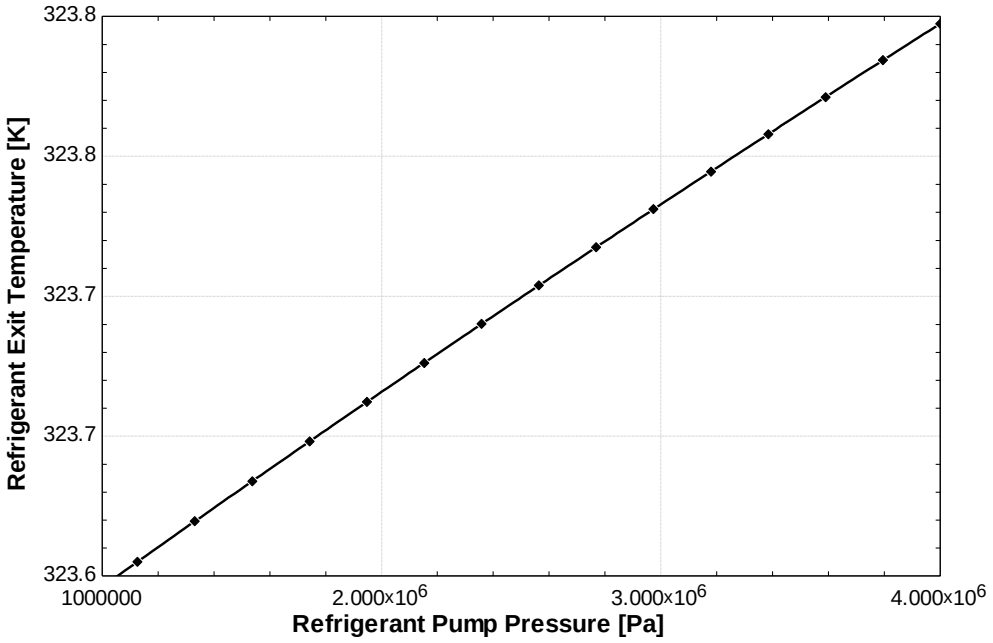

Figure 4.19: Effect of Refrigerant Pump Pressure on Refrigerant Exit Temperature

4.6.2 Effect of Refrigerant Pump Pressure on Quantity of Heat Energy Transferred

The total heat energy transferred between the fluids varies inversely to the refrigerant pump pressure of the cycle, although a significant change in the pressure of the refrigerant pump results in less significant change in the quantity of the heat transferred to it from the heat transfer fluid as shown in Figure 4.20.

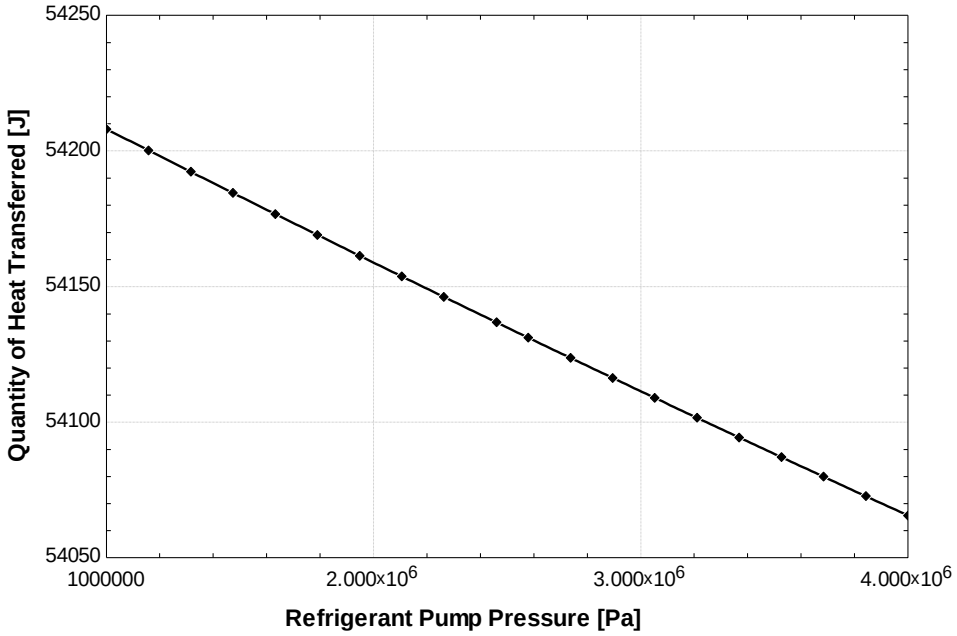

Figure 4.20: Effect of Refrigerant Pump Pressure on Quantity of Heat Energy Transferred

4.6.3 Effect of Refrigerant Pump Pressure on Net Power Output

The net power produced from the ORC presented with a pump pressure of the refrigerant of 2.46 MPa is 9.4 kW. However, Figure 4.21 shows that a net power output of 29.7 kW can be obtained when the pump pressure of the refrigerant is at 1.32 MPa. At this pressure value of 1.32 MPa, the cycle is observed to produce its optimum power output.

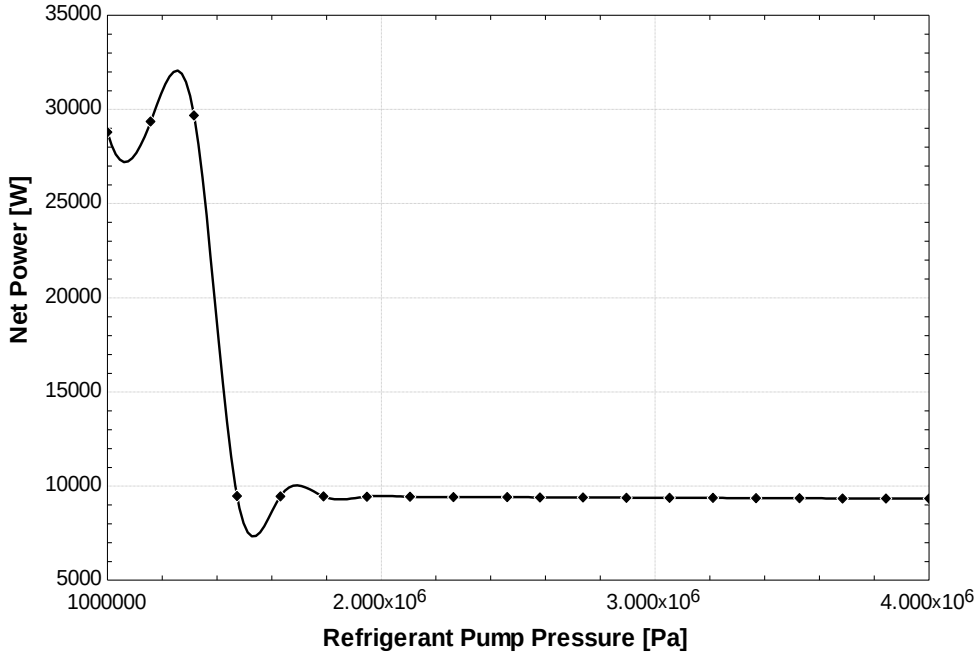

Figure 4.21: Effect of Refrigerant Pump Pressure on Net Power Output

4.6.4 Effect of Refrigerant Pump Pressure on its Cycle Efficiency

Similar to the effect of the refrigerant pump pressure on the net power generated from the cycle, Figure 4.22 shows the effect of the refrigerant pump pressure on the cycle efficiency of the ORC. The efficiency of the cycle increases to 22.6% at a pressure of 1.32 MPa of the refrigerant similar to the effect of the refrigerant pump pressure on the cycle power output.

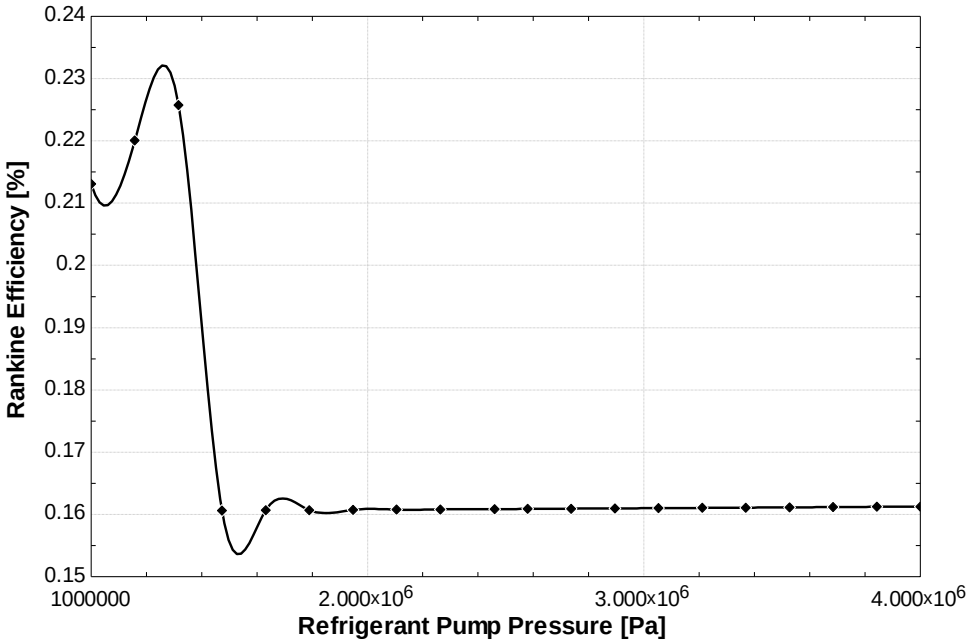

Figure 4.22: Effect of Refrigerant Pump Pressure on its Cycle Efficiency

4.6.5 Effect of Refrigerant Pump Pressure on Rotational Speed of Turbine Blades

The effect of the change in the refrigerant pressure operating within the ORC system is shown in Figure 4.23. It is seen that the rotational speed on the turbine blade decreases rapidly from 12,700 rpm to 2,130 rpm as the pressure of the refrigerant is increased from 0.5 MPa to1.97 MPa. Between 1.97 MPa and 4 MPa, the speed of the rotation on the turbine blade remained largely constant at 1500 rpm.

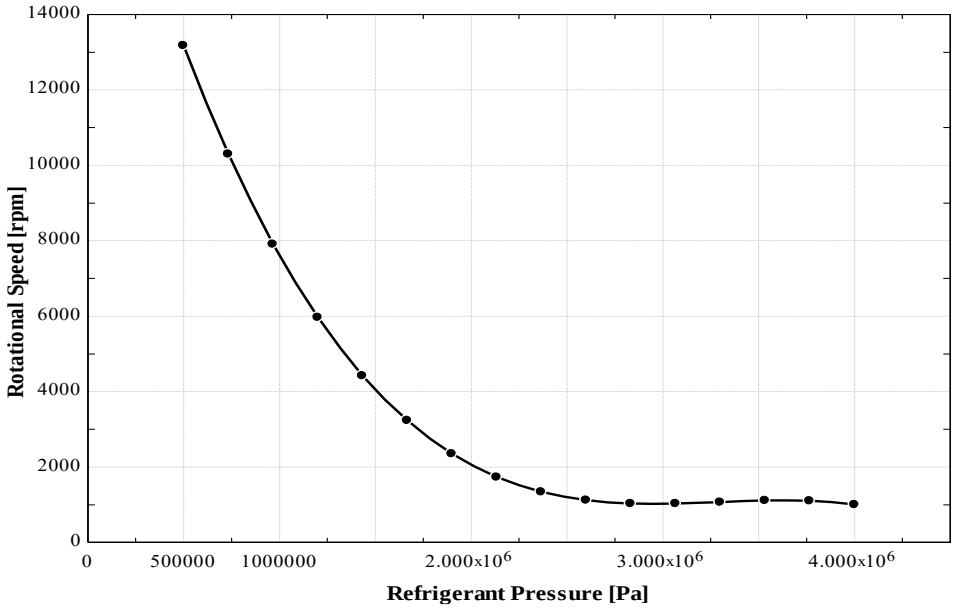

Figure 4.23: Effect of Refrigerant Pump Pressure on Rotational Speed of Turbine Blades

4.6.6 Effect of Refrigerant Pump Pressure on Torque

The torque generated on a rotating system is inversely proportional to the rotational speed of the system. This is shown by Equation 4.1

$$Rotational\ Speed = \frac{Power}{2*\pi*\tau} \quad 4.1$$

Where $\tau = Torque$

The torque generated by the turbine blade due to rotation increases as the refrigerant pressure operating within the ORC system increases. This is shown in Figure 4.24.

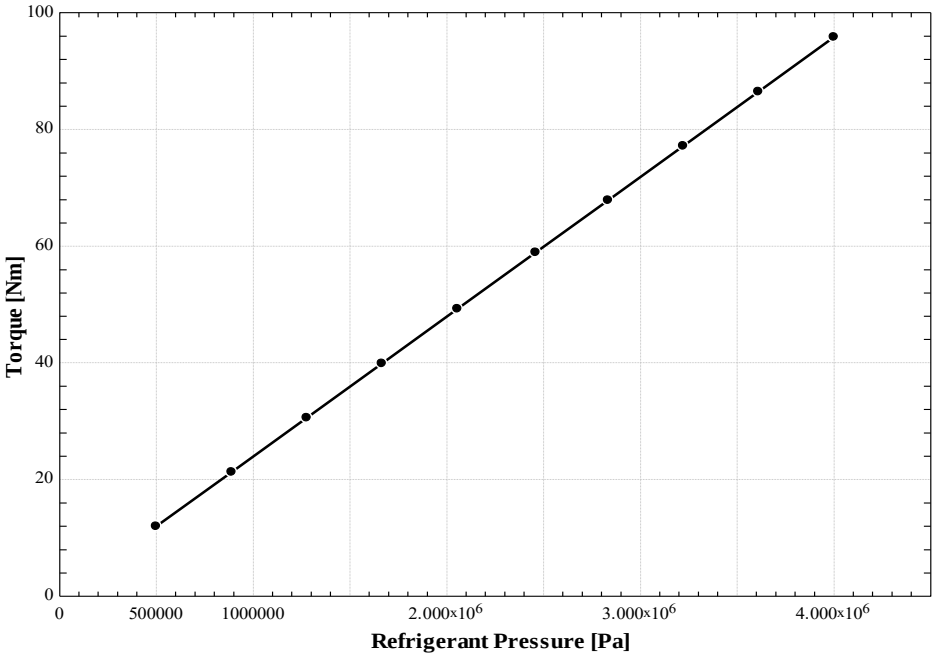

Figure 4.24: Effect of Refrigerant Pump Pressure on Torque

The torque increases from 11.99 Nm to 95.82 Nm as the pressure is varied from 0.5 MPa to 4 MPa.

4.7 Influence of Power on the Rotational Speed of the Turbine Blade

The net power generated by the ORC system varies directly with the speed of rotation caused by the impact of the refrigerant fluid on the blades of the turbine. Figure 4.25 shows a linear increase of the net power generated by the ORC system as the speed of rotation of the turbine blades increases. This relationship is supported by Equation 4.1.

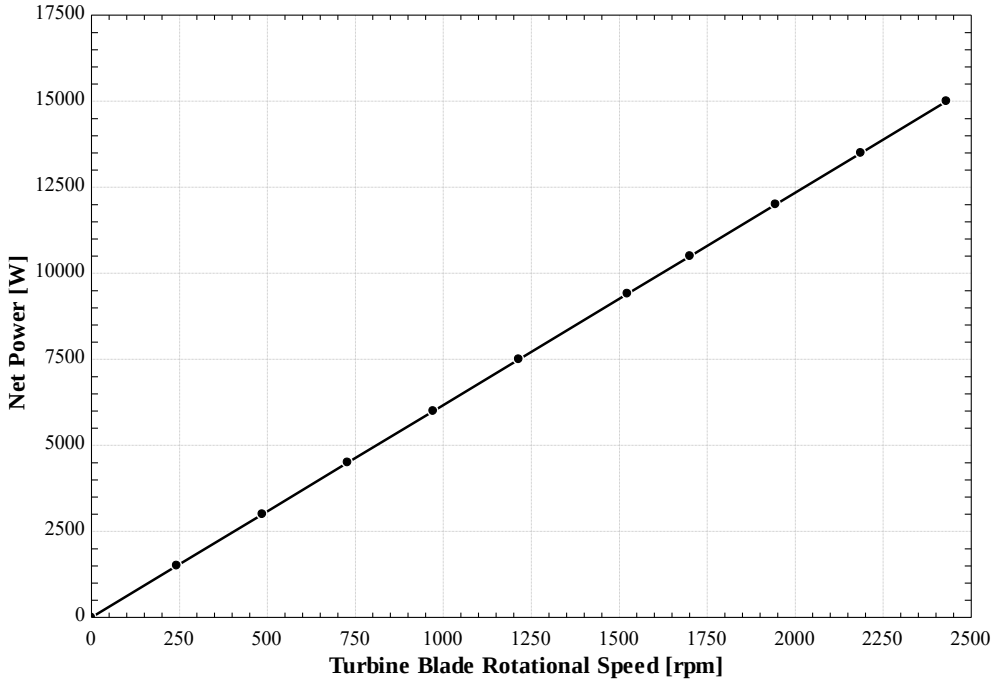

Figure 4.25: Influence of Power on the Rotational Speed of the Turbine Blade

The summary of the simulation results can be seen in Table 4.3 to Table 4.6. Table 4.3 shows how the heat source temperature influences performance of the ORC such as the cycle power output and efficiency. From the data presented, it can be seen that the increase in the temperature of the heat source will also increase the performance of the cycle's components thereby leading to an overall increased cycle performance.

The effects of the refrigerant pump pressure on the performance of the ORC are presented in Table 4.4. As the refrigerant pump pressure is increased, the power consumed by the pump, $\dot{W}_p$, is observed to increase as well. However, the heat transfer in the evaporator $\dot{Q}_b$ is seen to decrease gradually to a point where the refrigerant pump pressure is 1.32 MPa, after which there is a sharp decline, followed by a gentle decline. Turbine work is observed to increase from 8 kW to 30 kW at 1.32 MPa and then drop sharply to 9.9 kW followed by a steady increase, while the cycle efficiency increases to 22.5 % at 1.32 MPa. Given that the HTF characteristics of pressure, temperature and flow rate remain unchanged, the optimum pressure for the refrigerant circulation pump was observed to be 1.32 MPa.

Table 4.3: Variation of ORC Units and Performance with Heat Source Temperature

$T_{h,in}$ [K]	$\dot{W}_p$ [W]	$\dot{Q}_b$ [J]	$\dot{W}_t$ [W]	$\dot{Q}_c$ [W]	$\dot{W}_{net}$ [W]	Efficiency [%]
303	810.7	32510	4103	29218	3292	0.1013
307	810.7	34488	4477	30821	3667	0.1063
311	810.7	36479	4871	32419	4060	0.1113
315	810.7	38485	5284	34011	4474	0.1162
319	810.7	40506	5717	35600	4906	0.1211
323	810.7	42544	6169	37185	5359	0.126
327	810.7	44598	6641	38768	5831	0.1307
331	810.7	46671	7134	40348	6323	0.1355
335	810.7	48764	7646	41929	6835	0.1402
339	810.7	50878	8179	43510	7369	0.1448
343	810.7	53016	8734	45093	7923	0.1494
347	810.7	55178	9310	46679	8499	0.154
351	810.7	57368	9909	48270	9098	0.1586
355	810.7	59589	10531	49869	9720	0.1631
359	810.7	61843	11177	51477	10367	0.1676
363	810.7	64136	11850	53097	11039	0.1721
367	810.7	66472	12550	54733	11740	0.1766
371	810.7	68859	13281	56389	12470	0.1811
375	810.7	71306	14045	58071	13234	0.1856
379	810.7	73824	14847	59788	14036	0.1901
383	810.7	76434	15693	61551	14882	0.1947

Table 4.4: Variation of ORC Units and Performance with Refrigerant Pump Pressure

P_c [Pa]	$\dot{W}_p$ [W]	$\dot{Q}_b$ [J]	$\dot{W}_t$ [J]	$\dot{Q}_c$ [W]	$\dot{W}_{net}$ [W]	Efficiency [%]
100000	16.56	142695	8150	134562	8133	0.057
300000	83.93	141206	19889	121402	19805	0.1403
500000	151.3	139626	24480	115297	24329	0.1742
700000	218.6	137930	27032	111117	26813	0.1944
900000	286	136086	28573	107799	28287	0.2079
1.10E+06	353.3	134040	29529	104864	29176	0.2177
1.30E+06	420.6	131703	30085	102040	29664	0.2252
1.50E+06	487.9	58923	9953	49457	9465	0.1606
1.70E+06	555.1	58826	10008	49374	9452	0.1607
1.90E+06	622.4	58731	10062	49291	9440	0.1607
2.10E+06	689.6	58638	10117	49211	9427	0.1608
2.30E+06	756.9	58547	10172	49131	9415	0.1608

2.50E+06	824.1	58457	10228	49053	9404	0.1609
2.70E+06	891.3	58368	10284	48976	9392	0.1609
2.90E+06	958.5	58281	10340	48900	9381	0.161
3.10E+06	1026	58196	10396	48825	9371	0.161
3.30E+06	1093	58111	10453	48751	9360	0.1611
3.50E+06	1160	58028	10510	48678	9350	0.1611
3.70E+06	1227	57947	10567	48607	9340	0.1612
3.90E+06	1294	57866	10624	48536	9330	0.1612

The quantity of heat energy transferred between the fluids in the evaporator is influenced by the availability of the surface area where they interact with each other. The effect of this is represented in Table 4.5.

Table 4.5: Variation of ORC Units and Performance with Heat Transfer Area

HTA [m^2]	$\dot{W}_p$ [W]	$\dot{Q}_b$ [J]	$\dot{W}_t$ [W]	$\dot{Q}_c$ [J]	$\dot{W}_{net}$ [W]	**Efficiency** [%]
0.1	810.7	9227	1125	8913	314.2	0.03405
0.25	810.7	21594	2358	20046	1547	0.07165
0.4	810.7	31881	3987	28704	3177	0.09964
0.55	810.7	40444	5703	35551	4893	0.121
0.7	810.7	47576	7353	41033	6543	0.1375
0.85	810.7	53520	8867	45464	8056	0.1505
1	810.7	58474	10217	49069	9406	0.1609
1.15	810.7	62605	11399	52017	10588	0.1691
1.3	810.7	66048	12422	54437	11611	0.1758
1.45	810.7	68916	13298	56428	12488	0.1812
1.6	810.7	71304	14044	58070	13234	0.1856
1.75	810.7	73290	14675	59425	13865	0.1892
1.9	810.7	74939	15206	60543	14396	0.1921
2.05	810.7	76306	15651	61466	14841	0.1945
2.2	810.7	77438	16023	62226	15212	0.1964
2.35	810.7	78374	16332	62853	15521	0.198
2.5	810.7	79146	16589	63368	15778	0.1994
2.65	810.7	133560	34774	99596	33963	0.2543
2.8	810.7	134042	34935	99917	34125	0.2546
2.95	810.7	134426	35064	100172	34254	0.2548

The effect of the refrigerant mass flow rate is seen in Table 4.6. As the refrigerant mass flow rate is increased, the rate of heat transfer in the evaporator also increases and, consequently, the

power produced at the turbine increases. The same increase is observed for the power consumed by the refrigerant pump. However, it is observed that the highest power output of 11.489 kW was obtained at a refrigerant mass flow rate of 0.16 kg/s which can be taken as the optimum flow rate of the refrigerant at which maximum power can be generated.

Table 4.6: Variation of ORC Units and Performance with Refrigerant Mass Flow Rate

$\dot{m}_c$ [kg/s]	$\dot{W}_p$ [W]	$\dot{Q}_b$ [J]	$\dot{W}_t$ [W]	$\dot{Q}_c$ [J]	$\dot{W}_{net}$ [W]	Efficiency [%]
0.01	16.97	2847	745.1	2119	728.2	0.2558
0.06	101.8	17081	4471	12712	4369	0.2558
0.11	186.6	31268	8181	23274	7994	0.2557
0.16	271.5	45069	11760	33580	11489	0.2549
0.21	356.3	34312	7134	27534	6777	0.1975
0.26	441.1	40505	8186	32760	7745	0.1912
0.31	526	45770	8957	37339	8431	0.1842
0.36	610.8	50254	9508	41357	8897	0.177
0.41	695.6	54094	9891	44899	9195	0.17
0.46	780.5	57405	10149	48037	9368	0.1632
0.51	865.3	60282	10314	50833	9449	0.1567
0.56	950.1	62799	10411	53338	9461	0.1507
0.61	1035	65016	10458	55593	9423	0.1449
0.66	1120	66982	10468	57634	9348	0.1396
0.71	1205	68735	10452	59488	9247	0.1345
0.76	1289	70307	10417	61179	9127	0.1298
0.81	1374	71722	10368	62728	8994	0.1254
0.86	1459	73002	10311	64151	8851	0.1212
0.91	1544	74166	10247	65462	8703	0.1174
0.96	1629	75227	10181	66675	8552	0.1137

4.8 Summary

Computer based simulation and modelling as a tool in engineering has become essential and often reliable in predicting the performance of various engineering systems with known input or working parameters. Consequently, this engineering tool was adopted in analyzing the performance of an ORC system for power generation from a renewable thermal source. The simulation results of the modelled ORC system were then presented and the effects of various changes in the operating conditions of the system on its output performance were presented.

Selected performance of the system will be compared with the performance obtained from experimental investigation performed using a real life ORC system in Chapter 5.

CHAPTER 5 : EXPERIMENTAL INVESTIGATION

5.1 Introduction

This chapter presents the laboratory experiment using an ORC IT10 Infinity Turbine system with a maximum possible power generating capacity of 10 kW supplied by Global Energy and Infinity Turbine LLC Madison, Wisconsin, USA. The experiment was conducted at the Mechanical Engineering laboratory of the Howard College Campus of the University of KwaZulu-Natal, Durban using an ORC system with a simulated Heat Transfer Fluid system of a typical geothermal resource. The effectiveness of the ORC in harnessing and converting low-grade waste heat energy into power for domestic application is investigated. The heat source characteristics was substituted using a hot water geyser whose temperature rise was restricted with the aid of a thermo-regulator to 80^0C, typical of temperature profiles of a geothermal resource found in Limpopo province, South Africa [35].

5.2 Detailed Description of Experimental Setup Units

The experimental setup comprises of two different units, the hot water geyser (heat source) and the main ORC system. Both units are described in details in subsections 5.2.1 and 5.2.2.

5.2.1 Description of the Hot Water Geyser System

The heat source adopted is a hot water geyser supplied by Kwikot (Pty) Ltd, Durban, South Africa. The geyser unit has a volume capacity of 450 liters which was connected to a 3-phase circuit main for this laboratory experiment [48]. The HTF temperature within the geyser was restricted to a maximum temperature of 353K (80^0C) with the aid of a thermostat supplied by Wire-Ohms, Durban, South Africa. The hot water geyser is connected to the evaporator heat exchanger through a flexible hot water hose which facilitates the flow of the HTF from the geyser to the evaporator for the system heat transfer. An in-line hot water circulation pump is installed along the hose to aid in the circulation of the HTF from the geyser to the evaporator by providing additional pressure to the HTF. The cross-section of the heat source (hot water geyser) can be seen in Figure 5.1.

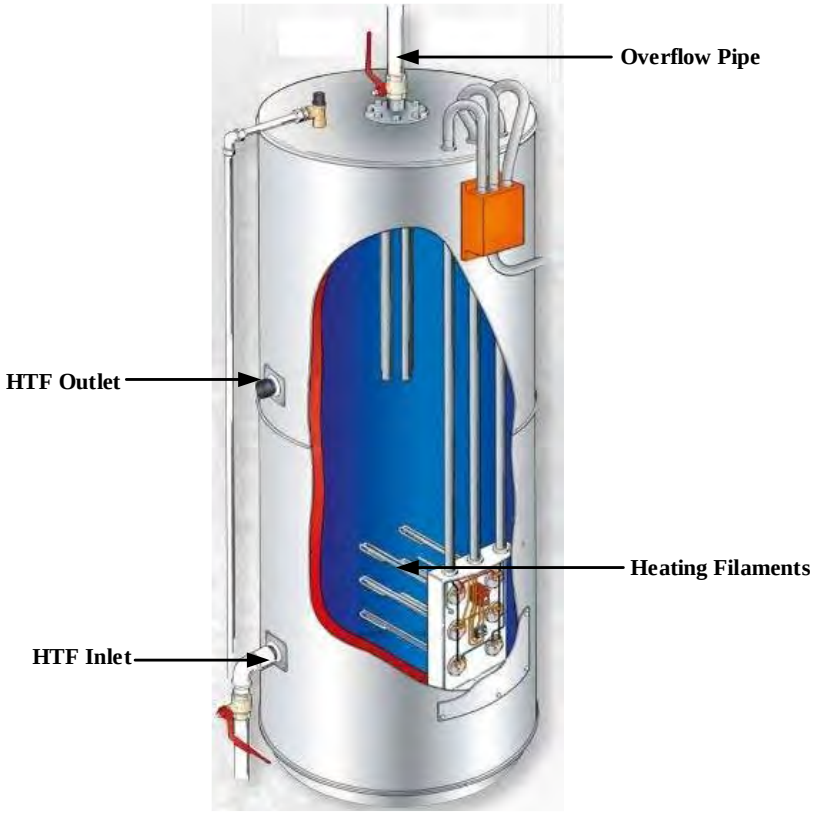

Figure 5.1 Cross-section of the Heat Source (Hot Water Geyser)

5.2.2 Description and Details of the IT10 ORC

The ORC system designed for this research has four basic components and was supplied by Global Energy and Infinity Turbine. There was no further installation required other than to connect the desired heat source, heat sink and provide an electrical load for utilizing the power generated. The installed heat exchangers are flat plate and the turbine is a radial (IFR 90^0) Turbine [49]. The refrigerant pump is powered by a programmable Titan C series sensor-less / space vector control which is connected to AC mains in the laboratory [50]. Figure 5.2 shows the IT10 ORC unit detailing its component parts.

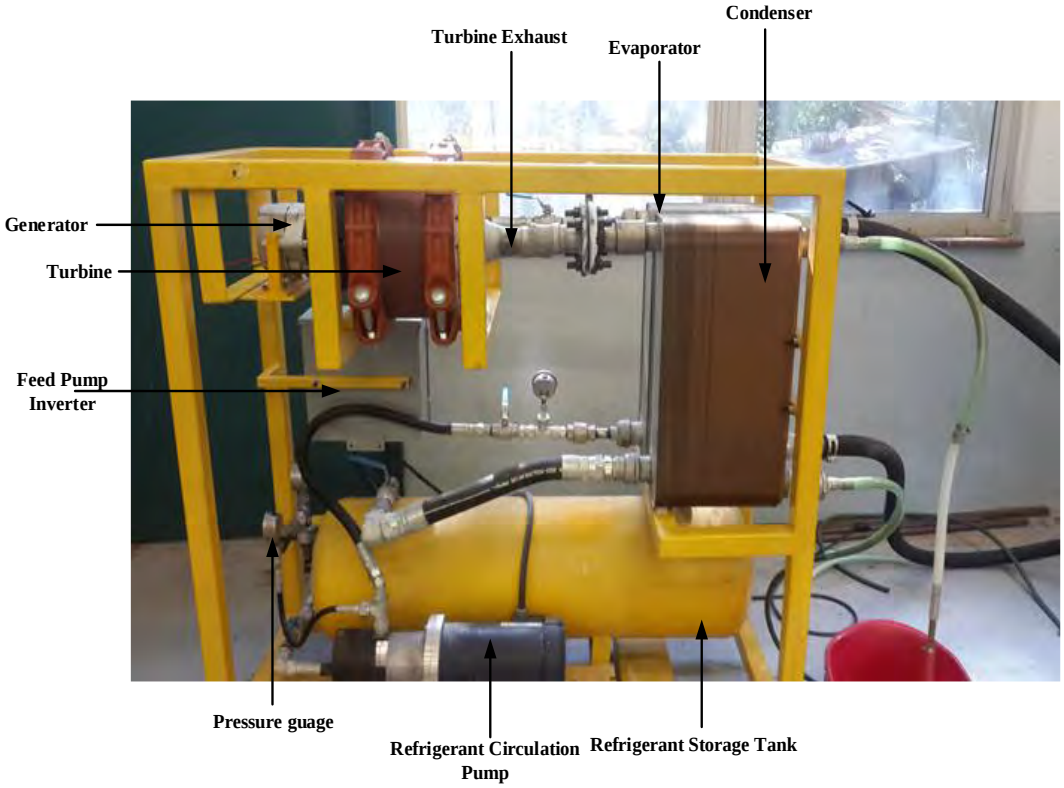

Figure 5.2: IT10 Organic Rankine Cycle Unit

5.3 Cycles in the Experimental Setup

The experiment consists of three cycles through which the HTF, Working Fluid (WF) and Cooling Fluid (CF) flows. These cycles are further explained in the next subsections.

5.3.1 The Heat Transfer Fluid (HTF) Cycle

The HTF (hot water) flows from the geyser into the connecting hot water pipe, through a hot water circulation pump for additional pressure as it makes its way into the evaporator. At the evaporator, it interacts with the WF transferring thermal energy to it through convection. The flow pattern of both the HTF and the WF within the evaporator is counter-current to each other and they do not mix. The HTF exits the evaporator heat exchanger depleted of thermal energy and is returned to the hot water geyser to be re-heated to complete the cycle. Figure 5.3 shows the schematic representation of the HTF cycle.

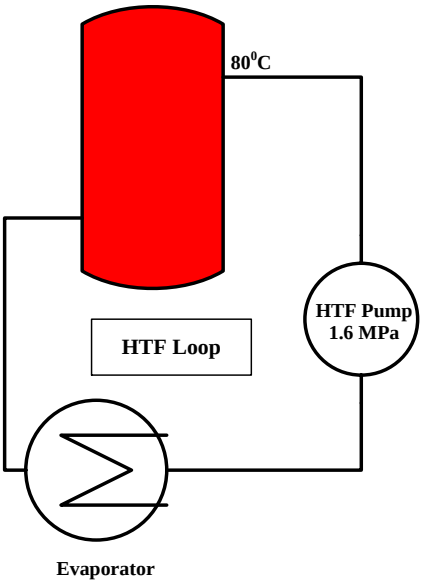

Figure 5.3 Schematic of the HTF Cycle

5.3.2 The Working Fluid (WF) Cycle

The WF adopted for the experimental investigation was the R-134a refrigerant. This was an acceptable alternative to R-245fa as suggested by the IT10 supplier [49]. The WF moves from storage and is pumped by the refrigerant pump into the evaporator unit where its temperature is raised and there a phase change from liquid to vapor phase occurs. In vapor phase, the refrigerant moves into the turbine where it is expanded and work is done at the turbine. The WF leaves the turbine and proceeds to the condenser where heat is removed, its temperature is further reduced, and a phase change to liquid state occurs. The WF is passed from the condenser into the storage tank and the cycle is repeated. Figure 5.4 shows a schematic layout of the WF cycle.

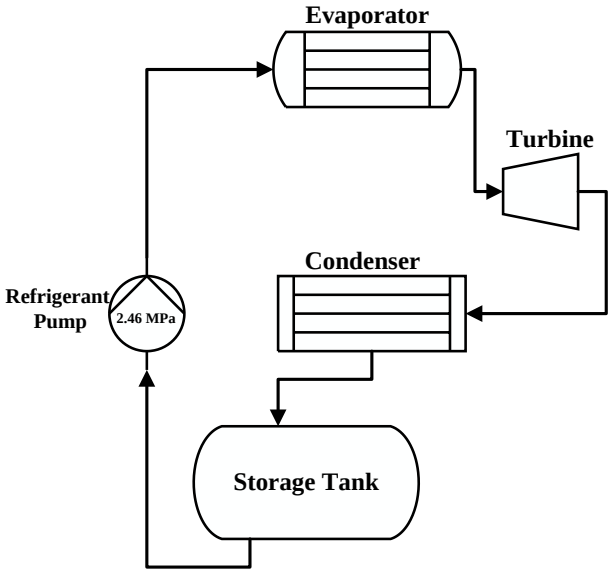

Figure 5.4 Schematic Layout of the WF cycle

5.3.3 The Cooling Fluid (CF) Cycle

The CF cycle, unlike the other two cycles which are closed cycles, is an open flow cycle, with water as the cooling fluid. The cooling fluid (water) at room temperature (23^0C) is released from the mains and allowed to run through the condenser. The CF absorbs heat from the WF in the condenser through a convection process and the heat-laden CF is expelled at the condenser exit through a discharge pipe outside the operating area as shown schematically in Figure 5.5.

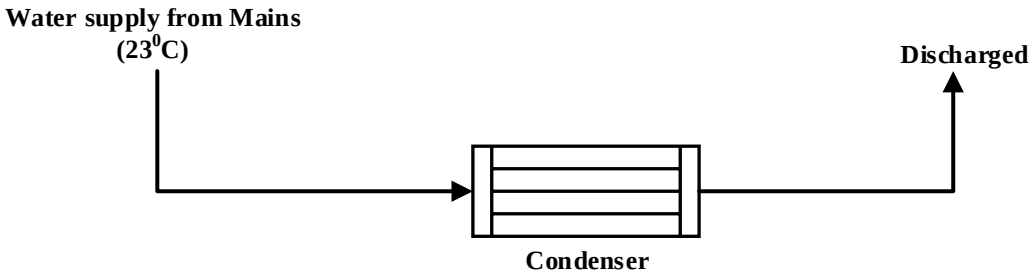

Figure 5.5 Schematic of Cooling Fluid Cycle

5.4 Experimental Methodology

The experimental methodology for this research is divided into three main processes which include: leak testing of the ORC system, charging of the refrigerant into the system storage, and experimentation. The leak test procedures are explained in subsection 5.4.1. Subsection 5.4.2 details the charging procedures for the refrigerant while experimentation and analysis of experimental data is contained in subsection 5.4.3.

5.4.1 Leak Testing on the ORC System

The ORC operates on a principle of constant volume, viz, at no point during the operation of the ORC setup should there be a decrease in the volume of the refrigerant used. To ensure this, the piping joints and connecting hoses of the ORC system were inspected physically after which four leakage test procedures were performed on the system to ensure it is leak-free.

5.4.1.1 Air Leak Test

The purpose of this test and other leak tests is to ensure that there is no loss of refrigerant to the surrounding from any joint or vessel of the ORC system. After properly tightening all the joints and hoses on the ORC and ensuring no physical damage exists, the ORC system was filled with atmospheric air up to a maximum of 690 kPa (100 psi). The pressurized unit was monitored for 3 hours to detect any leaks within the system components or the joints. The air leak test produced a satisfactory result with no significant change in the pressure reading at the start and at the end of the test. Figure 5.6 shows the air compressor used to supply compressed air to the ORC system.

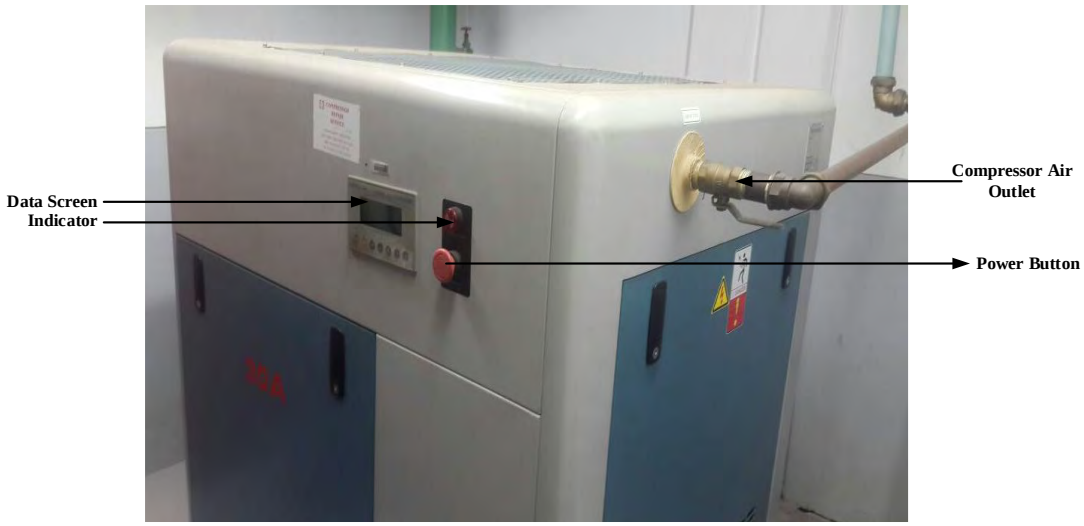

Figure 5.6 Air Compressor Unit

5.4.1.2 Nitrogen Leak Test

The second stage of the leak test involves the use of nitrogen gas to pressurize the ORC system to check for tiny leaks which might have gone undetected by the air leak test. The air was evacuated from the system and nitrogen gas was pumped into the system at a pressure of 1034 kPa (150 psi). The pressurized system was then observed for 24 hours to check for a drop in system pressure resulting from leak. On first observation, it was observed that there was a decrease in system pressure and loss of the gas to the surrounding due to leaks within the system. With a suitable amount of gas within the system, the bolts, joints, pipes and vessels such as exchangers, storage tanks, and turbine flanges were examined for leakages by applying soapy solution across them. Escaping gas from the system produced air bubbles around points of leaks such as the joints which were consequently tightened. More nitrogen gas was added to the system to make up for the losses and the system pressure increased to the required test pressure of 1034 kPa and observed for 24 hours. On the second observation, the system unit was determined leak-free, after which the nitrogen gas was recovered into the nitrogen cylinder. The setup of the nitrogen cylinder for this test is as shown in Figure 5.7.

Figure 5.7: Nitrogen Charging Setup

5.4.1.3 Ultrasonic Leak Test

Having satisfied the Nitrogen leak test, the system is then filled with dry Nitrogen gas at a pressure of 860 kPa and subjected to an ultrasonic leak detector. There was no leak detected in the system or its joints thereby ensuring conservation of fluid throughout the system operation.

5.4.1.4 Vacuuming

After recovery of the nitrogen gas from the system, the system is then vacuumed to remove remaining traces of nitrogen gas and / or moisture within the system. This procedure is carried out using a vacuum pump. Figure 5.8 shows the vacuuming unit. The system is vacuumed to a pressure less than 500 microns (mercury) by connecting the vacuum pump to the system and setting it in operation for 24 hours. The vacuum pump is switched off and disconnected and the gauge observed for 10 minutes to check for pressure change. The system was then asserted tight as it was observed that there was no increase in pressure within the system after observation. The system was determined to be moisture free making way for the next phase of experimentation.

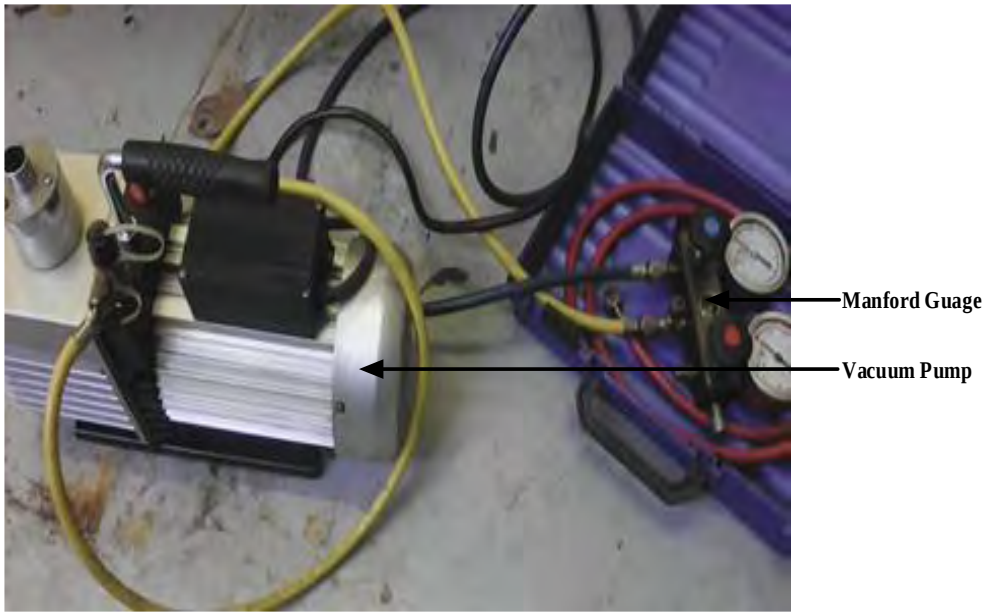

Figure 5.8: System Vacuuming Pump Setup

5.4.2 Refrigerant Charging

The ORC system is such that the working fluid begins the cycle in a liquid state. As a result, the R134a refrigerant has to be charged into the system storage in a liquid state. The necessity of this detail informs the charging method and/or procedure used in feeding the refrigerant into the ORC system. To ensure the proper state phase of the refrigerant during charging, the gravity mode of charging was adopted as shown in Figure 5.9. The ORC reservoir was charged with 58 kg of the R134a refrigerant and the system was ready to be run.

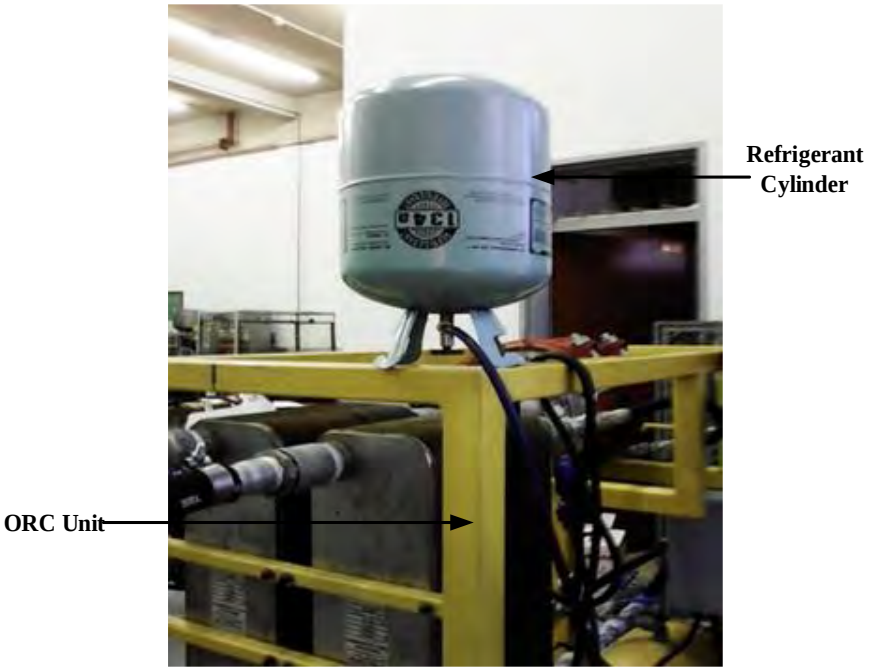

Figure 5.9: Refrigerant Charging

5.4.3 Experimental Result and Analysis

The geyser is switched on and the HTF temperature rises to the maximum of 80^0C. The exit valve of the geyser is opened and the heated HTF is allowed to flow through the circulation pump in the HTF loop. The pump is switched on to provide additional pressure for the fluid as it passes through the evaporator and finally into the geyser where it is reheated, thus completing the HTF cycle.

The ORC system valves are opened to allow the refrigerant to fill the system. The system / refrigerant circulation pump is switched on and programmed to the desired operating pressures. The ORC system starts as the refrigerant is pumped from the system storage through the circulation pump into the evaporator. At the evaporator, heat energy is transferred to the working fluid from interaction with the HTF thereby causing the refrigerant to gain energy and change phase into saturated vapor. The vaporized refrigerant then enters the turbine causing the rotation of the turbine blades. This mechanical energy is then converted into power by the generator which is coupled to the turbine through a shaft. The schematic diagram for the experimental setup is presented in Figure 5.10 showing the three fluid cycles, the HTF storage and the ORC system unit.

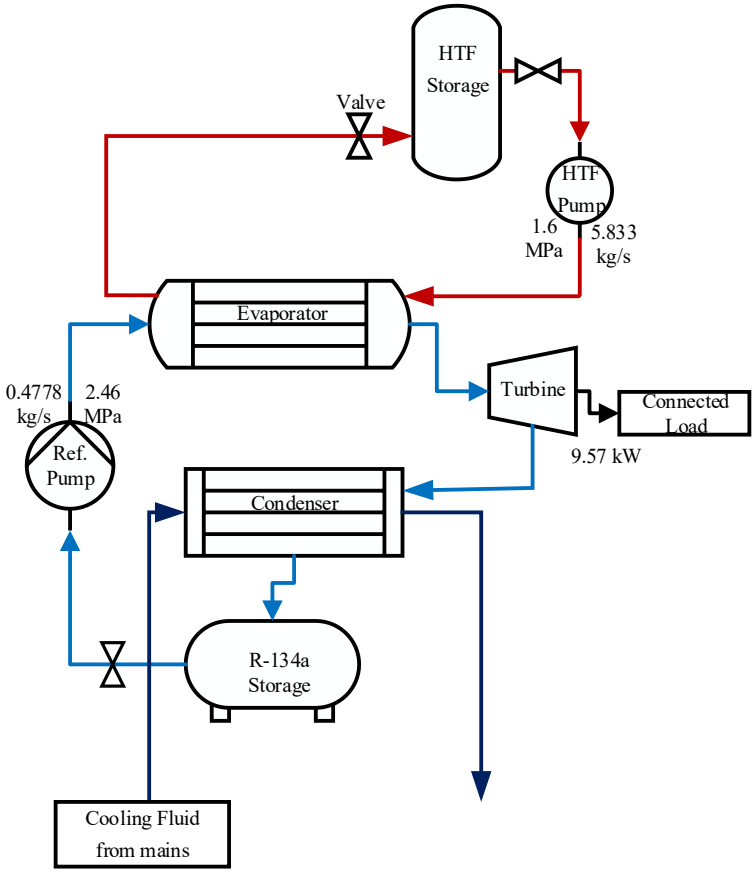

Figure 5.10: Schematic Diagram of Experimental Setup

Having a programmable Titan series refrigerant pump as part of its component, the variable input for the IT10 ORC system is the system operating pressure which was varied as the HTF source temperature is held constant at 80^0C. The time taken for the HTF to attain maximum temperature within the geyser is observed and recorded in subsection 5.4.3.1. Rotational speed of the turbine blade, the torque produced and the power generated at the different system pressure values are obtained by means of auxiliary equipment. The influence of the system working pressure on system outputs is discussed in subsections 5.4.3.2 to 5.4.3.4.

5.4.3.1 Rise in HTF Temperature

The temperature of the HTF is raised from room temperature (23 ^{0}C) to 80 ^{0}C within the geyser and the rise in temperature is measured against the time taken as shown in Figure 5.11 by using an infrared thermo-gun.

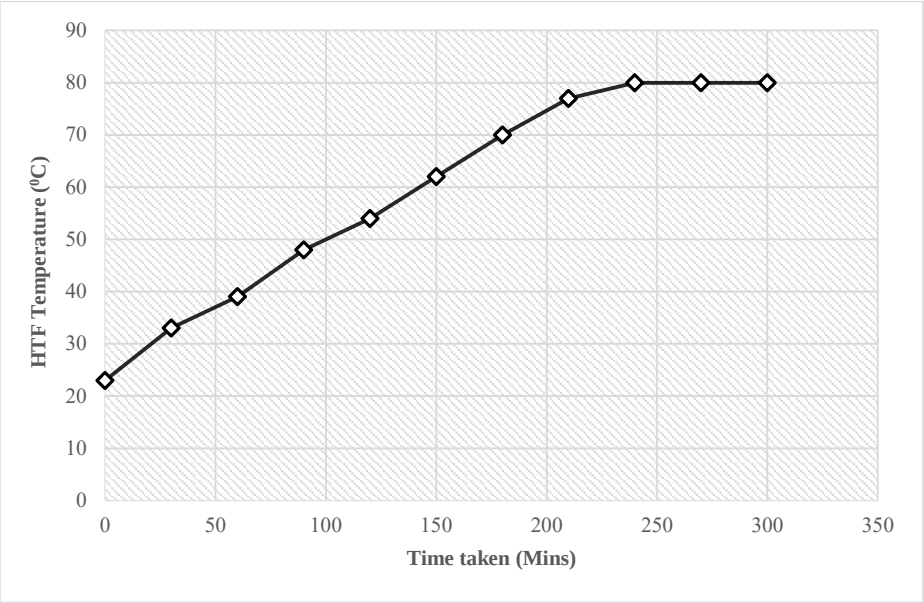

Figure 5.11: Rise in HTF Temperature with Time

The study of the temperature profile of a potential renewable heat source can help determine how much power can be generated from it. The choice of working fluid that best suits the ORC operation can also depend on the temperature profile study.

5.4.3.2 Influence of System Working Pressure on Rotational Speed

The speed at which the turbine blade rotates is dependent on the pressure with which the refrigerant enters the turbine. The speed of rotation is measure by directing a laser beam tachometer at the exposed end of the shaft connected to the turbine blade. Readings are taken from the digital display on the tachometer and recorded for varying values of system working fluid pressure. This relationship is shown by the plot on Figure 5.12.

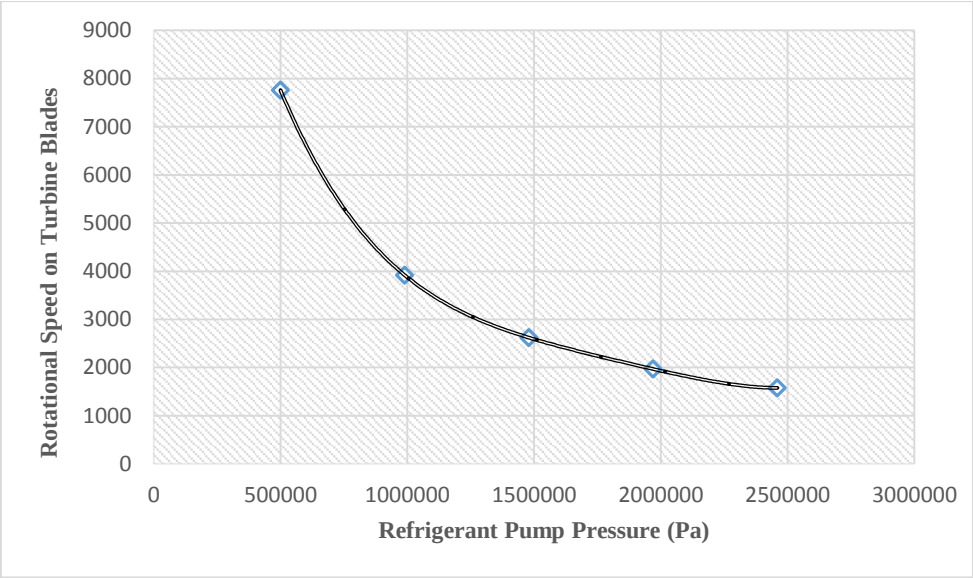

Figure 5.12: Variation of Rotational Speed of Turbine with Refrigerant Pressure

From Figure 5.11, it is deduced that the turbine speed decreases with subsequent increase in the system operating pressure. The equation of best fit for the plot is given as;

$$y = 10^{-21}x^4 - 8 * 10^{-15}x^3 + 2 * 10^{-8}x^2 - 0.0296x + 17841 \qquad 5.1$$

Where x and y represents the values of the system operating pressure and the corresponding turbine speed respectively. The coefficient of determination (R^2) value of 1 obtained for Equation 5.1 shows that other values of rotational speed for the system can be predicted with known value of operational pressure of the ORC system should other parameter remain unchanged.

5.4.3.3 Influence of System Working Pressure on Torque

The torque generated by the rotation of the blade in the turbine is also dependent on the system working pressure. This can be established by the mathematical relationship represented by Equation 5.2.

$$\tau = F * D_t \qquad 5.2$$

Where τ is Torque on Turbine blades and D_t is Turbine Blade diameter.

Figure 5.13 shows how the system working pressure affects the torque generated at the turbine blades.

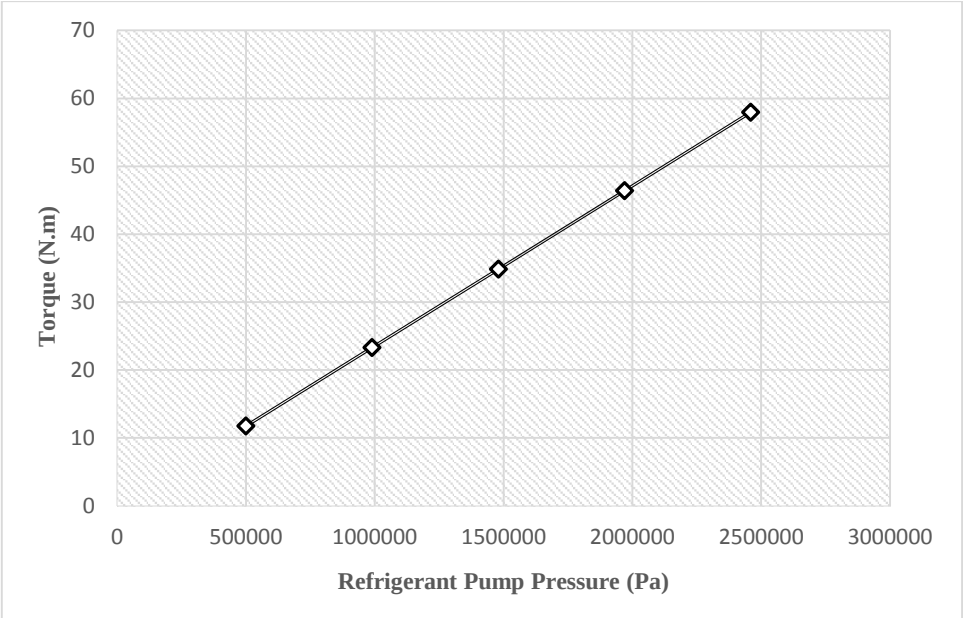

Figure 5.13: Variation of Torque with Refrigerant Pressure

From calculations, it can be seen that the relationship between the torque and the system operating pressure is represented by the linear equation in Equation 5.3. The coefficient of determination (R^2) value of 1 shows the equation's reliability to predict other values of torque given known values on system working pressure.

$$y = 2 * 10^{-5}x + 0.0014 \qquad 5.3$$

Where x and y represents the values of the system operating pressure and the corresponding torque on turbine blades.

5.4.3.4 Influence of System Working Pressure on Power

The IT10 infinity turbine was designed to generate 10 kW of power from renewable heat source. However, the output power generated is largely dependent on the pressure at which the system operates. The value of output power calculated by taking the current and voltage reading on a multi-meter connected to the contact points of the generator at different system operating pressures. This is represented on the plot shown in Figure 5.14.

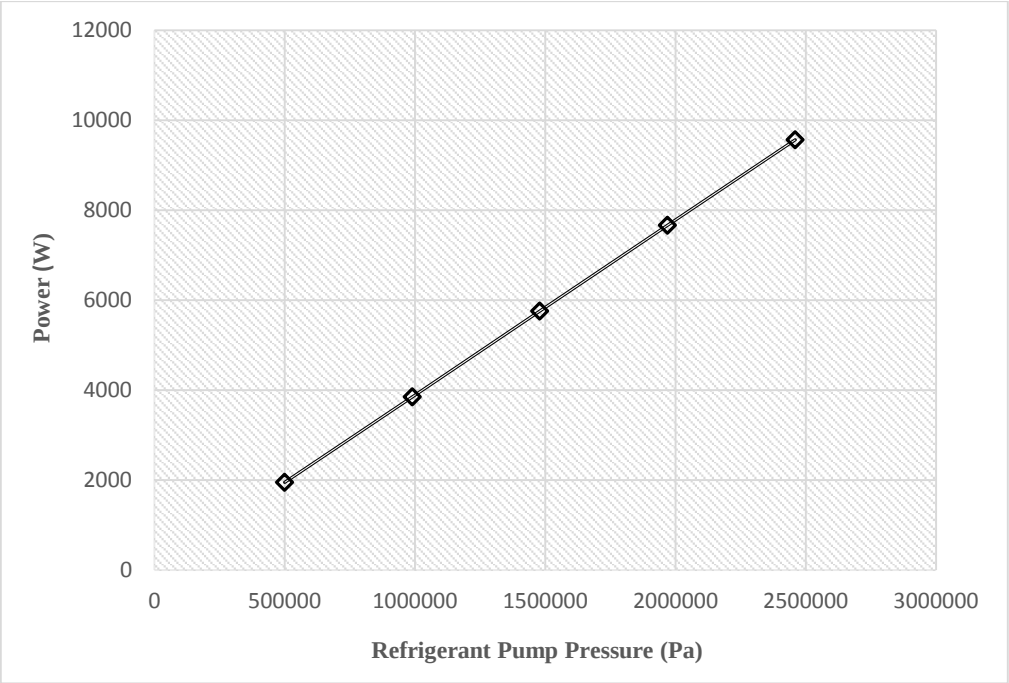

Figure 5.14: Variation of Power with Refrigerant Pressure

The plot shown in Figure 5.14 indicates that there is a linear relationship between the operating system pressure and the power generated by the turbine. This relationship is further presented by Equation 5.4

$$y = 0.0039x + 1.2 \qquad 5.4$$

Where x and y represents the values of the system operating pressure and the corresponding power output at the turbine. The Equation 5.4 has coefficient of determination (R^2) value of 1 suggesting its suitability in predicting other values of turbine power when values of pressures are known.

5.4.3.5 Influence of Power Output on Turbine Speed

Figure 5.15 shows increase in the load connected to the generator result to a proportional increase in the power generated which also increases the speed of rotation of turbine blades. This plot is similar to the plot obtained from the IT10 manufacturer shown in Figure 5.16. The equation for the plot in Figure 5.15 is given as;

$$y = 0.1648x - 0.0079 \qquad 5.5$$

The coefficient of determination (R^2) value of 1 indicates that values of turbine speed can be determined with known values of the generator power output using Equation 5.5

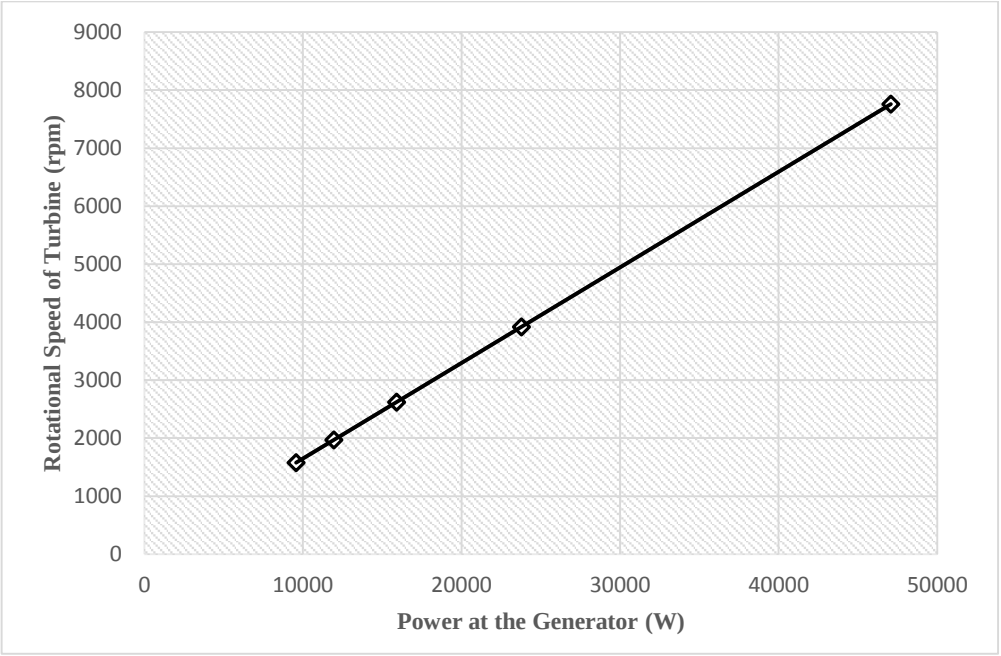

Figure 5.15: Generator Power versus Turbine Speed

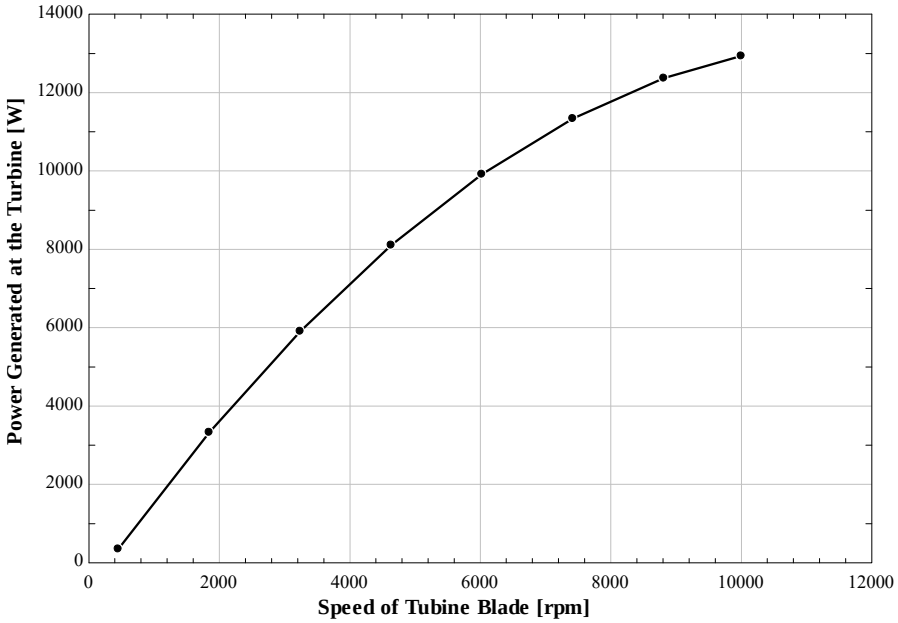

Figure 5.16: Turbine Speed and Generator Characteristics [49]

5.4.3.6 Electrical Load Connection and Measurements

The electrical load measurement connected to the ORC generator was taken at various working pressures of the system with the aid of AC voltmeter at the generator end, DC voltmeter and DC ammeter at the load end. The electrical circuit and load connection is shown in Figure 5.17.

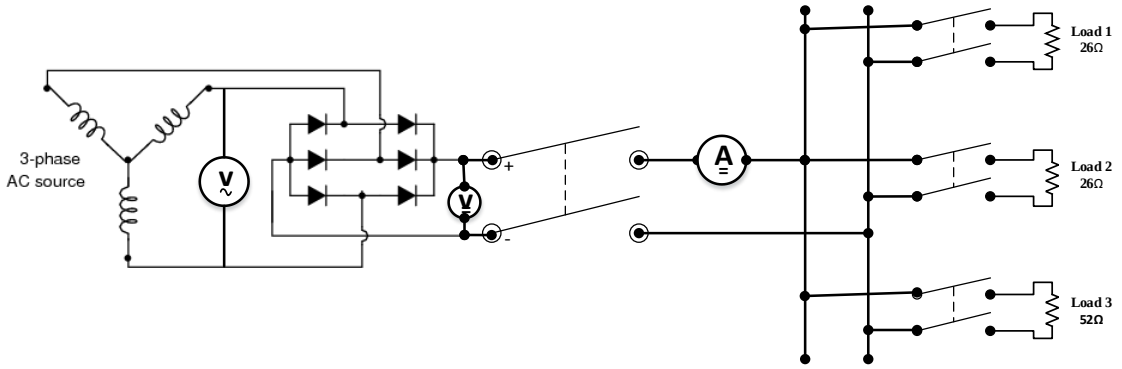

Figure 5.17: Schematic Showing the Load Connection on the ORC

At each system working pressure, a load, or combination of loads are added by closing the switch of the load circuit. The load adopted was three immersion electric heating elements connected in a parallel circuit to use the power produced at the generator. They are identified as 'Load 1', 'Load 2' and 'Load 3' as shown in Figure 5.16.

Load 1 and Load 2 both have 26 Ω resistance each while Load 3 has a resistance of 53 Ω. At system operating pressure of 0.5 MPa, Load 1 alone is connected and an ammeter reading of 8.65 A was obtained. Load 1 and Load 3 were connected in parallel to give a combined resistance of 17.46 Ω and an ammeter reading of 10.66 A was obtained. Load 1 and Load 2 were connected in parallel to give a combined resistance of 13 Ω and an ammeter reading of 12.24 A. Finally, all three loads were connected in parallel to give a combined resistance of 10.43 Ω and an ammeter reading of 13.66 A. This process is then repeated for the different operating pressures. Figure 5.18 shows how the current varies with load resistance at different system operating pressures.

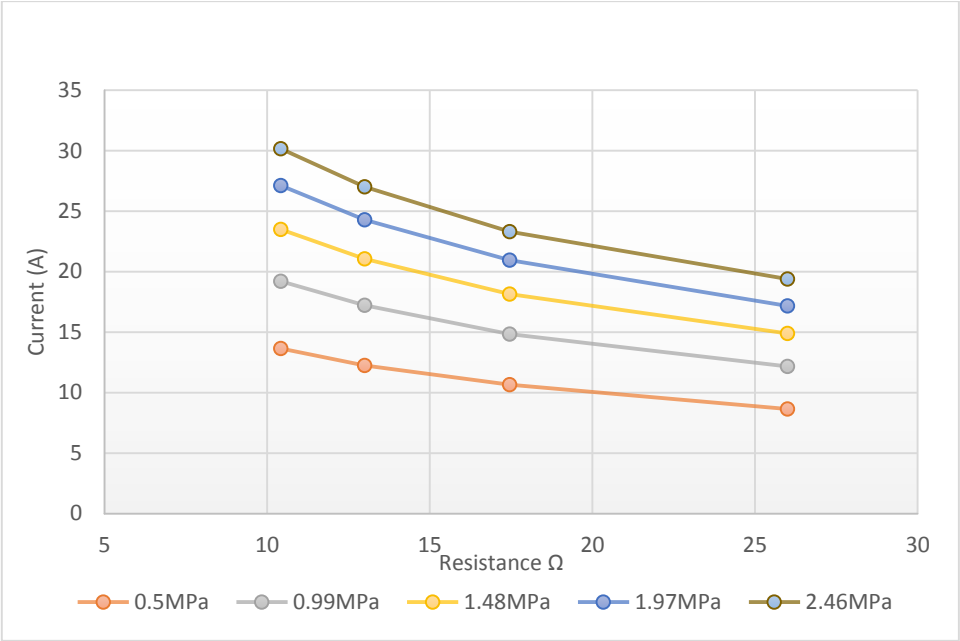

Figure 5.18: Current Variation with Load Resistance at Different System Operating Pressures

From Figure 5.18, it is observed that an increase in load connected results in a decrease in resistance provided by the load thereby causing an increase in the current consumed by the heating element. A combination of different load results in a decreased value of resistance provided which then results in greater flow of current to the heating elements. These processes are repeated at different system operating pressures. The increase in the system operating pressure results in an increase in power produced at the generator, hence, the current supply to the heating element is also increased.

5.5 Model Validation with Experimental Results

A model for an ORC was developed as part of the methodological approach in this research. The model considered various operating parameters which are obtainable in the components of an ideal ORC system. Furthermore, the properties of the refrigerant fluid and the HTF were monitored at critical state points within the system. The performance of this model was then determined through simulation and the results are presented in Chapter 4 of this dissertation.

The experimental investigation using a real life ORC system and an improvised heat source was carried out using an Infinity Turbine IT10 ORC model. The operating conditions of refrigerant type, heat source temperature and refrigerant pressure from the model were adopted as input parameters for the experimental investigation. The correlation between the model system

performance and experimental system performance are discussed in Section 5.5.1 to Section 5.5.3.

5.5.1 System Refrigerant Pressure against Rotational Speed of Turbine blade

The output of the speed of rotation at the turbine is plotted against the refrigerant pressure operating within the system for the model and the experimental investigation as shown in Figure 5.19. The simulation result from the model showed a decrease in rotational speed of the turbine from 19600 rpm to 8000 rpm as the pressure is varied from 0.5 MPa to 1 MPa, while at the same range of operating pressure, the experimental outcome of turbine speed decreases from 6500 rpm to 4500 rpm. The divergence in the simulation and experimental outputs of the rotational speed as the pressure increases from 0.5 MPa to 1.5 MPa is due to variable input parameters which had a greater degree of control while developing and running the simulation model but which are not so easily controlled on the prototype IT10 ORC system available for the experiment.

However, as the refrigerant operating pressure is increases from 1.9 MPa to 4 MPa, the rotational speed of the turbine blades for both the model and the experiment show a strong correlation as seen in Figure 5.19.

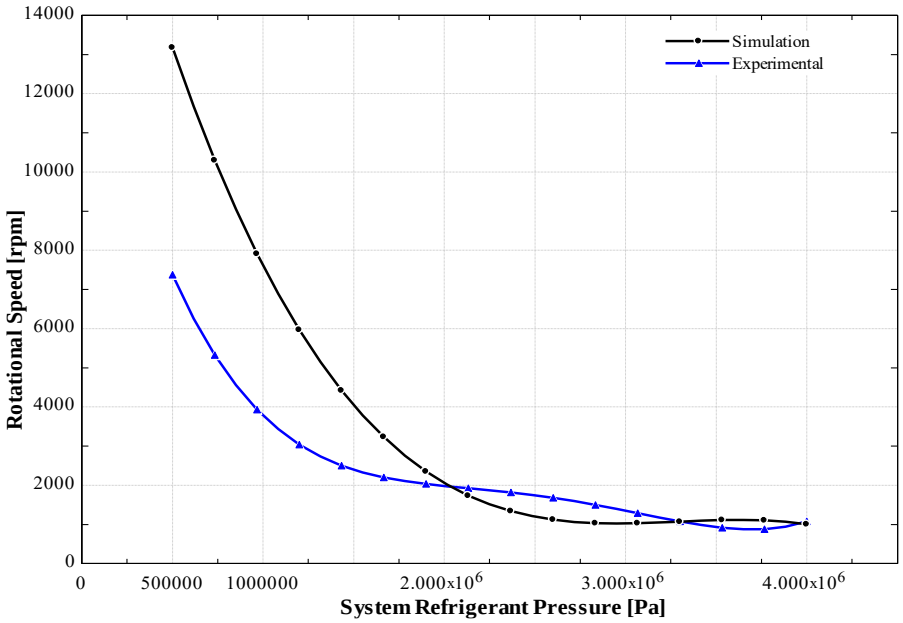

Figure 5.19: Model Validation for Rotational Speed of Turbine blade

This shows the reliability of the model in determining the performance operation of the ORC turbine at system operating pressure range of 1.9 MPa to 4 MPa.

5.5.2 System Refrigerant Pressure against Torque

The values torque generated at the turbine is observed to increase for both the simulation model and the experimental investigation for increasing values of pressures from 0.5 MPa to 4 MPa as shown in Figure 5.20.

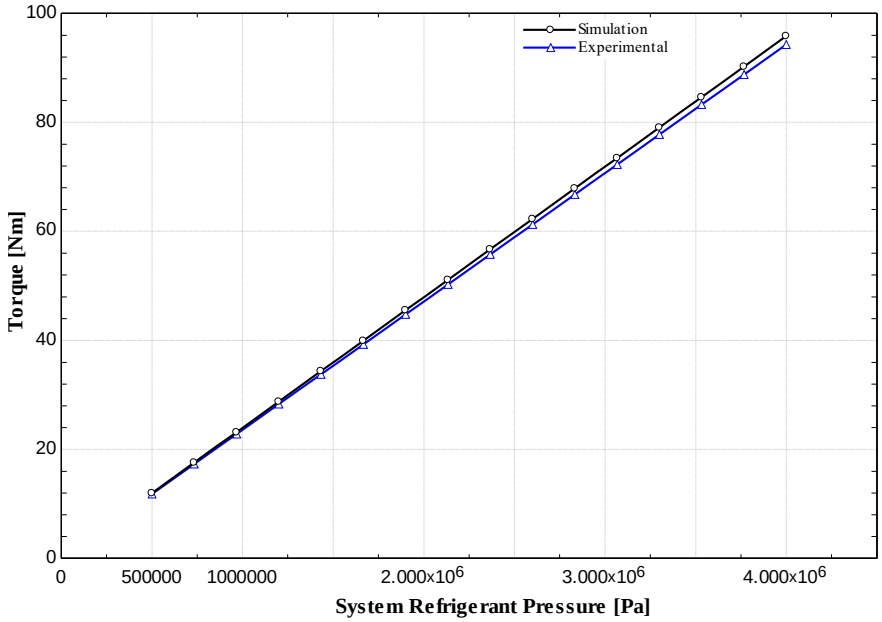

Figure 5.20: Model Validation for Torque Produced at the Turbine

The model shows that the torque produced increases from 11.98 Nm to 95.82 Nm when the pressure is increased from 0.5 MPa to 4 MPa, while for the same variation of refrigerant pressure operating within the system, the experimental investigation shows a linear increase in the torque generated at the turbine from 11.78 Nm to 94.25 Nm. The agreement between the outcomes of the torque values obtained from the model and the values of torque generated through experimental investigation further shows the validity of the ORC model developed.

5.5.3 Power Output against Turbine Speed

The relationship between the rotational speed of the turbine blade and the net power of the ORC system is linear, that is, as the rotational speed of the blades about the shaft increases, there is a

proportional increase in the power obtained at the generator. This relationship holds true for outputs from both the model simulation and the experimental investigation as can be observed in Figure 5.21.

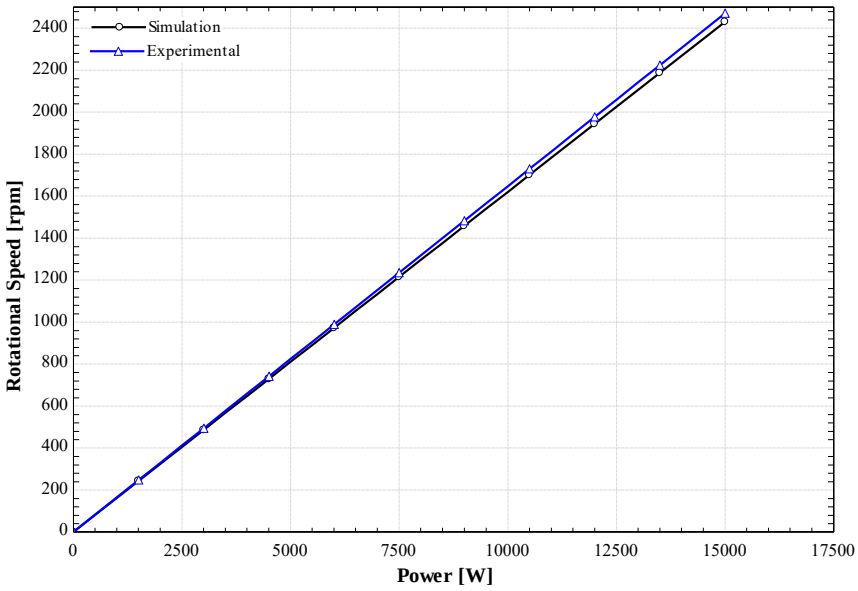

Figure 5.21: Model Validation for Power Output versus Turbine Speed

The model presented shows how the rotational speed of the turbine blade increases linearly from 0 rpm to 2431 rpm when net power produced by the ORC system increase from 0 kW to 15 kW. Similarly, for the same variation of net power produced by the ORC system, the experimental investigation also shows linear increase in the rotational speed of the turbine blade from 0 rpm to 2471 rpm. Similarities in values obtained from the performance of the ORC model and the experimental investigation presented in Figure 5.21, further shows the reliability of the research model presented in Chapter 3 in determining the relationship between the rotational speed of the turbine blades and the power produced at the generator of the IT10 ORC system.

5.6 Summary

The outcome of the experimental investigation presented in this Chapter allude to the fact that power generation from low thermal sources using the ORC system is obtainable and also sustainable. The IT10 ORC system from Infinity Turbine are obtained and installed to generate power as required for domestic as well as industrial use, sustainably.

The IT10 is designed to have a power generating capacity of 10 kW from renewable heat energy source. The experimental investigation conducted shows that the system generated a power output of 9.57 kW at a system working pressure of 2.46 MPa and an HTF temperature of 80^0C. Rural and satellite regions which are off grid can benefit from this technology by harnessing the renewable energy resources located around them using the Rankine technology.

Power generation from renewable and sustainable source are taking central focus in the energy industries globally. In South Africa, plans are ongoing to introduce alternative energy sources in form of nuclear power to replace the traditional power source which is coal. Although this is a step in the right direction, the potentials inherent in the other sources with low to medium thermal contents such as waste heat and geothermal sources in producing renewable energy for domestic and industrial usage, are yet to be fully maximized. Power generation from these green sources using the ORC technology, proposes to further serve as long term solution to the energy crises faced by increased industrialization in developed and developing nations.

The agreements between the simulation performance presented in chapter 4 and the performance of the ORC system from experiments in this Chapter shows that the model developed and presented in Chapter 3 holds a high degree of reliability.

CHAPTER 6 : CONCLUSIONS AND RECOMMENDATIONS

6.1 Conclusions

This study has presented the findings of the power generating capacity of ORC system from a renewable energy source and also the performance of a computer-based simulation of an ORC system given different operating conditions. The advantages of harnessing energy from these alternate energy sources cannot be over emphasized given the current trend in global climatic changes. Among the various techniques available today for harnessing green energy, the recovery of thermal heat from the earth through the use of the Rankine cycle technology using organic fluid as refrigerant was adopted. A major advantage in the use of organic refrigerant as working fluid, as compared to water, is its low boiling temperature which allows for a low system operational temperature. This impacts positively on overall cost of generation of renewable energy using the ORC technology. Other factors such as ozone layer friendliness and less negative environmental impact, also lend credibility to the use of organic refrigerant.

In line with the objectives set out for this study, a generic model of an ORC system which can be used to determine the amount of power that can be harnessed from renewable sources was developed and presented. The optimum operating parameters of pressure and flowrate for the refrigerant's circulation pump and the optimum HTA for the evaporator was presented. The agreement between obtained output power from the model and that obtained from David, et al. [33] when the same input parameters were used further gave credit to the model. Furthermore experimental outputs of the IT10 Infinity Turbine obtained from laboratory investigation shows that ORC technology can be utilized in power generation from renewable sources thereby reducing adverse impact on the environment to the barest minimum, among other benefits as stated in Section 1.3.

Outcomes from this research study shows that communities with inadequate supply of power from the national grid can be directly impacted from the development of this technology by generating their own power from available renewable sources using the ORC, and perhaps also feed the excess into the national grid. It is important to note that the global energy trend is shifting from conventional energy source to more green and eco-friendly sources. Consequently, research on how these green sources can be harnessed and maximally utilized becomes vital.

6.2 Recommendations

On the basis of the challenges encountered during the course of this extensive research, the following recommendations are made:

- That proper instrumentation should be incorporated to the ORC system to allow for more accurate reading of input data and working fluid properties at various points within the system.
- That recommended refrigerant be made available for future experimental investigation using the IT10 ORC system.
- That an auxiliary load setup capable of accurately measuring various system output while also providing discharge of generated power be made available for future operation.

The results obtained in this research shows a high thermal energy potential of the heat transfer fluid after its first cycle. This high thermal energy can be further harnessed for domestic use in the form of domestic washing, or underfloor heating and can also serve as a heat source in a two-phased ORC system.

REFERENCES

[1] B. F. Tchanche, "Low-Grade Heat Conversion Into Power Using Small Scale Organic Rankine Cycles," Ph.D, Department of Natural Resources And Agricultural Engineering, Agricultural University of Athens, 2010.

[2] K. Li, H. Bian, C. Liu, D. Zhang, and Y. Yang, "Comparison of geothermal with solar and wind power generation systems," *Renewable and Sustainable Energy Reviews,* vol. 42, pp. 1464-1474, 2015.

[3] REN21, "RENEWABLES2014 Global Status Report," Renewable Energy Policy Network 2014.

[4] R. ElSayed, E. A. Shalaby, and M. A. Karim, "Life cycle analysis as a tool of pollution prevention," *Polymer-Plastics Technology and Engineering,* vol. 43, pp. 1601-1616, 2004.

[5] P. Viebahn, S. Kronshage, F. Trieb, and Y. Lechon, "Final Report on Technical Data, Costs and Life Cycle Inventories of Solar Thermal Power Plants," German Aerospace Center (DLR). Centre in Energy, Environment and Technology (CIEMAT)2008.

[6] B. Saadatfar, R. Fakhrai, and TorstenFransson, "Waste heat recovery Organic Rankine cycles in sustainable energy conversion: A state-of-the-art review," *The Journal of MacroTrends in Energy and Sustainability,* vol. 1, 2013.

[7] G. Qiu, Y. Shao, J. Li, H. Liu, and S. B. Riffat, "Experimental investigation of a biomass-fired ORC-based micro-CHP for domestic applications," *Fuel,* vol. 96, pp. 374-382, 2012.

[8] J. Hnat, J. Patten, J. Cutting, and L. Bartone, "Industrial heat recovery with organic Rankine cycles," 1982.

[9] T. Yamamoto, T. Furuhata, N. Arai, and K. Mori, "Design and testing of the Organic Rankine Cycle," *Energy,* vol. 26, pp. 239-251, 2001.

[10] V. Minea, "Power generation with ORC machines using low-grade waste heat or renewable energy," *Applied Thermal Engineering,* vol. 69, pp. 143-154, 2014.

[11] W. Gu, Y. Weng, Y. Wang, and B. Zheng, "Theoretical and experimental investigation of an organic Rankine cycle for a waste heat recovery system," *Proceedings of the Institution of Mechanical Engineers, Part A: Journal of Power and Energy,* vol. 223, pp. 523-533, 2009.

[12] M. T. Dunham and B. D. Iverson, "High-efficiency thermodynamic power cycles for concentrated solar power systems," *Renewable and Sustainable Energy Reviews,* vol. 30, pp. 758-770, 2014.

[13] R. Kapooria, S. Kumar, and K. Kasana, "An analysis of a thermal power plant working on a rankine cycle: A theoretical investigation," *Journal of Energy in Southern Africa,* vol. 19, pp. 77-83, 2008.

[14] S. Quoilin and V. Lemort, "The Organic Rankine Cycle: Thermodynamics, Applications and Optimization," ed Oxford, UK: UNESCO-EOLSS Publishers, 2011.

[15] S. Masheiti, B. Agnew, and S. Walker, "An Evaluation of R134a and R245fa as the Working Fluid in an Organic Rankine Cycle Energized from a Low Temperature Geothermal Energy Source," *Journal of Energy and Power Engineering,* vol. 5, pp. 392-402, 2011.

[16] H. Leibowitz, I. Smith, and N. Stosic, "Cost effective small scale ORC systems for power recovery from low grade heat sources," in *International Mechanical Engineering Congress and Exposition ASME*, 2006, pp. 521-527.

[17] J. B. Obi, "State of Art on ORC Applications for Waste Heat Recovery and Micro-cogeneration for Installations up to 100 kWe," *Energy Procedia,* vol. 82, pp. 994-1001, 2015.

[18] R. A. Victor, J.-K. Kim, and R. Smith, "Composition optimisation of working fluids for Organic Rankine Cycles and Kalina cycles," *Energy,* vol. 55, pp. 114-126, 2013.

[19] M. Yari, A. S. Mehr, V. Zare, S. M. S. Mahmoudi, and M. A. Rosen, "Exergoeconomic comparison of TLC (Trilateral Rankine Cycle), ORC (Organic Rankine Cycle) and Kalina Cycle using a low grade heat source," *Energy,* 2015.

[20] J. Nouman, "Comparative studies and analyses of working fluids for Organic Rankine Cycles – ORC," Master of Science Thesis Master of Science Thesis, Department of Energy Technology, The Royal Institute of Technology(KTH), Stockholm, Sweden, 2012.

[21] Z. Zhang, Z. Guo, Y. Chen, J. Wu, and J. Hua, "Power generation and heating performances of integrated system of ammonia–water Kalina–Rankine cycle," *Energy Conversion and Management,* vol. 92, pp. 517-522, 2015.

[22] X. Zhang, M. He, and Y. Zhang, "A review of research on the Kalina Cycle," *Renewable and Sustainable Energy Reviews,* vol. 16, pp. 5309-5318, 2012.

[23] P. A. Lolos and E. D. Rogdakis, "A Kalina Power Cycle driven by Renewable Energy Sources," *Energy,* vol. 34, pp. 457-464, 2009.

[24] S. Ogriseck, "Integration of Kalina Cycle in a Combined Heat and Power Plant, A Case Study," *Applied Thermal Engineering,* vol. 29, pp. 2843-2848, 2009.

[25] R. V. Padilla, G. Demirkaya, D. Y. Goswami, E. Stefanakos, and M. M. Rahman, "Analysis of Power and Cooling Cogeneration using Ammonia-Water Mixture," *Energy,* vol. 35, pp. 4649-4657, 2010.

[26] M. Jonsson, "Advanced Power Cycles with Mixtures as the Working Fluid," Doctoral Doctoral Thesis, Department of Chemical Engineering and Technology, Royal Institute of Technology (KTH), Stockholm, Sweden, 2003.

[27] F. Xu, D. Yogi Goswami, and S. S. Bhagwat, "A Combined Power/Cooling Cycle," *Energy,* vol. 25, pp. 233-246, 2000.

[28] J. Fischer, "Comparison of Trilateral Cycles and Organic Rankine Cycles," *Energy,* vol. 36, pp. 6208-6219, 2011.

[29] Y. Li, "Analysis of Low Temperature Organic Rankine Cycles for Solar Applications," 2013.

[30] V. T. Cheang, R. A. Hedderwick, and C. McGregor, "Benchmarking Supercritical Carbon dioxide Cycles against Steam Rankine Cycles for Concentrated Solar Power," *Solar Energy,* vol. 113, pp. 199-211, 2015.

[31] Y. Dai, J. Wang, and L. Gao, "Parametric Optimization and Comparative study of organic Rankine Cycle (ORC) for Low Grade Waste Heat Recovery," *Energy Conversion and Management,* vol. 50, pp. 576-582, 2009.

[32] C. Zhang, G. Shu, H. Tian, H. Wei, and X. Liang, "Comparative Study of Alternative ORC-based Combined Power Systems to Exploit High Temperature Waste Heat," *Energy Conversion and Management,* vol. 89, pp. 541-554, 2015.

[33] M. David, W. Choon, E. Frithjof, and K. Susan, "Design and build of 1 kilowatt Organic Rankine Cycle power generator," in *35th New Zealand Geothermal Workshop*, 2013, pp. 17-20.

[34] G. Zyhowski, A. Brown, and A. Achaichia, "HFC-245fa working fluid in organic Rankine cycle-a safe and economic way to generate electricity from waste heat," in *Proceedings of 23 rd Annual ECOS Conference*, 2010.

[35] Taufeeq Dhansay, Maarten de Wit, and A. Patt, "An evaluation for harnessing low-enthalpy geothermal energy in the Limpopo Province, South Africa," *South African Journal of Science,* 2014.

[36] W. Husband and A. Beyene, "Low-grade heat-driven Rankine cycle, a feasibility study," *International Journal of Energy Research,* vol. 32, pp. 1373-1382, 2008.

[37] X. Wang, L. Zhao, J. Wang, W. Zhang, X. Zhao, and W. Wu, "Performance evaluation of a low-temperature solar Rankine cycle system utilizing R245fa," *Solar Energy,* vol. 84, pp. 353-364, 2010.

[38] G. J. Zyhowski, A. P. Brown, and A. Achaichia, "HFC-245fa Working Fluid in Organic Rankine Cycle - A Safe and Economic Way to Generate Electricity from Waste Heat," presented at the ECOS2010, Lausanne, Switzerland, 2010.

[39] X. Wang and L. Zhao, "Analysis of zeotropic mixtures used in low-temperature solar Rankine cycles for power generation," *Solar Energy,* vol. 83, pp. 605-613, 2009.

[40] P. Garg, P. Kumar, K. Srinivasan, and P. Dutta, "Evaluation of isopentane, R-245fa and their mixtures as working fluids for organic Rankine cycles," *Applied Thermal Engineering,* vol. 51, pp. 292-300, 2013.

[41] T. F. Bertrand, G. Papadakis, G. Lambrinos, and A. Frangoudakis, "Criteria for working fluids selection in low-temperature solar organic Rankine cycles," presented at the EUROSUN2008, Lisbon, Portugal, 2008.

[42] H. Chen, D. Y. Goswami, and E. K. Stefanakos, "A review of thermodynamic cycles and working fluids for the conversion of low-grade heat," *Renewable and Sustainable Energy Reviews,* vol. 14, pp. 3059-3067, 2010.

[43] E. Macchi, "The Choice of Working Fluid: The most important step for a successful organic rankine cycle (and an efficient turbine)," in *ASME ORC 2013*, Rotherdam, Netherland, 2013, pp. 4-8.

[44] A. Borsukiewicz-Gozdur, "Pumping work in the Organic Rankine Cycle," *Applied Thermal Engineering,* vol. 51, pp. 781-786, 2013.

[45] S. Quoilin, M. V. D. Broek, S. Declaye, P. Dewallef, and V. Lemort, "Techno-economic survey of Organic Rankine Cycle (ORC) systems," *Renewable and Sustainable Energy Reviews,* vol. 22, pp. 168-186, 2013.

[46] T. L. Bergman, F. P. Incropera, and A. S. Lavine, *Fundamentals of heat and mass transfer*: John Wiley & Sons, 2011.

[47] EngineersEdge. (03/02/2016). *Convective Heat Transfer Coeffficients Table Chart*. Available: http://www.engineersedge.com/heat_transfer/convective_heat_transfer_coefficients__13378.htm

[48] *Kwikot Product Bronchures, Kwikot Kwa-Zulu Natal Division*. Available: www.kwikot.co.za

[49] "Infinity Turbine LLC. ORC Engine Generator Set IT10 kWe Full Build Version 11 Installation Manual," ed, 2012.

[50] "Cerus Industrial Corporaton, Titan_C_Series_User_Manual, ed. 153rd Drive Suite 318 Beaverton," 2013.

APPENDIXES

Appendix I: Simulation Codes and Formatted Equations

EES Ver. 10.119: #3144: For use only in Mechanical Engineering Univ. of Kwazulu-Natal, Durban, South Africa

```
$UnitSystem SI K Pa J mass radian

T_h_in=353[K]                                   "Inlet temperature of Water"

T_c_in=233[K]                                   "Inlet Temperture of R-134a"

P_h_in=1.6[MPa]*convert(MPa,Pa)                 "water Pump Pressure"

P_c_in=2.46[MPa]*convert(MPa,Pa)                "Refrigerant pump Pressure"

U=851.17[W/m^2*K]                               "Heat Transfer Co-efficient"

A=1[m^2]                                        "Heat Transfer Area"

m_dot_h=5.8333[kg/s]                            "Hot Water Mass flow rate"

m_dot_c=0.4778[kg/s]                            "Refrigerant Mass flow rate"

F$='r134a'                                      "Refrigerant"

c_p_c=cp(F$,T=T_c_in,P=P_c_in)                  "Specific Heat Capacity of Refrigerant"

c_p_h=cp(Water,T=T_h_in,P=P_h_in)               "Specific Heat Capacity of water"

C_h=m_dot_h*c_p_h                               "Heat Capacity of water"

C_c=m_dot_c*c_p_c                               "Heat Capacity of refrigerant"

C_r=C_c/C_h                                     "Heat Capacity ratio"

NTU=U*A/C_c                                     "Number of transfer Units"

q_max=C_c*(T_h_in-T_c_in)                       "maximum heat transfer possible"

epsilon=(1-exp(-NTU*(1-C_r)))/(1-C_r*exp(-NTU*(1-C_r)))  "Evaporator Effectiveness"

q=epsilon*q_max                                 " heat transfer"

T_h_out=T_h_in-q/(m_dot_h*c_p_h)                "Exit Temperature of Hot water from Evaporator"

T_c_out=T_c_in+q/(m_dot_c*c_p_c)                "Exit Temperature of Refrigerant from Evaporator"

"state 1"                                       "determine Entropy and Pressure"

s[1]=s[4]                                       "specific entropy"
P[1]=P[2]                                       "pressure"
h[1]=enthalpy(F$,s=s[1],P=P[1])                 "specific enthalpy"
T[1]=temperature(F$,s=s[1],P=P[1])              "temperature"

"state 2"                                       "determine Pressure and Temperature"

P[2]=P_c_in                                     "boiler pressure"
T[2]=T_c_out                                    "boiler temperature"
h[2]=enthalpy(F$,P=P[2],T=T[2])                 "specific enthalpy"
s[2]=entropy(F$,P=P[2],T=T[2])                  "entropy"

"state 3"                                       "determine Entropy and Pressure"

s[3]=s[2]                                       "specific entropy"
```

```
P[3]=P[4]                                   "pressure"
h[3]=enthalpy(F$,s=s[3],P=P[3])             "specific enthalpy"
T[3]=temperature(F$,s=s[3],P=P[3])          "temperature"

"state 4"                                   "determine Quality and Temperature"

x[4]=0                                      "quality"
T[4]=T_c_in                                 "condenser temperature"
P[4]=pressure(F$,x=x[4],T=T[4])             "pressure"
h[4]=enthalpy(F$,x=x[4],T=T[4])             "specific enthalpy"
s[4]=entropy(F$,x=x[4],T=T[4])              "specific entropy"

"Energy Balances across components"

W_dot_p\m_dot_c=h[1]-h[4]                   "Pump"
Q_dot_b\m_dot_c=h[2]-h[1]                   "Boiler"
W_dot_t\m_dot_c=h[2]-h[3]                   "Turbine"
Q_dot_c\m_dot_c=h[3]-h[4]                   "Condenser"

"Overall Energy Balance"

Check_1=W_dot_t\m_dot_c+Q_dot_c\m_dot_c-W_dot_p\m_dot_c-Q_dot_b\m_dot_c     "overall balance"

"Net Power produced by Rankine Cycle"

W_dot_net\m_dot_c=W_dot_t\m_dot_c-W_dot_p\m_dot_c          "net power produced per mass flow rate"

W_dot_net=W_dot_net\m_dot_c*m_dot_c                        "net power produced"

"energy transfer across units"

W_dot_p=W_dot_p\m_dot_c*m_dot_c                            "pump"
Q_dot_b=Q_dot_b\m_dot_c*m_dot_c                            "boiler"
W_dot_t=W_dot_t\m_dot_c*m_dot_c                            "turbine"
Q_dot_c=Q_dot_c\m_dot_c*m_dot_c                            "condenser"

"Rankine Thermal Efficiency"

eta_Rankine=W_dot_net\m_dot_c/Q_dot_b\m_dot_c              "ratio of net work to heat input"

"Backwork ratio"                                           "ratio of pump work to turbine work"

bwr=W_dot_p/W_dot_t                                        "Back-work ratio"

V=220[V]

r=0.005[m]

Di_turbineblade=0.305[m]

W_dot_net=I*V

CSA_t_in=Pi*r^2

P_c_in=F/CSA_t_in

tau=F*Di_turbineblade
```

```
118:  S_r=W_dot_net*60/(2*Pi*tau)
```

$T_{h,in} = 353$ [K] *Inlet temperature of Water*

$T_{c,in} = 233$ [K] *Inlet Temperature of R-134a*

$P_{h,in} = 1.6$ [MPa] $\left| 1000000 \cdot \frac{Pa}{MPa} \right|$ *water Pump Pressure*

$P_{c,in} = 2.46$ [MPa] $\left| 1000000 \cdot \frac{Pa}{MPa} \right|$ *Refrigerant pump Pressure*

$U = 851.17$ [W/m^2°K] *Heat Transfer Co-efficient*

$A = 1$ [m^2] *Heat Transfer Area*

$\dot{m}_h = 5.8333$ [kg/s] *Hot Water Mass flow rate*

$\dot{m}_c = 0.4778$ [kg/s] *Refrigerant Mass flow rate*

$F\$ = 'r134a'$ *Refrigerant*

$c_{p,c} = Cp[F\$, T = T_{c,in}, P = P_{c,in}]$ *Specific Heat Capacity of Refrigerant*

$c_{p,h} = Cp[water, T = T_{h,in}, P = P_{h,in}]$ *Specific Heat Capacity of water*

$C_h = \dot{m}_h \cdot c_{p,h}$ *Heat Capacity of water*

$C_c = \dot{m}_c \cdot c_{p,c}$ *Heat Capacity of refrigerant*

$C_r = \frac{C_c}{C_h}$ *Heat Capacity ratio*

$NTU = U \cdot \frac{A}{C_c}$ *Number of transfer Units*

$q_{max} = C_c \cdot [T_{h,in} - T_{c,in}]$ *maximum heat transfer possible*

$\varepsilon = \frac{1 - \exp[-NTU \cdot (1 - C_r)]}{1 - C_r \cdot \exp[-NTU \cdot (1 - C_r)]}$ *Evaporator Effectiveness*

$\dot{q} = \varepsilon \cdot q_{max}$ *heat transfer*

$T_{h,out} = T_{h,in} - \frac{\dot{q}}{\dot{m}_h \cdot c_{p,h}}$ *Exit Temperature of Hot water from Evaporator*

$T_{c,out} = T_{c,in} + \frac{\dot{q}}{\dot{m}_c \cdot c_{p,c}}$ *Exit Temperature of Refrigerant from Evaporator*

state 1

determine Entropy and Pressure

$s_1 = s_4$ *specific entropy*

$P_1 = P_2$ *pressure*

$h_1 = h[F\$, s = s_1, P = P_1]$ *specific enthalpy*

$T_1 = T[F\$, s = s_1, P = P_1]$

temperature

state 2

determine Pressure and Temperature

$P_2 = P_{c,in}$ *boiler pressure*

$T_2 = T_{c,out}$ *boiler temperature*

$h_2 = h[F\$, P = P_2, T = T_2]$ *specific enthalpy*

$s_2 = s[F\$, P = P_2, T = T_2]$ *entropy*

state 3

determine Entropy and Pressure

$s_3 = s_2$ *specific entropy*

$P_3 = P_4$ *pressure*

$h_3 = h[F\$, s = s_3, P = P_3]$ *specific enthalpy*

$T_3 = T[F\$, s = s_3, P = P_3]$ *temperature*

state 4

determine Quality and Temperature

$x_4 = 0$ *quality*

$T_4 = T_{c,in}$ *condenser temperature*

$P_4 = P[F\$, x = x_4, T = T_4]$ *pressure*

$h_4 = h[F\$, x = x_4, T = T_4]$ *specific enthalpy*

$s_4 = s[F\$, x = x_4, T = T_4]$ *specific entropy*

Energy Balances across components

$\dot{W}'_{pm_c} = h_1 - h_4$ *Pump*

$\dot{Q}'_{bm_c} = h_2 - h_1$ *Boiler*

$\dot{W}'_{tm_c} = h_2 - h_3$ *Turbine*

$\dot{Q}'_{cm_c} = h_3 - h_4$ *Condenser*

Overall Energy Balance

$Check_1 = \dot{W}'_{tm_c} + \dot{Q}'_{cm_c} - \dot{W}'_{pm_c} - \dot{Q}'_{bm_c}$ *overall balance*

Net Power produced by Rankine Cycle

$\dot{W}'_{netm_c} = \dot{W}'_{tm_c} - \dot{W}'_{pm_c}$ *net power produced per mass flow rate*

$\dot{W}_{net} = \dot{W}_{netm_s} \cdot \dot{m}_s$ *net power produced*

energy transfer across units

$\dot{W}_p = \dot{W}_{pm_c} \cdot \dot{m}_c$ *pump*

$\dot{Q}_b = \dot{Q}_{bm_c} \cdot \dot{m}_c$ *boiler*

$\dot{W}_t = \dot{W}_{tm_c} \cdot \dot{m}_c$ *turbine*

$\dot{Q}_c = \dot{Q}_{cm_c} \cdot \dot{m}_c$ *condenser*

Rankine Thermal Efficiency

$\eta_{Rankine} = \frac{\dot{W}_{netm_c}}{\dot{Q}_{bm_c}}$ *ratio of net work to heat input*

Backwork ratio

ratio of pump work to turbine work

$bwr = \frac{\dot{W}_p}{\dot{W}_t}$ *Back-work ratio*

$V = 220$ [V]

$r = 0.005$ [m]

$Di_{turbineblade} = 0.305$ [m]

$\dot{W}_{net} = I \cdot V$

$CSA_{t,in} = \pi \cdot r^2$

$P_{c,in} = \frac{F}{CSA_{t,in}}$

$\tau = F \cdot Di_{turbineblade}$

$S_r = \dot{W}_{net} \cdot \frac{60}{2 \cdot \pi \cdot \tau}$

Appendix II: Simulation Results

SOLUTION

Unit Settings: SI K Pa J mass rad

$A = 1$ [m^2]
$Check_1 = 0$
$C_c = 596.9$ [J]
$c_{p,c} = 1249$ [J/kgK]
$C_r = 0.02442$
$\varepsilon = 0.7558$
$F = 193.2$ [N]
$I = 42.75$ [A]
$\dot{m}_h = 5.833$ [kg/s]
$P_{c,in} = 2.460E+06$ [Pa]
$q = 54137$ [J]
$\dot{Q}_{b/m\_dot,c} = 122383$
$\dot{Q}_{c/m\_dot,c} = 102697$
$r = 0.005$ [m]
$\tau = 58.93$ [Nm]
$T_{c,out} = 323.7$ [K]
$T_{h,out} = 350.8$ [K]
$V = 220$ [V]
$\dot{W}_{net/m\_dot,c} = 19686$
$\dot{W}_{p/m\_dot,c} = 1697$
$\dot{W}_{t/m\_dot,c} = 21383$

$bwr = 0.07935$
$CSA_{c,in} = 0.00007854$
$C_h = 24446$ [J]
$c_{p,h} = 4191$ [J/kgK]
$D_{turbinetube} = 0.305$ [m]
$\eta_{Rankine} = 0.1609$
$F\$ = 'r134a'$
$\dot{m}_c = 0.4778$ [kg/s]
$NTU = 1.426$
$P_{h,in} = 1.600E+06$ [Pa]
$\dot{Q}_b = 58474$
$\dot{Q}_c = 49069$
$q_{max} = 71628$ [J]
$S_r = 1524$ [rpm]
$T_{c,in} = 233$ [K]
$T_{h,in} = 353$ [K]
$U = 851.2$ [W/m^2*K]
$\dot{W}_{net} = 9406$ [W]
$\dot{W}_p = 810.7$ [W]
$\dot{W}_t = 10217$ [W]

Appendix III: Parametric Tables for Plots

Parametric Table: HTA against Refrigerant-temp-out

	A [m^2]	$T_{c,out}$ [K]
Run 1	0.1	*248.9*
Run 2	0.2	*262.7*
Run 3	0.3	*274.6*
Run 4	0.4	*284.9*
Run 5	0.5	*293.9*
Run 6	0.6	*301.6*
Run 7	0.7	*308.4*
Run 8	0.8	*314.2*
Run 9	0.9	*319.3*
Run 10	1	*323.7*
Run 11	1.1	*327.5*
Run 12	1.2	*330.8*
Run 13	1.3	*333.7*
Run 14	1.4	*336.2*
Run 15	1.5	*338.4*
Run 16	1.6	*340.3*
Run 17	1.7	*342*
Run 18	1.8	*343.4*
Run 19	1.9	*344.7*
Run 20	2	*345.7*
Run 21	2.1	*346.7*
Run 22	2.2	*347.5*
Run 23	2.3	*348.2*
Run 24	2.4	*348.8*
Run 25	2.5	*349.4*
Run 26	2.6	*349.9*
Run 27	2.7	*350.3*
Run 28	2.8	*350.6*
Run 29	2.9	*350.9*
Run 30	3	*351.2*
Run 31	3.1	*351.4*
Run 32	3.2	*351.6*
Run 33	3.3	*351.8*
Run 34	3.4	*352*
Run 35	3.5	*352.1*
Run 36	3.6	*352.2*
Run 37	3.7	*352.3*
Run 38	3.8	*352.4*
Run 39	3.9	*352.5*
Run 40	4	*352.6*
Run 41	4.1	*352.6*
Run 42	4.2	*352.7*
Run 43	4.3	*352.7*
Run 44	4.4	*352.7*
Run 45	4.5	*352.8*
Run 46	4.6	*352.8*
Run 47	4.7	*352.8*
Run 48	4.8	*352.9*
Run 49	4.9	*352.9*
Run 50	5	*352.9*

Parametric Table: HTA against Heat Quantity

	A [m^2]	q [J]
Run 1	0.1	*9505*
Run 2	0.2	*17725*
Run 3	0.3	*24840*
Run 4	0.4	*31002*
Run 5	0.5	*36344*
Run 6	0.6	*40975*
Run 7	0.7	*44993*
Run 8	0.8	*48480*
Run 9	0.9	*51508*
Run 10	1	*54137*
Run 11	1.1	*56420*
Run 12	1.2	*58405*
Run 13	1.3	*60129*
Run 14	1.4	*61627*
Run 15	1.5	*62930*
Run 16	1.6	*64063*
Run 17	1.7	*65047*
Run 18	1.8	*65904*
Run 19	1.9	*66648*
Run 20	2	*67296*
Run 21	2.1	*67859*
Run 22	2.2	*68349*
Run 23	2.3	*68776*
Run 24	2.4	*69146*
Run 25	2.5	*69469*
Run 26	2.6	*69749*
Run 27	2.7	*69993*
Run 28	2.8	*70206*
Run 29	2.9	*70391*
Run 30	3	*70551*
Run 31	3.1	*70691*
Run 32	3.2	*70813*
Run 33	3.3	*70919*
Run 34	3.4	*71011*
Run 35	3.5	*71091*
Run 36	3.6	*71161*
Run 37	3.7	*71221*
Run 38	3.8	*71274*
Run 39	3.9	*71320*
Run 40	4	*71360*
Run 41	4.1	*71395*
Run 42	4.2	*71425*
Run 43	4.3	*71451*
Run 44	4.4	*71474*
Run 45	4.5	*71494*
Run 46	4.6	*71512*
Run 47	4.7	*71527*
Run 48	4.8	*71540*
Run 49	4.9	*71551*
Run 50	5	*71561*

Parametric Table: HTA against Power

	A [m^2]	$\dot{W}_{net}$ [W]
Run 1	0.1	*314.2*
Run 2	0.2263	*1315*
Run 3	0.3526	*2642*
Run 4	0.4789	*4081*
Run 5	0.6053	*5513*
Run 6	0.7316	*6874*
Run 7	0.8579	*8131*
Run 8	0.9842	*9272*
Run 9	1.111	*10293*
Run 10	1.237	*11199*
Run 11	1.363	*11997*
Run 12	1.489	*12696*
Run 13	1.616	*13305*
Run 14	1.742	*13834*
Run 15	1.868	*14291*
Run 16	1.995	*14686*
Run 17	2.121	*15025*
Run 18	2.247	*15316*
Run 19	2.374	*15565*
Run 20	2.5	*15778*

Parametric Table: HTA against Efficiency

	A [m^2]	$\eta_{Rankine}$
Run 1	0.1	*0.03405*
Run 2	0.2	*0.06038*
Run 3	0.3	*0.08188*
Run 4	0.4	*0.09964*
Run 5	0.5	*0.1145*
Run 6	0.6	*0.1269*
Run 7	0.7	*0.1375*
Run 8	0.8	*0.1465*
Run 9	0.9	*0.1542*
Run 10	1	*0.1609*
Run 11	1.1	*0.1666*
Run 12	1.2	*0.1715*
Run 13	1.3	*0.1758*
Run 14	1.4	*0.1795*
Run 15	1.5	*0.1828*
Run 16	1.6	*0.1856*
Run 17	1.7	*0.1881*
Run 18	1.8	*0.1902*
Run 19	1.9	*0.1921*
Run 20	2	*0.1937*
Run 21	2.1	*0.1952*
Run 22	2.2	*0.1964*
Run 23	2.3	*0.1975*
Run 24	2.4	*0.1985*
Run 25	2.5	*0.1994*
Run 26	2.6	*0.2001*
Run 27	2.7	*0.2544*

Parametric Table: HTA against Efficiency

	A [m²]	$\eta_{Rankine}$
Run 28	2.8	*0.2546*
Run 29	2.9	*0.2547*
Run 30	3	*0.2549*
Run 31	3.1	*0.255*
Run 32	3.2	*0.2551*
Run 33	3.3	*0.2552*
Run 34	3.4	*0.2553*
Run 35	3.5	*0.2553*
Run 36	3.6	*0.2554*
Run 37	3.7	*0.2555*
Run 38	3.8	*0.2555*
Run 39	3.9	*0.2555*
Run 40	4	*0.2556*
Run 41	4.1	*0.2556*
Run 42	4.2	*0.2556*
Run 43	4.3	*0.2556*
Run 44	4.4	*0.2557*
Run 45	4.5	*0.2557*
Run 46	4.6	*0.2557*
Run 47	4.7	*0.2557*
Run 48	4.8	*0.2557*
Run 49	4.9	*0.2557*
Run 50	5	*0.2557*

Parametric Table: HTA against BWR

	A [m²]	bwr
Run 1	0.1	*0.7207*
Run 2	0.2	*0.431*
Run 3	0.3	*0.2818*
Run 4	0.4	*0.2033*
Run 5	0.5	*0.1579*
Run 6	0.6	*0.1294*
Run 7	0.7	*0.1102*
Run 8	0.8	*0.09674*
Run 9	0.9	*0.08684*
Run 10	1	*0.07935*
Run 11	1.1	*0.07354*
Run 12	1.2	*0.06895*
Run 13	1.3	*0.06526*
Run 14	1.4	*0.06225*
Run 15	1.5	*0.05978*
Run 16	1.6	*0.05772*
Run 17	1.7	*0.056*
Run 18	1.8	*0.05454*
Run 19	1.9	*0.05331*
Run 20	2	*0.05226*
Run 21	2.1	*0.05136*
Run 22	2.2	*0.05059*
Run 23	2.3	*0.04993*
Run 24	2.4	*0.04936*
Run 25	2.5	*0.04887*

Parametric Table: HTA against BWR

	A [m^2]	bwr
Run 26	2.6	*0.04844*
Run 27	2.7	*0.02327*
Run 28	2.8	*0.0232*
Run 29	2.9	*0.02315*
Run 30	3	*0.02309*
Run 31	3.1	*0.02305*
Run 32	3.2	*0.02301*
Run 33	3.3	*0.02298*
Run 34	3.4	*0.02295*
Run 35	3.5	*0.02293*
Run 36	3.6	*0.02291*
Run 37	3.7	*0.02289*
Run 38	3.8	*0.02287*
Run 39	3.9	*0.02286*
Run 40	4	*0.02285*
Run 41	4.1	*0.02284*
Run 42	4.2	*0.02283*
Run 43	4.3	*0.02282*
Run 44	4.4	*0.02281*
Run 45	4.5	*0.02281*
Run 46	4.6	*0.0228*
Run 47	4.7	*0.0228*
Run 48	4.8	*0.02279*
Run 49	4.9	*0.02279*
Run 50	5	*0.02279*

Parametric Table: Water-temp-in against Refrigerant-temp-out

	$T_{h,in}$ [K]	$T_{c,out}$ [K]
Run 1	303	*285.9*
Run 2	305.4	*287.8*
Run 3	307.9	*289.6*
Run 4	310.3	*291.5*
Run 5	312.8	*293.3*
Run 6	315.2	*295.2*
Run 7	317.7	*297*
Run 8	320.1	*298.9*
Run 9	322.6	*300.7*
Run 10	325	*302.6*
Run 11	327.5	*304.4*
Run 12	329.9	*306.3*
Run 13	332.4	*308.1*
Run 14	334.8	*310*
Run 15	337.3	*311.8*
Run 16	339.7	*313.7*
Run 17	342.2	*315.5*
Run 18	344.6	*317.4*
Run 19	347.1	*319.2*
Run 20	349.5	*321.1*
Run 21	352	*322.9*
Run 22	354.4	*324.8*
Run 23	356.9	*326.6*

Parametric Table: Water-temp-in against Refrigerant-temp-out

	$T_{h,in}$ [K]	$T_{c,out}$ [K]
Run 24	359.3	*328.5*
Run 25	361.8	*330.3*
Run 26	364.2	*332.2*
Run 27	366.7	*334*
Run 28	369.1	*335.9*
Run 29	371.6	*337.7*
Run 30	374	*339.6*
Run 31	376.5	*341.4*
Run 32	378.9	*343.3*
Run 33	381.4	*345.1*
Run 34	383.8	*347*
Run 35	386.3	*348.8*
Run 36	388.7	*350.7*
Run 37	391.2	*352.5*
Run 38	393.6	*354.4*
Run 39	396.1	*356.3*
Run 40	398.5	*358.1*
Run 41	401	*360*
Run 42	403.4	*361.8*
Run 43	405.9	*363.7*
Run 44	408.3	*365.5*
Run 45	410.8	*367.4*
Run 46	413.2	*369.2*
Run 47	415.7	*371.1*
Run 48	418.1	*372.9*
Run 49	420.6	*374.8*
Run 50	423	*376.6*

Parametric Table: Water-temp-in against Heat Quantity

	$T_{h,in}$ [K]	q [J]
Run 1	300	*30226*
Run 2	302.6	*31394*
Run 3	305.2	*32561*
Run 4	307.8	*33729*
Run 5	310.4	*34896*
Run 6	312.9	*36064*
Run 7	315.5	*37232*
Run 8	318.1	*38399*
Run 9	320.7	*39567*
Run 10	323.3	*40735*
Run 11	325.9	*41902*
Run 12	328.5	*43070*
Run 13	331.1	*44238*
Run 14	333.6	*45405*
Run 15	336.2	*46573*
Run 16	338.8	*47741*
Run 17	341.4	*48908*
Run 18	344	*50076*
Run 19	346.6	*51244*
Run 20	349.2	*52412*
Run 21	351.8	*53579*

Parametric Table: Water-temp-in against Heat Quantity

	$T_{h,in}$ [K]	q [J]
Run 22	354.4	*54747*
Run 23	356.9	*55915*
Run 24	359.5	*57083*
Run 25	362.1	*58251*
Run 26	364.7	*59419*
Run 27	367.3	*60587*
Run 28	369.9	*61754*
Run 29	372.5	*62922*
Run 30	375.1	*64090*
Run 31	377.6	*65258*
Run 32	380.2	*66426*
Run 33	382.8	*67594*
Run 34	385.4	*68762*
Run 35	388	*69931*

Parametric Table: Water-temp-in against Power

	$T_{h,in}$ [K]	$\dot{W}_{net}$ [W]
Run 1	300	*3024*
Run 2	304.2	*3404*
Run 3	308.4	*3804*
Run 4	312.6	*4227*
Run 5	316.8	*4670*
Run 6	321.1	*5136*
Run 7	325.3	*5623*
Run 8	329.5	*6133*
Run 9	333.7	*6665*
Run 10	337.9	*7219*
Run 11	342.1	*7797*
Run 12	346.3	*8399*
Run 13	350.5	*9026*
Run 14	354.7	*9678*
Run 15	358.9	*10358*
Run 16	363.2	*11066*
Run 17	367.4	*11806*
Run 18	371.6	*12579*
Run 19	375.8	*13389*
Run 20	380	*14243*

Parametric Table: Water-temp-in against Efficiency

	$T_{h,in}$ [K]	$\eta_{Rankine}$
Run 1	303	*0.1013*
Run 2	307.2	*0.1066*
Run 3	311.4	*0.1118*
Run 4	315.6	*0.117*
Run 5	319.8	*0.1221*
Run 6	324.1	*0.1272*
Run 7	328.3	*0.1322*
Run 8	332.5	*0.1372*

Parametric Table: Water-temp-in against Efficiency

	$T_{h,in}$ [K]	$\eta_{Rankine}$
Run 9	336.7	*0.1421*
Run 10	340.9	*0.147*
Run 11	345.1	*0.1519*
Run 12	349.3	*0.1567*
Run 13	353.5	*0.1615*
Run 14	357.7	*0.1662*
Run 15	361.9	*0.1709*
Run 16	366.2	*0.1757*
Run 17	370.4	*0.1804*
Run 18	374.6	*0.1851*
Run 19	378.8	*0.1899*
Run 20	383	*0.1947*

Parametric Table: Ref mass-flow against Ref-outlet-temp

	$\dot{m}_c$ [kg/s]	$T_{c,out}$ [K]
Run 1	0.01	*353*
Run 2	0.06211	*353*
Run 3	0.1142	*352.7*
Run 4	0.1663	*351*
Run 5	0.2184	*347.6*
Run 6	0.2705	*343.1*
Run 7	0.3226	*338.2*
Run 8	0.3747	*333.2*
Run 9	0.4268	*328.3*
Run 10	0.4789	*323.6*
Run 11	0.5311	*319.2*
Run 12	0.5832	*315.2*
Run 13	0.6353	*311.4*
Run 14	0.6874	*307.9*
Run 15	0.7395	*304.7*
Run 16	0.7916	*301.7*
Run 17	0.8437	*298.9*
Run 18	0.8958	*296.3*
Run 19	0.9479	*293.9*
Run 20	1	*291.7*

Parametric Table: Ref mass-flow against Heat Quantity

	$\dot{m}_c$ [kg/s]	q [J]
Run 1	0.01	*1499*
Run 2	0.06211	*9310*
Run 3	0.1142	*17076*
Run 4	0.1663	*24507*
Run 5	0.2184	*31262*
Run 6	0.2705	*37214*
Run 7	0.3226	*42393*
Run 8	0.3747	*46886*
Run 9	0.4268	*50794*
Run 10	0.4778	*54137*

Parametric Table: Ref mass-flow against Heat Quantity

	$\dot{m}_c$ [kg/s]	q [J]
Run 11	0.5311	*57206*
Run 12	0.5832	*59856*
Run 13	0.6353	*62211*
Run 14	0.6874	*64316*
Run 15	0.7395	*66206*
Run 16	0.7916	*67913*
Run 17	0.8437	*69461*
Run 18	0.8958	*70871*
Run 19	0.9479	*72159*
Run 20	1	*73341*

Parametric Table: Ref mass-flow against Power

	$\dot{m}_c$ [kg/s]	$\dot{W}_{net}$ [W]
Run 1	0.01	*728.2*
Run 2	0.06211	*4522*
Run 3	0.1142	*8296*
Run 4	0.1663	*11912*
Run 5	0.2184	*6962*
Run 6	0.2705	*7911*
Run 7	0.3226	*8567*
Run 8	0.3747	*9000*
Run 9	0.4268	*9265*
Run 10	0.4778	*9406*
Run 11	0.5311	*9461*
Run 12	0.5832	*9449*
Run 13	0.6353	*9389*
Run 14	0.6874	*9296*
Run 15	0.7395	*9178*
Run 16	0.7916	*9044*
Run 17	0.8437	*8899*
Run 18	0.8958	*8746*
Run 19	0.9479	*8589*
Run 20	1	*8430*

Parametric Table: Ref mass-flow against Efficiency

	$\dot{m}_c$ [kg/s]	$\eta_{Rankine}$
Run 1	0.01	*0.2558*
Run 2	0.06211	*0.2558*
Run 3	0.1142	*0.2556*
Run 4	0.1663	*0.2548*
Run 5	0.2184	*0.1965*
Run 6	0.2705	*0.1898*
Run 7	0.3226	*0.1824*
Run 8	0.3747	*0.1749*
Run 9	0.4268	*0.1677*
Run 10	0.4789	*0.1607*
Run 11	0.5311	*0.1541*
Run 12	0.5832	*0.148*

Parametric Table: Ref mass-flow against Efficiency

	$\dot{m}_c$ [kg/s]	$\eta_{Rankine}$
Run 13	0.6353	*0.1422*
Run 14	0.6874	*0.1368*
Run 15	0.7395	*0.1317*
Run 16	0.7916	*0.127*
Run 17	0.8437	*0.1226*
Run 18	0.8958	*0.1184*
Run 19	0.9479	*0.1146*
Run 20	1	*0.1109*

Parametric Table: Ref Pump Pressure against Ref-outlet-temp

	$P_{c,in}$ [Pa]	$T_{c,out}$ [K]
Run 1	100000	*323.5*
Run 2	305263	*323.5*
Run 3	510526	*323.6*
Run 4	715789	*323.6*
Run 5	921053	*323.6*
Run 6	1.126E+06	*323.6*
Run 7	1.332E+06	*323.6*
Run 8	1.537E+06	*323.6*
Run 9	1.742E+06	*323.6*
Run 10	1.947E+06	*323.7*
Run 11	2.153E+06	*323.7*
Run 12	2.358E+06	*323.7*
Run 13	2.563E+06	*323.7*
Run 14	2.768E+06	*323.7*
Run 15	2.974E+06	*323.7*
Run 16	3.179E+06	*323.7*
Run 17	3.384E+06	*323.8*
Run 18	3.589E+06	*323.8*
Run 19	3.795E+06	*323.8*
Run 20	4.000E+06	*323.8*

Parametric Table: Ref Pump Pressure against Heat Quantity

	$P_{c,in}$ [Pa]	q [J]
Run 1	1000000	*54208*
Run 2	1.158E+06	*54200*
Run 3	1.316E+06	*54192*
Run 4	1.474E+06	*54184*
Run 5	1.632E+06	*54177*
Run 6	1.789E+06	*54169*
Run 7	1.947E+06	*54161*
Run 8	2.105E+06	*54154*
Run 9	2.263E+06	*54146*
Run 10	2.460E+06	*54137*
Run 11	2.579E+06	*54131*
Run 12	2.737E+06	*54124*
Run 13	2.895E+06	*54116*
Run 14	3.053E+06	*54109*

Parametric Table: Ref Pump Pressure against Heat Quantity

	$P_{c,in}$ [Pa]	q [J]
Run 15	3.211E+06	*54102*
Run 16	3.368E+06	*54094*
Run 17	3.526E+06	*54087*
Run 18	3.684E+06	*54080*
Run 19	3.842E+06	*54073*
Run 20	4.000E+06	*54066*

Parametric Table: Ref Pump Pressure against Power

	$P_{c,in}$ [Pa]	$\dot{W}_{net}$ [W]
Run 1	1000000	*28787*
Run 2	1.158E+06	*29355*
Run 3	1.316E+06	*29687*
Run 4	1.474E+06	*9467*
Run 5	1.632E+06	*9457*
Run 6	1.789E+06	*9447*
Run 7	1.947E+06	*9437*
Run 8	2.105E+06	*9427*
Run 9	2.263E+06	*9417*
Run 10	2.421E+06	*9408*
Run 11	2.579E+06	*9399*
Run 12	2.737E+06	*9390*
Run 13	2.895E+06	*9382*
Run 14	3.053E+06	*9373*
Run 15	3.211E+06	*9365*
Run 16	3.368E+06	*9357*
Run 17	3.526E+06	*9349*
Run 18	3.684E+06	*9341*
Run 19	3.842E+06	*9333*
Run 20	4.000E+06	*9326*

Parametric Table: Ref Pump Pressure against Efficiency

	$P_{c,in}$ [Pa]	$\eta_{Rankine}$
Run 1	1000000	*0.2131*
Run 2	1.158E+06	*0.2201*
Run 3	1.316E+06	*0.2258*
Run 4	1.474E+06	*0.1606*
Run 5	1.632E+06	*0.1607*
Run 6	1.789E+06	*0.1607*
Run 7	1.947E+06	*0.1607*
Run 8	2.105E+06	*0.1608*
Run 9	2.263E+06	*0.1608*
Run 10	2.460E+06	*0.1609*
Run 11	2.579E+06	*0.1609*
Run 12	2.737E+06	*0.1609*
Run 13	2.895E+06	*0.161*
Run 14	3.053E+06	*0.161*
Run 15	3.211E+06	*0.161*
Run 16	3.368E+06	*0.1611*

Parametric Table: Ref Pump Pressure against Efficiency

	$P_{c,in}$ [Pa]	$\eta_{Rankine}$
Run 17	3.526E+06	*0.1611*
Run 18	3.684E+06	*0.1612*
Run 19	3.842E+06	*0.1612*
Run 20	4.000E+06	*0.1613*

Parametric Table: Refrigerant Pressure against Rotational Speed

	$P_{c,in}$ [Pa]	S_r [rpm]
Run 1	500000	12397
Run 2	758889	10658
Run 3	990000	8573
Run 4	1.278E+06	5542
Run 5	1.480E+06	4050
Run 6	1.667E+06	*2261*
Run 7	1.970E+06	*1909*
Run 8	2.056E+06	*1828*
Run 9	2.460E+06	*1524*
Run 10	2.883E+06	*1297*
Run 11	3.222E+06	*1159*
Run 12	3.611E+06	*1032*
Run 13	4.000E+06	*929.4*

Parametric Table: Refrigerant Pressure against Torque

	$P_{c,in}$ [Pa]	τ [Nm]
Run 1	500000	*11.98*
Run 2	888889	*21.29*
Run 3	1.278E+06	*30.61*
Run 4	1.667E+06	*39.92*
Run 5	2.056E+06	*49.24*
Run 6	2.460E+06	*58.93*
Run 7	2.833E+06	*67.87*
Run 8	3.222E+06	*77.19*
Run 9	3.611E+06	*86.5*
Run 10	4.000E+06	*95.82*

Parametric Table: Power against Rotational Speed

	$\dot{W}_{net}$ [W]	S_r [rpm]
Run 1	0	*0*
Run 2	1500	*243.1*
Run 3	3000	*486.1*
Run 4	4500	*729.2*
Run 5	6000	*972.3*
Run 6	7500	*1215*
Run 7	9406	*1524*
Run 8	10500	*1702*
Run 9	12000	*1945*

Parametric Table: Power against Rotational Speed

	$\dot{W}_{net}$ [W]	S_r [rpm]
Run 10	13500	*2188*
Run 11	15000	*2431*

Appendix IV: IT10 Infinity Turbine Data Sheet

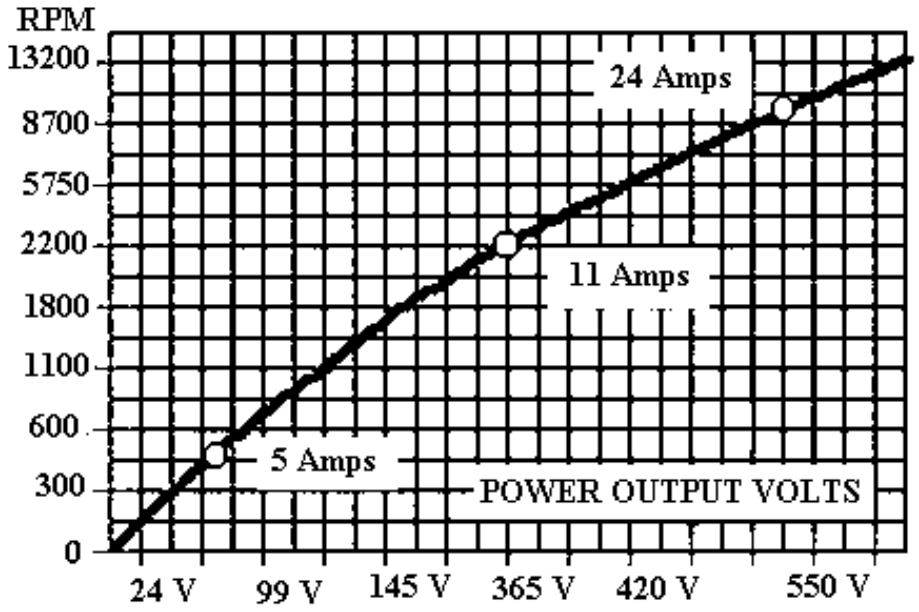

RPM-Volt characteristics of DC generator [49]

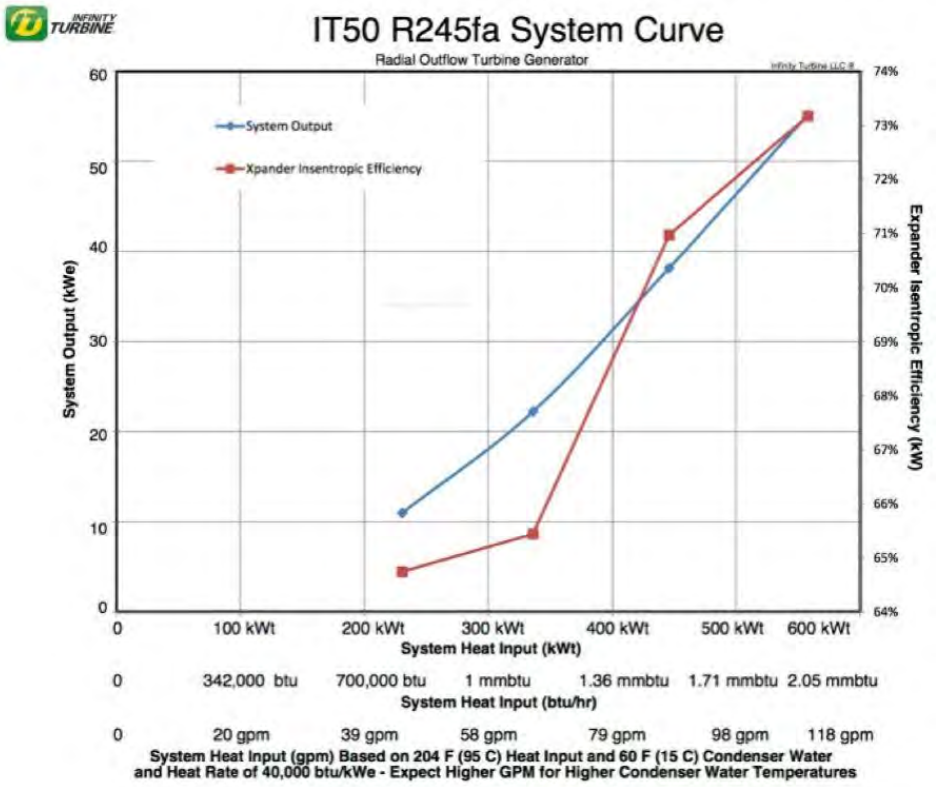

System Heat Input versus System Output [49]